

Photocopy and Use Authorization

In presenting this dissertation in partial fulfilment of the requirement for an advanced degree at Idaho State University; I agree that the Library shall make it freely available for inspection. I further state that permission for extensive copy of my dissertation for scholarly purposes may be granted by the Dean of the Graduate School, Dean of my academic division, or by the University Librarian. It is understood that any copying or publication of this dissertation for financial gain shall not be allowed without my written permission.

Signature_____

Adamu Kadiri

Date_____

**SHIELDING UPGRADE AND BEAM DUMP DESIGN ANALYSIS FOR A
40-MeV ELECTRON LINEAR ACCELERATOR AT IDAHO
ACCELERATOR CENTER**

By

Adamu Kadiri

A dissertation

submitted in partial fulfilment

of the requirements for the degree of

Doctor of Philosophy in Nuclear Science and Engineering

Idaho State University

December 2017

To the Graduate Faculty:

The members of the committee appointed to examine the dissertation of **Adamu Kadiri** find it satisfactory and recommended that it be accepted.

Dr. Richard Brey

Major Advisor

Dr. Thomas F. Gesell

Committee Member

Dr. George Imel

Committee Member

Dr. Chad Pope

Committee Member

Dr. Rene Rodriguez

Graduate Faculty Representative

ACKNOWLEDGMENTS

I would like to thank my major advisor, Dr. Richard Brey for his unwavering support, encouragement and advice. I would like to thank my committee members Dr. Thomas F. Gesell, Dr. George Imel, and Dr. Chad Pope for reading though and making valuable comments on my dissertation and for their time. I would like to thank Dr. Rene Rodriguez for serving as a Graduate Faculty Representative on my committee. I want to appreciate my family for their relentless support, patience and prayers for the past eight years since I left home in pursuit of educational dream. Most importantly, I give all glory to God for giving me the strength and health to study.

TABLE OF CONTENTS

LIST OF FIGURES	viii
LIST OF TABLE	ix
ABSTRACT	x
1. INTRODUCTION	1
1.1. Description and Statement of Problem	1
1.1.1. Cu-67 Production at Idaho Accelerator Center	4
1.2. Objectives	10
1.3. Hypothesis Statements	13
2. LITERATURE REVIEW	15
2.1. Particle Accelerator	15
2.2. Electron Linear Accelerators	16
2.3. The IAC Electron Accelerator	19
2.4. Activation Process in an Electron Accelerator	20
2.5. Radiation Associated with Electron LINACs	22
2.6. Shielding Considerations	23
2.7. Shielding Against Photons	23
2.8. Shielding Against Neutrons	25
2.9. History of Medical Radionuclide Production	26
2.10. Selection of radionuclide for Potential use in Nuclear medicine	29
2.10.1 Using Accelerator for Medical Radionuclide Production and Nuclear Research	30
2.11. Beam Dump Designs	31
3. MATERIALS AND METHOD	
3.1. Instruments used	35
3.2. Monte Carlo Neutral Transport Code (MCNP6)	35
3.2.1. The Title Block	36
3.2.2. The Cell Block	36
3.2.3. The Surface Block	37
3.2.4. Data Card	37
3.3. Data Acquisition	38
3.4. Methodology Part I	39
3.4.1. Target Study	39
3.4.2. The Experiment	40

3.4.3. Simulations	44
3.5.Methodology Part II	47
3.5.1. Benchmarking MCNP6 using Dose Equivalent Rate	47
3.5.2. Shielding/Being Dump Design Analysis using MCNP6	49
4. RESULTS AND DISCUSSION	55
4.1.Experimental Data Collected	55
4.2.Comparison between Experimental Fluence and Simulated Fluence Rates	57
4.3.Experimental Dose Rates Map	60
4.4.Caparison between Experimental and Simulated Dose Equivalent Rates	61
4.5.Comparison between Radiation Survey Data and Simulated Dose Equivalent Rates for Cu-67 Production	67
4.6.Predicted Dose Equivalent Rate Results for Zn-68 and that of the Two New Target Holders	71
4.7.Predicted Dose Equivalent Rate around the White Room without Shield Upgrade or Beam Dump	72
4.8. Predicted Dose Equivalent Rate around the White Room with Shield Upgrade and Beam Dump	73
4.9.Predicted Dose Equivalent Rate around the White Room when Beam Dump is immersed in Cooling Tank	77
5. CONCLUSION	81
6. FUTURE WORK	83
7. REFERENCES	84
8. APPENDIX A	86
9. APPENDIX B	96
10. APPENDIX C	106
11. APPENDIX D	116
12. APPENDIX E	126
13. APPENDIX G	133

LIST OF FIGURES

Figure 1.1: Top View of the White Room	2
Figure 1.2: Side View of the White Room	2
Figures 1.3 Plan View of the Target Room in the White Room (Left) Elevation View of the Target Room in the White Room (Right)	4
Figure 1.4. Decay Scheme of Copper-67 (ICRP 38)	5
Figures 1.5 Diagram of the Beam Window and the Zn-68 Target	8
Figures 1.6 Setup for Target Holder 1 (Left) Setup for Target Holder 2 (Right)	10
Figure 2.1: Bremsstrahlung Continuum	21
Figure 3.1. A schematic diagram of the data acquisition Station	38
Figure 3.2 Experimental Setup	41
Figure 3.3 Dose equivalent Rate Map	44
Figure 3.4. Location of the Spherical Phantoms	46
Figure 3.5. Plan View of the White Room with Shield Upgrade	48
Figure 3.6. The beam dump designs modeled using MCNP: Beam dump encased in concrete (Left) beam dump immersed in water tank (Right)	53
Figures 3.7 Elevation View of the Target Room in the White Room	54
Figure 4.1 Comparing Predicted and Measured Photon Fluence Rate	60
Figure 4.2 Comparing Predicted and Measured Neutron Fluence Rate	60
Figure 4.3 A Plot Comparing Predicted and Experimental Photon Dose Equivalent Rate	64
Figure 4.4 A Plot Comparing Predicted and Experimental Neutron Dose Equivalent Rate	65
Figure 4.5 Comparing Neutron Predicted and Survey Dose Equivalent Rates around the white room During Cu-67 Production	69
Figure 4.6 Comparing Photon Predicted Dose Equivalent Rate to Survey Dose Equivalent Rates around the white room During Cu-67 Production	70
Figure 4.7 The equivalent dose rate in units of mSvhr^{-1} around the white	

room without beam dump and shield upgrade	73
Figure 4.8 The Predicted equivalent dose rate in units of mSvhr^{-1} around the white room using Al Beam Dump surround by concrete	74
Figure 4.9 The Predicted equivalent dose rate in units of mSvhr^{-1} around the white room using C Beam Dump surround by concrete	75
Figure 4.10 The Predicted Dose Equivalent Rate in units of mSvhr^{-1} around the White Room using Cu Beam Dump Surround by Concrete	76
Figure 4.11 The Predicted Dose Equivalent Rate in units of mSvhr^{-1} around the White Room using Ordinary Concrete as Beam Dump Material	77
Figure 4.12 The Predicted Dose Equivalent Rate in units of mSvhr^{-1} around the White Room using Cu Beam Dump Surround by Water	78
Figure 4.13 The Predicted Dose Equivalent Rate in units of mSvhr^{-1} around the White Room using C Beam Dump Surround by Water	79
Figure 4.14 The Predicted Dose Equivalent Rate in units of mSvhr^{-1} around the White Room using C Beam Dump Surround by Water	80

LIST OF TABLES

Table 1.1 Primary reactions of Cu-67 production (Ayzatskiy et al. 2007)	7
Table 3.1 Characteristic of Materials chosen for Beam Dump Design Analysis	50
Table 4.1. Experimental Data	55
Table 4.2 Conversion of MCNP F2 Tally Output to Fluence Rate	56
Table 4.3 Simulated and Experimental Flux Results	58
Table 4.4. Neutron and Photon Dose Rates for the Location Shown on the Dose Rate Map	61
Table 4.5 Dose Equivalent Rate comparison between simulation and experimental result at 1 kW	63
Table 4.6 Dose equivalent Rate Comparison between Simulation and Experiment at 10 kW Power	66
Table 4.7 Radiation Survey Data for Cu-67 Production	68
Table 4.8 Predicted Radiation Results for Cu-67 Production	69
Table 4.9 The Dose equivalent Rate results from Zn-68 for a 10-kW Beam	71
Table 4.10 Dose Equivalent Rate for Kr/Xe Target Holder 1 at 10-kW	72
Table 4.11 Dose Equivalent rate for Kr/Xe Target Holder 2 at 10-kW	72

ABSTRACT

Shielding analyses undertaken for the Idaho Accelerator Center at Idaho State University was accomplished in two parts. The first part consisted of an analysis of the utility of the shielding design to determine if it would be adequate for a larger machine producing higher energy radiation at larger magnitudes. The analyses in question involved the shielding of the accelerator room called “the white room” designated to house the new 40-MeV linear accelerator. This linear accelerator was going to be used for medical radionuclide production and other research. The main radionuclide that would be produced was copper-67 from the irradiation of a zinc-68 target. The study was performed to evaluate the integrity of the shielding of the white room to ascertain whether radiation that would be generated by the 40-MeV and 10-kW linear accelerator that was being built could be contained in the accelerator hall. Instead of operating the linear accelerator at full capacity to determine the integrity of the shielding of the accelerator hall, Monte Carlo simulations were performed for this purpose. Therefore, a low power experiment was performed at 1-kW power to obtain data for fluence rates around the surfaces of a cylindrical surrogate target and dose equivalent rates at several locations of interest around the white room. The data collected from the experiment was used as reference to develop an input file in Monte Carlo Neutral Particle transport code to benchmark the simulation for unit power (i.e. output per kW) conditions. After the benchmark, the code was used to determine the dose equivalent rate at the various locations of interest for a 10-kW power operation. The simulations performed for a 10-kW power operation of the linear accelerator would produce a combined neutron and photon dose rate of 0.47-mSv per hour in front of the white room door. In addition, the highest combined neutron and photon dose equivalent rate on top of the earthen material on the concrete ceiling was 0.14-mSv per hour. The predicted dose equivalent rates were greater than the 0.02-mSv in any one hour determined to be

the administrative design base, This value is consistent with the recommendations promulgated by the United States Nuclear Regulatory Commission for the public. Therefore, it was concluded that the shielding of the white room needed to be upgraded before the linear accelerator began operating at 10-kW. After the white room shielding was upgraded there were still some locations of interest that had elevated neutron and photon dose equivalent rates. In view of this problem and the need to introduce the use of two new target holders for gas irradiations, another evaluation was performed to determine the effect that the two new target holders would have on the neutron and photon dose equivalent rates at the various locations of interest around the white room. The target holders are made of aluminum to hold gas targets such as krypton and xenon for irradiation. Again, radiation surveys were performed during copper-67 production to determine the locations with elevated dose equivalent rate. During copper-67 production the linear accelerator is operated using a 7.24-kW electron beam. The data collected were used as reference to benchmark a model developed in the Monte Carlo Neutral Particle transport code for this shielding evaluation. The code was then used to determine the dose equivalent rates that would be produced at the locations of interest around the white room by copper-67 and the two new target holders when the accelerator was operated at a 10-kW electron beam power. The predicted dose equivalent rates around the white room predicted for the three different targets were compared to determine the target that would have the highest dose equivalent. Based on the model predictions the zinc-68 target appeared to be capable of producing the largest ancillary radiation fields and thus was used as a basis for the shielding design. Based on the zinc-68 target, a beam dump made of ordinary concrete was incorporated into the target room and the thickness of the shield materials covering the top of the target room were also adjusted to suppress the elevated dose equivalent observed at some locations of interest during copper-67 production.

Chapter 1: INTRODUCTION

1.1 Description and Statement of Problem

During 2012, the Idaho Accelerator center (IAC) located at Idaho State University (ISU), began construction of a new 40-MeV linear-accelerator (LINAC) with an intended maximum power output of 10-kW. The LINAC was to be used for medical radionuclide production and research. While the construction of the accelerator was in progress, it was deemed appropriate to evaluate the integrity of the shielding in the accelerator vault with respect to the enhanced accelerator deployment plan. The evaluation was imperative because the room was designed for a purpose other than housing a 40-MeV, 10-kW, linear accelerator. Staff of the IAC needed to determine if the shielding of the accelerator vault (or “white room” as the vault is called), as it was, would be sufficient to attenuate the dose equivalent rate that could be produced when the new linear accelerator came online for medical radionuclide production. Therefore, the task of evaluating the current condition of the white room with respect to shielding was assigned to the author. It was important that we use methods that would not violate regulatory requirement but still to ascertain the credibility of shielding of the white room before a 40-MeV, 10-kW power accelerator became operational. The dimensions of the white room are 1463 ± 1 -cm long, 566 ± 1 -cm wide and a height of 365 ± 1 -cm as shown in Figures. 1.1 and 1.2. The white room was built into the side of an earthen hill such that the west, east and south walls are covered with a substantial thickness of earthen material of over 10-m thick providing ample shielding in those directions. However, the wall on the north end of the accelerator vault is 76 ± 1 -cm thick. A concrete door on that wall with a thickness of 76 ± 1 -cm gives access to the accelerator vault. Beyond the accelerator vault’s north wall is a loading area which also contains the accelerator control booth.

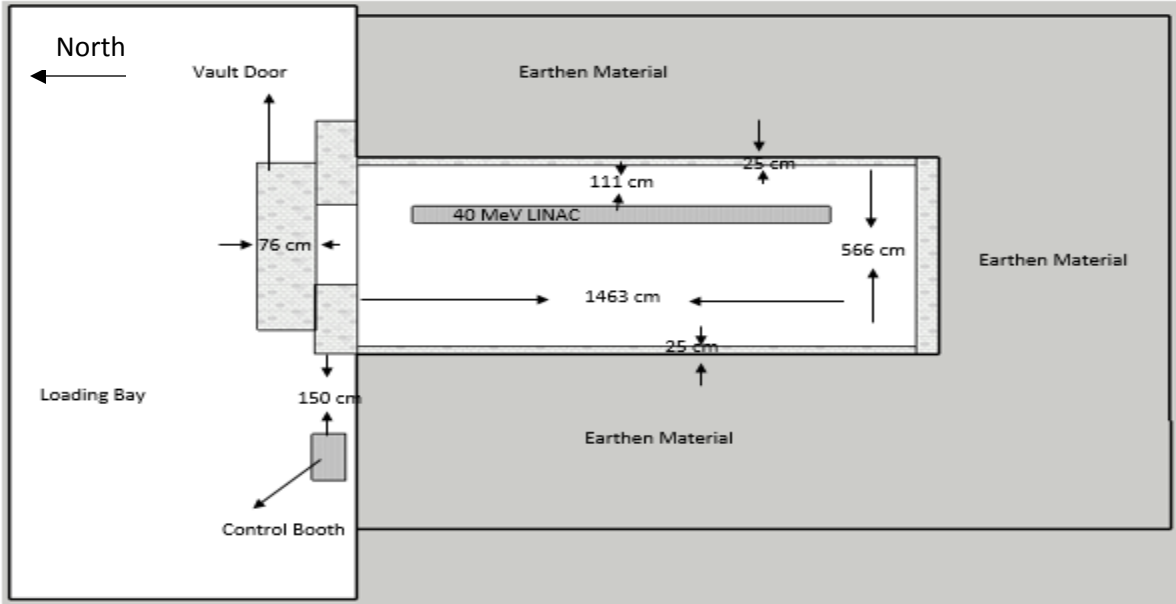


Figure 1.1: Plan View of the White Room

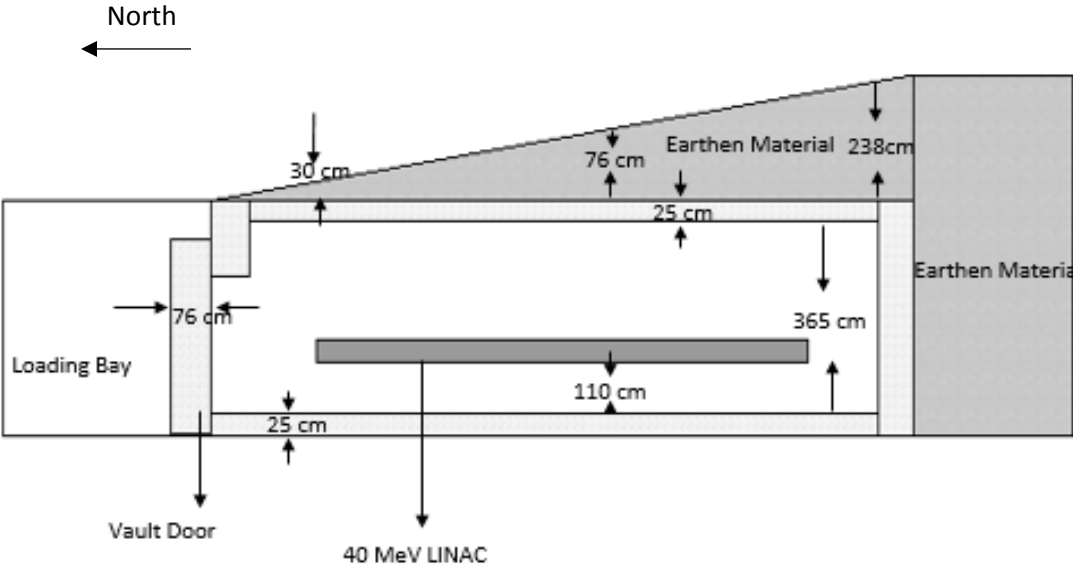


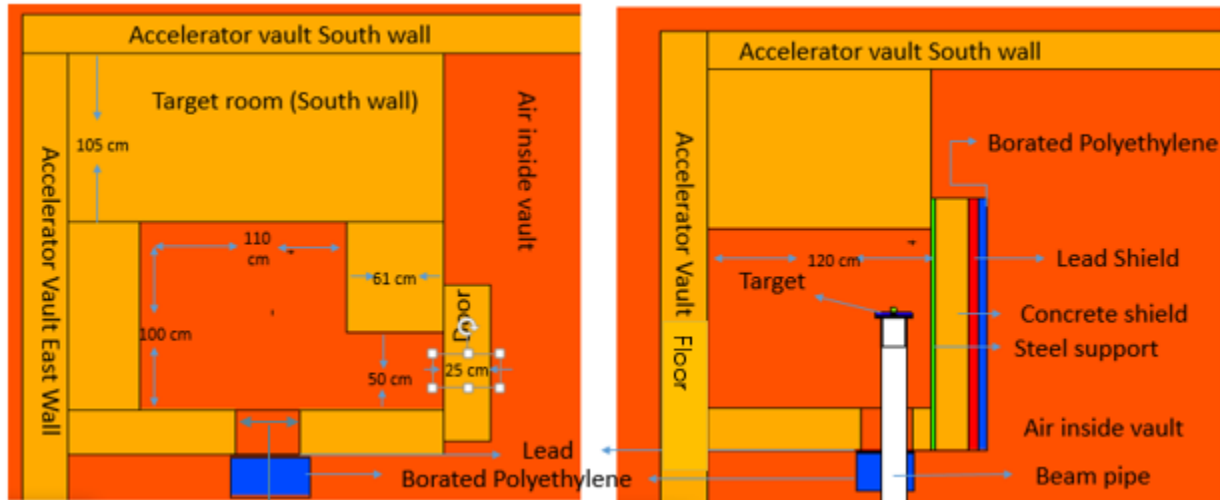
Figure 1.2: Elevation View of the White Room

The accelerator control (booth) area is located 150 ± 1 -cm away from the 76 ± 1 -cm thick part of the north wall of the accelerator vault. This area was of concern because the accelerator

operator(s) will occupy the control booth when the accelerator is in use. The other area of concern was the top of the white room, which is made from a 25 ± 1 -cm thick concrete. The concrete ceiling is covered with earthen material. Unfortunately, the amount of earthen materials is not uniform across the surface. Therefore, a metal rod was driven into the hill at random on the north, south and, middle sections of the earthen material. This was done 20 times on each section to determine average thickness of soil. Using the measurements, the average thickness of each location and variation in thickness as expressed using the standard deviation was calculated. The earthen material sloped from a high point of 238 ± 15 -cm on the south end above the ceiling concrete, to 76 ± 4 -cm midway between the south and north ends and to about 30.5 ± 2 -cm at the north end as shown in Figure 1.2. The linear accelerator stands at a distance of 111 ± 1 -cm away from and parallel to the east wall as shown in Figure 1 and is 110 ± 1 -cm high from the floor. The beam window is perpendicular to the south wall at a distance of 156 ± 1 -cm from the wall.

Analyses performed to substantiate the credibility of the shield surrounding the white room showed that at a power of 10-kW, the existing shielding was inadequate to suppress the dose equivalent rate on top of the earthen material above the concrete ceiling. The dose equivalent rate was measured 100-cm from the surface of the earthen material to the approximate center of the detector to be more than 0.02-mSv in any one hour. This was also the case beyond the white room door in the north direction at a distance of 100 ± 1 -cm away. Due to the outcome of this analysis, the management of the IAC upgraded the shield thickness in the white room. Instead of retrofitting the entire shielding of the white room, a suggestion to shield only the beam window and the target was accepted. The shielding approach involved building a “room-inside-a-room” (i.e. a smaller room covering the target and the beam window inside the LINAC vault). The smaller room or “target room”, which is located at the southeast corner of the accelerator vault, has inner

dimensions of 100 ± 1 -cm (length) by 120 ± 1 -cm (height) by 110 ± 1 -cm (width). The east and north walls of the target room are 41 ± 1 -cm thick, the west wall is 61 ± 1 -cm thick. The south wall is 105 ± 1 -cm thick as shown in Figure 1.3 on the left.



Figures 1.3 Plan View of the Target Room in the White Room (left), Elevation View of the Target Room in the White Room (right)

A 100 ± 1 -cm by 50.0 ± 1 -cm opening in the west wall of the target room is covered by a 25.0-cm thick concrete sliding door, allows access to the target room. A rectangular hole of dimensions 28 ± 1 -cm by 20 ± 1 -cm in the north wall provides passage of the beam pipe into the target room as shown in Figure. 1.3a. Different types of materials cover the top of the target room shield to address the different types of radiation produced during accelerator operation. A 17.5 ± 1 -cm thick layer of brick follows a 2 ± 1 -cm thick steel sheet, which provides support for the shielding materials covering the target room. Next is a 6.4 ± 1 -cm thick layer of lead blocks to shield photons. Finally, a 6.4 ± 1 -cm thick layer of borated polyethylene (suitable for neutron shielding) tops the composite shield as shown in Figure. 1.3 on the right.

1.1.1 Cu-67 Production at Idaho Accelerator Center

The major purpose for which this LINAC was assembled is to produce radionuclides for clinical uses; in particular copper-67 (Cu-67). Figure 1.4 shows the decay scheme of Cu-67. Cu-67 decays by isobaric transition to Zn-67 through the emission of a beta particle. During this transition, Cu-67 can decay via any of the beta particle depicted in the decay scheme by the arrows slanting down and to the left. When Cu-67 decays through beta 1, 2, or 3, the product of that decay (Zn-67) is in excited state. Therefore, for Zn-67 to achieve stability it decays by the isomeric transition or the emission of a gamma particle that is depicted in Figure 1.4 as any of the arrows pointing horizontally down. In all, there are six isomeric transitions that are possible in this decay scheme.

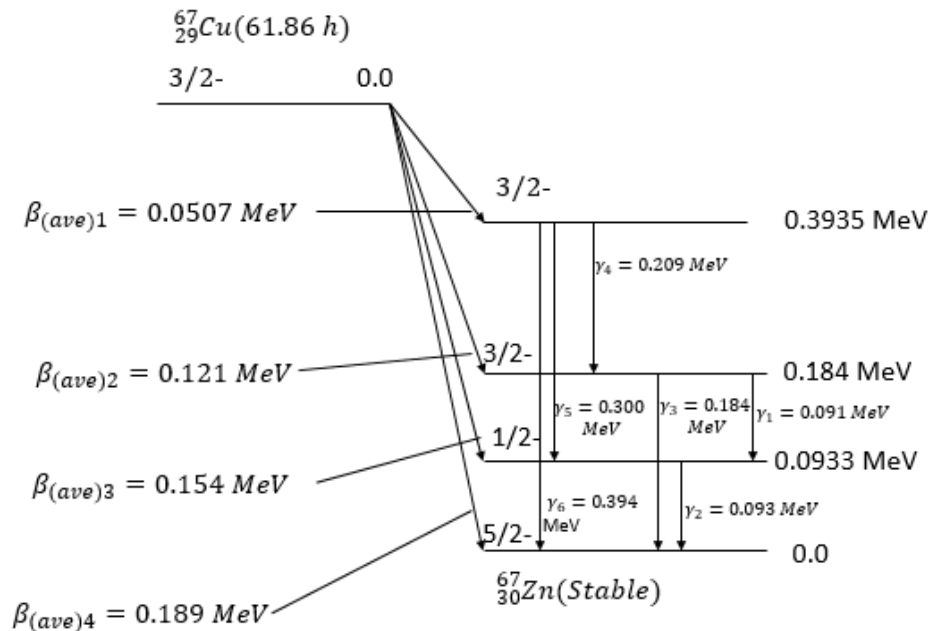


Figure 1.4. Decay Scheme of Copper-67 (ICRP 38)

Among the four beta particles emitted by Cu-67 these three with maximum energies of 377-keV, 468-keV and 561-keV with yields at 51%, 28% and 20% respectively are of interest (Novak-Hofer et. al. 2002). The Cu-67 beta particles have an average weighted energy of 141 keV and a mean negatron range of 0.2-mm in tissue (Novak-Hofer et. al. 2002). The Cu-67 isotope also emits four major gamma rays of 91-keV, 93-keV, 184-keV and 394-keV at yields of 6%, 35%, 45% and 0.6% respectively (Novak-Hofer et. al 2002). The photon energy range emitted by Cu-67 is suitable for pre-therapy diagnostic procedure with a gamma camera in nuclear medicine (Novak-Hofer et. al. 2002) (Starovoitova et. al 2011). Cu-67 has a half-life of 61.83 hours making it a viable choice because the half-life is long enough to produce effective treatment and short enough to reduce long term radiation effects on the patient (Starovoitova et. al 2011) and (Bindu et. al. 2013). All these physical features make Cu-67 a radioactive material potentially suitable for cancer therapy.

Several different nuclear interactions can lead to the production of Cu-67 as shown in Table 1.1 obtained from (Ayzatskiy et al. 2007). The tabulated data shows that photonuclear reaction cross section is an order of greater than that of (n,p) reaction cross section. Moreover, production of Cu-67 through the photonuclear method would be more attractive because of the relatively low cost of building electron accelerators and their low operational expenses compared to heavy particle accelerators. When compared to nuclear reactors, accelerator pose relatively lower environmental hazard (Ayzatskiy et. al 2007).

Table 1.1 Primary reactions of Cu-67 production (Ayzatskiy et al. 2007)

Particle	Reaction	Cross- section (mb)	Particle Energy Range (MeV)
p	$^{68}\text{Zn}(p, 2p) ^{67}\text{Cu}$	6	30-85
	$^{70}\text{Zn}(p, a) ^{67}\text{Cu}$	24.8	130-425
a	$^{64}\text{Ni}(a , p) ^{67}\text{Cu}$	34	22
n	$^{67}\text{Zn}(n,p) ^{67}\text{Cu}$	1.07	-
γ	$^{68}\text{Zn}(\gamma ,p) ^{67}\text{Cu}$	11	22

The reaction relevant to electron linear accelerators is the electron to gamma interactions where electrons are converted to Bremsstrahlung photons via interaction with a high-Z material (in this case tungsten metal). The photons in turn interact with a Zn-68 target to produce Cu-67 via the (gamma, p) reaction as listed on Table 1.1. Naturally occurring zinc can be used as a target for Cu- 67 production however, the use of zinc target that is enriched in Zn-68 improves the yield of Cu-67 and reduces the amount of activation product impurities that arise from interaction with other zinc isotopes (Zn-64, Zn-66, Zn-67, and Zn-70) contained in natural zinc. After exposure to the electron beam, the activated target contains Zn-68, Cu-67 and other radioactive materials collaterally produced in the process. These solid targets are chemically dissolved to separate the Cu-67 (Dolley S. G. 2006) and (Ayzatskiy et al. 2007). Any other isotope of copper that may be present would also be separated.

Figure 1.5 shows a schematic target arrangement for Cu-67 production at the IAC. An electron beam bombards three tungsten converters (each converter is 1.5-mm thick). These are water cooled to remove the heat generated by charged (electron) particle interaction. Photons (Bremsstrahlung) and unstopped electrons emanating from the converter further interact with the cylindrical Zn-68 target. The Zn-68 target has a radius of 2.5 cm and a length of 3 cm. The energy

(40 MeV) at which the electrons collide into the converter and target, results in a substantial amount of Bremsstrahlung radiation of energies between $0 < E(\text{beta}) < 40 \text{ MeV}$. Considering that the average binding energy per nucleon in atoms is approximately 8 MeV (Perrin et al. 2003; Ahlgren et al. 1988; Almen et al. 1991), the interaction of photons produced with the target will result in the generation of neutrons and protons in the same energy range. The radiation produced (electron from the LINAC, photons from conversion, neutrons and protons from photon interactions with the nuclei), if not adequately shielded may constitute a radiological hazard to both workers and members of the public. Regulatory compliance is accomplished by a combination of approaches including the use of beam dumps to absorb those particles that would otherwise add to the dose rate beyond walls of the vault or by increasing the shielding around the accelerator.

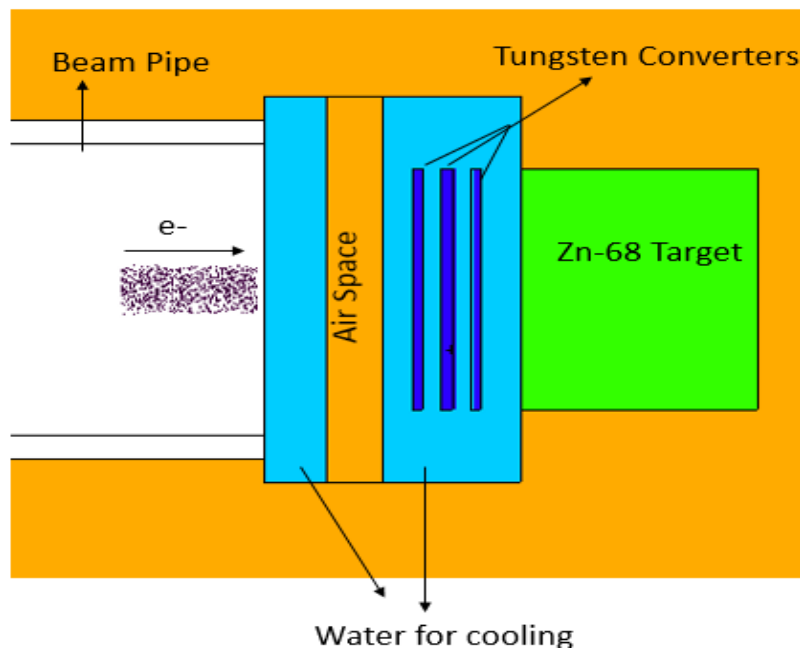


Figure 1.5 Diagram of the Beam Window and the Zn-68 Target

When the 40-MeV LINAC became operational in 2013, Cu-67 production commenced immediately. Radiation surveys performed during Cu-67 production demonstrated the combined

neutron and photon dose equivalent rate at some locations of interest were above the 0.02-mSv regulatory limit for members of the public. Therefore, the IAC was forced to demarcate the perimeter at the top of the vault to prevent unauthorized access by the public. In addition, the area in front of the vault door was posted with a radiation warning sign whenever the accelerator was in use. Signs and barriers were used to allow operations when Cu-67 was in production. This approach was used even though it was desirable to eliminate extraneous radiation field

During the summer of 2016, a project began using the 40-MeV electron LINAC in the white room to experiment with the irradiation of targets other than Zn-68. The first two targets considered for irradiation were krypton and xenon gases. Since the target materials are gases, a suitable target holder with chamber(s) to contain the gases had to be developed. The proposed targets holders were of two different designs each capable of holding either xenon or krypton gas sealed in an aluminum crucible. Both target holders were cylindrical in shape but the configuration of the chamber encasing krypton or xenon gas were of different designs. The first target holder had a height of 5.08-cm and a diameter of 3.81-cm with a cylindrical hollow center, wall thickness of the aluminum crucible was 0.3-cm. This was capable of holding about 0.6-ml of gas at standard temperature and pressure (STP). Target holder number two had height of 6.5-cm and 3.5-cm diameter. Inside the crucible there were 3-cylindrically shaped hollow spaces, each had a height of 3.5-cm and 0.9-cm diameter that encased either xenon or krypton gas. Three tungsten converters having a thickness of 1.5-cm always preceded the targets. These were continuously cooled by water as shown in Figures. 1.6a and b. Different isotope and/or composition of isotopes of either krypton or xenon gases were irradiated in these target containers. The various target compositions included natural krypton gas, natural xenon gas, Xenon gas enriched in Xe-136, Xe-134 or Xe-132. The products of interest from the irradiation of these

targets were Kr-85, Xe-135 and Xe-133 via the reactions Kr-84(n, gamma) Kr-85, Xe-136(gamma, n) Xe-135, various combinations of Xe-134(gamma, n) Xe-133 and Xe-132(n, gamma) Xe-133. These radionuclides are most commonly produced during fission of U-235 in nuclear reactors. Because of their usefulness in diagnostic medical procedures are extracted via complex chemical process to separate isotopes, and supplied to hospitals. Depending on the diagnosis desired, either of these can be administered to a patient in the hospital through inhalation. The IAC, at the request of the Idaho National Laboratory (INL) experimented to ascertain the feasibility of the production of these radioactive materials using LINAC technology. Subsequently, based on feasibility, the IAC may be requested to produce these radioactive materials using the 40-MeV electron LINAC through the reactions mentioned above for use in tracer studies. Because of the anticipated experimental irradiation with the new targets, the IAC decided to reevaluate the shielding configuration of the white room.

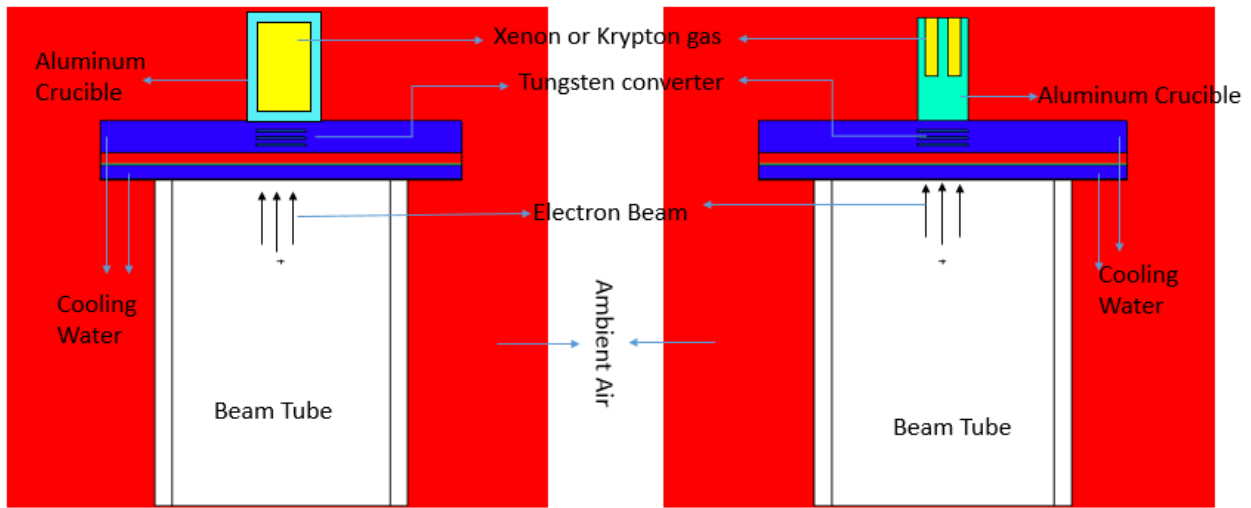


Figure 1.6 Setup for Target Holder 1 (left) Setup for Target Holder 2 (right)

1.2 Objectives

The objective of this study was to revisit the analysis performed on the white room in 2012 in which the author calculated the neutron and photon fluence rates emanating from the target and the neutron and photon dose equivalent rate around the white room. Based on the re-analysis, an improved understanding was obtained via Monte Carlo N Particle (MCNP)¹ modeling and modifications of the input file over the study performed in 2012. The new results presented include the simulation for neutron and photon fluence rates produced by the Zn-68 target and the dose equivalent rates at locations throughout the white room.

Based on these analyses, before the accelerator was brought back online for Cu-67 production, the IAC performed a shielding upgrade on the white room. The shielding upgrade suppressed the dose equivalent rates at the locations of interest. However, survey data obtained during Cu-67 production showed there were some locations around the white room that still had elevated dose equivalent rates. Further analyses and shielding design improvements were investigated to mitigate the problem of elevated dose equivalent rate observed at some of the locations of interest. Moreover, the consequence of new target configurations on the current shielding status of the white room was also investigated. To implement this evaluation and enhanced shielding design, radiation surveys were performed to collect dose equivalent rate data at locations around the white room that were considered to be of interest.

The radiation survey data was used as a reference in order to develop a new model of the white room in MCNP6 that would more closely and adequately simulate and reproduce the results obtained via radiation surveys conducted during Cu-67 production. Of course, this improved

¹ Los Alamos National Laboratory New Mexico 87545

model was intended to adhere to all conditions used during Cu-67 production. Developing a model in MCNP that can reproduce measured result allowed further analyses without having to perform real life measurements.

The irradiations heretofore were carried out with an electron beam power of approximately 7.24 kW. However, the accelerator has a maximum power of 10 kW. The 10 kW beam field characteristics can be obtained by scaling up from 7.24 kW, but the simulation was carried out to confirm that the scaled results were consistent with simulated results at this power. The simulation at 10 kW provided the best case scenario of operation for the dose equivalent rate around the white room.

In addition, the Zn-68 target in the input file would be modified using the parameters of the two new target holders to be used for xenon and krypton gas targets. Supplementary simulations at 10-kW beam power for these target configurations were also conducted. These simulations provided the results for neutron and photon dose equivalent rates for all locations of interest for these new targets holders.

The dose equivalent rate results obtained for Zn-68 and the two target holders simulated at 10-kW were compared for all locations of interest and one of these targets was selected for further analyses. The target selected as the design basis to carry out beam dump and shielding analyses was the target that showed the highest dose equivalent rate at most locations of interest. The idea behind this choice was that shielding the target that produced the highest dose equivalent rate at maximum power should adequately shield the other targets. Based on this choice, combined shielding upgrade and beam dump analyses were performed using a couple of different materials. It was anticipated that the adjustment of the shielding of the room-inside a-room and the addition of a beam dump to the design would better reduce the dose equivalent rate around the white room.

Moreover, considering the materials analyzed and used for beam dump in the simulations, the one with the most promising attributes would be suggested for actual application in order to accomplish better radiation control. The attributes considered were cost, availability of material used, ease of construction of such a beam dump, the ability of the material to withstand a great deal of heat and the amount of radiation attenuation the material provided.

1.3 Hypothesis Statement

Null Hypothesis 1

The radiation survey data collected at locations of interest around the white room will not be in agreement with the dose equivalent rate predicted by the model developed in MCNP

Alternate hypothesis 1

The radiation survey data collected at locations of interest around the white room will be in agreement with the dose equivalent rate predicted by the model developed in MCNP

Decision rule 1: the null hypothesis will be rejected if the dose equivalent rate obtained for all locations of interest are not statistically different to the dose equivalent rate predicted by MCNP. As such, the alternate hypothesis will be accepted

Null hypothesis 2

There will be no need for a shielding upgrade on the white room

Alternate hypothesis 2

There will be need for a shielding upgrade on the white room”

Decision rule 2: the null hypothesis will be rejected if the dose equivalent rate at locations of interest are greater 0.02 mSv in any one hour. Otherwise, the alternate hypothesis will be accepted

Null Hypothesis 3

Concrete beam dump will not perform as good as beam dumps made from conventional materials such as copper, aluminum and pyrolytic carbon

Alternate Hypothesis

Concrete beam dump will perform as good as beam dumps made from conventional materials such as copper, aluminum and pyrolytic carbon

Decision rule 3

The null hypothesis will be rejected if it is determined that concrete keeps the dose equivalent rate below 0.02 mSv in any one hour when used as beam dump under the same conditions as conventional materials. Consequently, the alternate hypothesis will be supported

Chapter 2: LITERATURE REVIEW

2.1 Particle Accelerators

Particle accelerators are devices built with the aim of adding kinetic energy to charged particles. Particles with sufficient energy may initiate nuclear reactions or be used for medical or industrial irradiations. Accelerators are classified in many different ways but the attributes that are of concern for radiation protection include the type of particle accelerated, the maximal energy, maximal intensity, the duty factor of the accelerated particle beams, and the types of media in the vicinity of locations struck by the beam (NCRP 2003). Currently, commonly accelerated particles include but are not limited to protons, ions and electrons. Protons or various ions may, upon interaction with certain targets, produce neutrons and other secondary particles. Accelerated electrons, incident on a high-Z target produce Bremsstrahlung radiations. These high-energy Bremsstrahlung photons may further interact with materials to produce neutrons or other particles. As the energy of the accelerated particle increases, so does the number, energy and variations in possible secondary radiation produced (Cossairt et. al. 2008).

Some of the secondary radiation generated is collateral to the main intention of the accelerator. Often such radiation is unwanted. These unwanted particles may leave the focused beam and produce substantial radiation fields at locations other than that which was anticipated. Sometimes these unwanted particles are capable of inducing radioactivity in accelerator components or nearby structural features. Consequently, they constitute a potential radiological hazard (NCRP 2003).

The radiation produced during operation of a LINAC is classified into two main categories; prompt radiation, which is produced only when the accelerator is being operated and

residual radiation that persists even after the device is shut down. The former is usually suppressed by the shielding that is placed around the accelerator. Moreover, primary radiation only arises when the accelerator is operating. During accelerator operation, the accelerator hall is not accessible to workers. Hence, worker exposure by prompt radiation is highly unlikely. However, from time to time under special circumstances workers may need to be in the accelerator hall during operation for maintenance of the LINAC. In these cases, the workers are at risk of acquiring potentially large radiation doses from prompt radiation.

Residual radiation on the other hand, can persist for years after a facility is shutdown (NCRP 2003). This is due to the induced activity produced by interaction of accelerated particles that constitute prompt radiation with accelerator components or structural materials. Induced activity is unavoidable in particle accelerator facilities so long as the particles accelerated have energy that is equal to or greater than the nuclear binding energy of one or more of the elemental constituents of materials around the accelerator. The radiation exposure received by workers from the induced radioactivity near an accelerator is limited by time distance and shielding, consistent with the philosophy of as low as reasonably achievable (ALARA). Workers should be as far as possible from a source to reduce exposure. Increasing the distance from a source usually reduces radiation intensity. Worker(s) could and should limit the length of time they spend near a source because the longer a worker stays around a source of radiation the higher the dose he or she will receive. If these two elements are not sufficient then shielding could be used to limit exposure.

2.2 Electron Linear Accelerator

The electron gun in a linear accelerator is a device used as the source of electrons. The electron gun typically consists of a metal oxide from which electrons are generated by the process of thermionic emission. The electrons produced are extracted from the electron gun by an applied

bias created by a high voltage power-supply. These electrons may be manipulated in many different ways to achieve various endpoints. Some machines employ bunchers to help focus the electron beam in time as well as in space. Sometimes a buncher provides the input to a resonant cavity in an accelerator. Either a magnetron or a klystron provides microwave energy to the resonant cavity for accelerating the free electrons. A klystron is an evacuated electron-beam tube in which an initial velocity modulation imparted to electrons in the beam results subsequently in density modulation of the beam. The buncher, when used, also regulates the speed of electrons pumped in by the electron gun so the electrons arrive in bunches at the output of the resonant cavity. A master pulse generator provides a timing signal for the electron gun, power supply, buncher, and klystron or magnetron. Both the radiofrequency system and the electron gun are designed with the intention for pulsed function at repetition rates that can be selected from several hertz up to few thousand hertz at maximum. Due to the very high voltage required for electron LINACs to operate, the function of these devices by default is in pulse mode. Microwave amplifiers can only supply the extremely large radiofrequency power needed in these devices at a comparatively low duty cycle and in pulsed operation. Collimation by focusing magnets is used before and after the electron stream is injected into the buncher to keep the solid angle of the beam to a few milliradian. The beam focus is accomplished with the help of focusing coils surrounding the LINAC tube. It is desirable for the energy of accelerated electron in a beam to be homogeneous. Uniformity is achieved by carrying out the injection at a chosen energy so that the electrons are readily captured in the accelerating region of the accelerator by the electric field in the resonant cavity. The electrons are accelerated by the microwaves in the resonant cavity and transferred in to the wave guide (Segebade et. al. 1988; Cossairt et. al. 2008)

The resonant cavity of the waveguide is the accelerator. The waveguide is a metal pipe with precisely machined void areas that allow for the creation of standing waves. This component is maintained often in a vacuum state. Sometime it is filled with gas dielectric that can be polarized by an electric field. The dielectric gas permits the continuous transfer of energy to the electron buncher from the electromagnetic standing waves established in the resonant cavity. Waveguides are produced to allow electromagnetic waves to be generated. Waveguides in electron accelerators are built with discs containing circular holes at the center that are strategically placed at appropriate distances inside the accelerating cavity. These circular holes serve as controls for the phase velocity of the accelerating wave which increases with increase in distance of the holes (or irises). If the irises are not in place, the phase velocity will surpass the speed of light and therefore become unfavorable for acceleration of particles (electrons) (Segebade et. al. 1988; Cossairt et. al 2008)

During acceleration in the waveguide, all other electrons are abandoned except those with phase velocity equivalent to that of the accelerating wave. Due to the manner by which the irises are spread out (in increasing distances) inside the buncher region the phase velocity of the traveling waves increases continuously until the traveling wave velocity approaches that of light. When the appropriate target velocity is reached, the spacing of the circular discs are kept at a constant distance. The beam travels through the rest of the waveguide and exits via the beam window, which is generally a thin metallic foil such as aluminum or titanium. Absorption of electrons exiting the beam window by a high Z material, most preferably, tungsten brings about the production of Bremsstrahlung radiation, which may for instance, be used in photon activation of materials (Segebade et. al. 1988; Cossairt et. al 2008).

2.3 The IAC Electron Linear Accelerator

The particle accelerator located in the white room of the IAC, accelerates electrons at a maximum energy of 40 MeV. Accelerated electrons are initially generated from a gridded thermionic electron gun biased at 20 kV. Electron production from the gun is gated by applying a pulsed bias through its grid for a series of 9 microsecond periods at a repetition rate that can range from 1 to 300-Hz by applying a positive pulse to the normally negatively biased grid of the gun. The entire gun assembly is biased to 20 kV, but the grid is biased to an additional 125 V. The grid or control grid is incorporated between the cathode and the anode of the electron gun. This used to vary the beam current over a wide range without varying the anode-to-cathode voltage (Karzmark et. al 1993). The operator at the control booth can vary the amplitude of the positive pulse that gates the electron gun on producing electrons.

The generated electron pluses arrives at the first cavity slightly after the radiofrequency (RF) pulse generated from two s-band klystrons arrives to fill the cavities. Thus, the klystrons is used as an amplifier in the microwave region (Karzmark et. al 1993). These 5-MW klystrons feed the two accelerating section that make up the LINAC. The IAC uses two klystrons to improve the power drive of the accelerator. To obtain the correct phase for the injected RF energy between the two accelerating guides, phase shift modules are used. This phase shift adjustment is done from the operator console. Other adjustable variables from the operator's control console includes amplitude of the RF, and adjustment of the high voltage applied to the klystrons.

Electrons traveling in the accelerating wave-guide in a given plane are kept focused by the use of several magnets along the first and second accelerating guide and the beamline. Other devices that aid in the transport of the beam include solenoids, steering, and quadrupole magnets. Also, located along the beamline are flags that may be used only at low beam power levels to aid

the operator in seeing the shape and position of the beam. Finally, at the end of the beamline is a calibrated bending magnet that acts as a spectrometer to help verify the beam energy.

The beam exits the vacuum system of the accelerator through a thin titanium window. The beam of electrons, upon exiting the window, interact with an assembly of water-cooled tungsten converters converting the electrons into a bremsstrahlung beam. The Bremsstrahlung photons in turn interact with the targets to produce activation.

2.4 Activation Process in an Electron Accelerator

When using electron LINACs, there is always the potential for photon production, which in turn may lead to photon induced activation if the energy is high enough. “Photon induced activation is a process where photons are used to bombard a target or material causing isomeric excitation, ionization, and a series of other nuclear reactions generated by nucleon ejection (protons and/or neutrons) by the incident photons. This process brings about the activation of the material” (Lutz 1970 and NCRP 2003). Classically, the production of electromagnetic radiation is inevitable whenever a charged particle travelling near relativistic velocity experiences a deflection from its path. The electromagnetic radiation is called Bremsstrahlung radiation. Depending on how the deflection occurs, the electron in question may lose only a small fraction or nearly all of its kinetic energy to the emitted photon (for a slight deflection). The emitted photon will have energy very close or equal to the initial energy of the travelling electron if the interaction is close to the nucleus of an atom in the target material. The Bremsstrahlung radiation is produced with a continuous energy spectrum. A plot of the photon fluence as a function of their energy known as the Bremsstrahlung continuum as shown in Figure 2.1 (Segebade et. al. 1988). The absorption of photons emitted during the deflection of accelerated electrons by the nucleus of an atom will cause it to become excited. The excitation energy of the newly formed unstable compound nucleus may

release another photon or other particles such as protons, neutrons (or photoneutrons), alpha particles, negatrons, or positrons to achieve stability. The loss or gain of a particle in the nucleus of a target material sometimes results in the activation of the material and eventually, the production of a new nuclide or radionuclide.

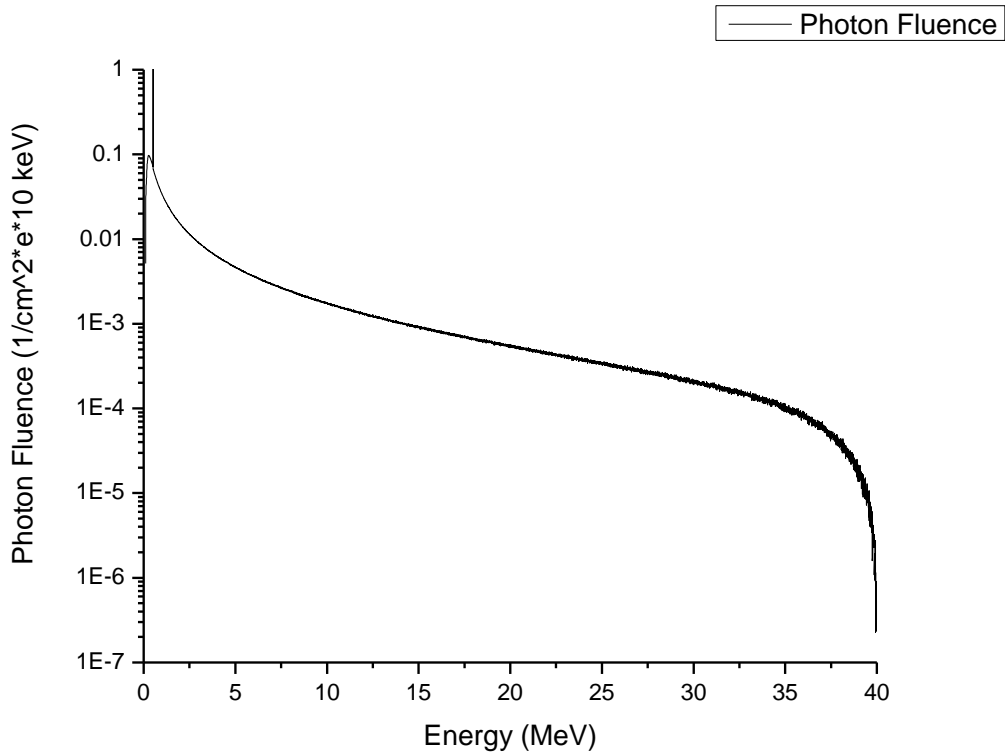


Figure 2.1: Bremsstrahlung Continuum

As the energy of a produced photon becomes greater than about 8-MeV (Perrin et al. 2003), (Ahlgren et al. 1988) (Almen et al. 1991), which is the average binding energy of most nucleons in nuclei, the photon acquires the minimum energy required to induce a photonuclear reaction. Depending on the bremsstrahlung continuum and the probability of a reaction occurring (usually expressed in terms of a cross section) different kinds of photonuclear reactions can occur, in the target or material such as; (gamma, n), (gamma, p), (gamma, np) and so on. Consequently,

a (gamma, n) reaction will produce an isotope with a mass number minus one (${}^X\text{A} + \gamma = {}^{X-1}\text{A} + \text{n}$) and a (gamma, p) reaction will produce an isotone with one less proton (${}^X\text{A} + \text{gamma} = {}^{X-1}\text{B} + \text{p}$) (Fischer et al. 2007). Induced activation may occur whether the target is placed deliberately in the line of the beam, or if it is a material lying in a place where it is collaterally exposed to the beam. If one considers the composition of the target or material, the energies in the bremsstrahlung continuum and the cross section of the different photonuclear reactions, it becomes evident that different activation products are possible (Perrin et al. 2003, Ahlgren et al. 1988 and Almen et al. 1991). Some of these products may be radioactive and therefore constitute ancillary exposure to workers during activation processes (Culp 2007) or during the use of an accelerator. As the energy of electrons increases, so does the energy of the photons that will be produced. The probability of interaction as expressed using the concept of cross section increases with photon energy. Increased photon energy also increase the possible types of radiation that will be produced. In fact, when beam energy begins to exceed about 45-MeV, air activation in the electron LINAC room becomes more and more probable (Almen et al. 1991).

2.5 Radiation Associated with Electron LINACs

Although electrons are the particles accelerated by an electron LINAC used for photon activation, the chief particles of concern from shielding point of view are bremsstrahlung photons and photoneutrons. This is true because the accelerated electrons that did not give off all their energy to produce electromagnetic radiation (photons) and are subsequently absorbed by surrounding materials. The absorbed electrons dissipate all their remaining energy in the material as heat due to the nature of electron interaction with matter.

2.6 Shielding Considerations

There are several factors known as a design basis that have to be considered when making shielding calculations. The objective of a shielding calculation is to estimate the amount of material and the thickness required for shielding. Therefore, the first and foremost design basis is to define what the rooms adjacent to the accelerator room(s) will be used for, i.e. whether the room(s) can be classified as controlled area(s) or uncontrolled area(s). A dose-equivalent rate limit is assigned to the room taking into consideration the average fraction of time the most exposed individual is likely to be present while the electron LINAC is on. The fraction of time is called occupancy factor or (T). Another important design basis factor is the estimate of the average time the accelerator is in operation facing a particular direction or the use factor (U). Other factors such as the primary barrier and the secondary barrier locations are also considered. The primary barrier is the portion of the accelerator room that is directly exposed to the primary beam. The secondary barrier(s) are the part(s) of the room that are exposed to scattered radiation from the primary beam and leakage radiation from the accelerator. Elaboration of these concepts may be found in “Structural Shielding Design for Medical X-Ray Imaging Facility” (NCRP 147).

2.7 Shielding Against Photons

When compared to the accelerators used in medical facilities, the use factor for accelerators employed in industry and research facilities by design and intention varies based on application, and as a result, the output has not been calculated. However, for radiation protection purposes in shielding calculations, it is recommended that a design basis of 10 hours in a 40 hour work week resulting in a use factor of $\frac{1}{4}$ with a typical workload range of 10^2 to 5×10^4 Gy m² per week be used (NCRP 2003). Given these design basis, there are four steps in calculating the required shield thickness for photons (NCRP 2003):

Step 1: Calculate the Unshielded Dose

$$H_{\text{Unshielded}} = \frac{WUT}{d^2} \quad (1)$$

$H_{\text{Unshielded}}$ = the dose equivalent rate at a given distance before shielding is placed around a source

W = Workload

U = Use factor (Defined as the quotient of the time the beam is oriented to a particular direction by the time of work in a week)

T = Occupancy factor

d = is the distance between the point of the beam exit to a point 30-cm beyond the shield barrier to a room adjacent to the accelerator vault or 50-cm above the floor of a room that is located above the vault or a distance of 2-m if the room is below the floor of the accelerator vault.

Step 2: Calculate the shielded dose by shield material

$$H_{\text{shielded}} = T(x) \times H_{\text{Unshielded}} \quad (2)$$

H_{shielded} = is the dose equivalent rate measured beyond the shield after placing a shield around a radiation source

$H_{\text{Unshielded}}$ = the dose equivalent rate at a given distance before shielding is placed around a source

T(x) = is the transmission factor or the reciprocal of the attenuation factor of the shield material

Step 3: Calculate desired transmission factor to acquire the appropriate thickness of shield barrier

$$T(x) = \frac{H_m d^2}{(WUT)} \quad (3)$$

$T(x)$ = is the transmission factor that will reduce the dose at the point of interest to the desired weekly dose equivalent limit

H_m = is the design goal for weekly dose

W = Workload,

U = Use Factor

T = Occupancy Factor

Step 4: Obtain the required shield thickness from graphs of transmission factor against shield thickness at different energies and for different shielding materials from the text “Radiation Protection for Particle Accelerator Facility” (NCRP 2003).

2.8 Shielding Against Neutrons

Neutron attenuation in shielding materials follows approximately an exponential function and while the neutrons are being thermalized and absorbed in the shield barrier, gamma rays are emitted by absorbing nuclei to achieve stability. This process contributes to the dose equivalent beyond the surface of the barrier. Thus, photons produced due to the absorption of slow neutrons should be taken into consideration during shielding design. When considering electron accelerators with energies less than 100 MeV, the most important source of neutrons are the photonuclear interaction in the target material. Photoneutron production is almost isotropic in nature, unlike the anisotropic photon field produced by these machines. While probably conservative, it was assumed that for Bremsstrahlung energy above approximately 15 MeV and electron beam power of 1 kW,

incident on a high Z target, the estimated neutron yield should be about 2×10^{12} neutrons per second (IAEA, 1979a). The dose equivalent transmission factor for the neutrons can then be calculated using Eq. 4.

$$H_n = \frac{H_m}{\left\{ \frac{T \sum \left[\frac{d\phi}{dt} \right] U_i}{d^2} \right\}} \quad (4)$$

H_n = is the coefficient (in $Svcm^{-2}n^{-1}$) relating the neutron dose-equivalent at the location in question to the unshielded neutron fluence

$\frac{d\phi}{dt}$ = is the neutron particle flux at the standard distance of 1 m from the target in the direction in question (in $n.cm^2week^{-1}m^2$)

d = is the distance between the neutron source and the location to be protected (in m)

H_m = is the maximal permissible dose-equivalent rate for the type of area

U is the use factor and it is summed for all machine orientations (NCRP 2003).

2.9 History of Medical Radionuclide Production

The use of radiation in medicine started within months following the discovery of x-ray by Wilhelm Roentgen in 1895. Within two months after the discovery of x-rays, Henri Becquerel discovered naturally occurring radioactivity and this set the stage for nuclear medicine. Becquerel observed that uranium salt wrapped in a photographic paper left very distinct outlines signifying that the salt continued to exhibit fluorescence even though there was no power source connected to the material. Becquerel concluded that uranium emitted penetrating radiation, apart from x-rays that fogged up a photographic plate and this discovery became the foundation for the research of uranium salts as a thesis topic for Marie Curie (Havesy 1984, Ice 1995 and Slater 2012).

Using pitchblende as sample material, Marie discovered that thorium is radioactive as well and she coined the word radioactivity when she observed that uranium electrified air using the piezoelectric sensor (a device that measures extremely low electrical current) Pierre and his brother invented. Becquerel, Marie and Pierre Curie shared the noble prize in 1903 for the discovery of radioactivity. Marie Curie was again awarded the Nobel Prize in Chemistry for the discovery of polonium and radium in 1911. It was estimated that 1,000 Ci of radium was used in medicine by 1963 (U.S. PHS 1963; Ice 1995; IAEA 2009). But the application of radioactive material in nuclear medicine was not limited to naturally occurring materials, and the full medical potential of radioactive material was not achieved until radionuclides could be produced artificially (IAEA 2009)

In 1934 Marie Curie's daughter Irene and her husband Frederic Joliot (both trained and worked in Marie Curie's lab) described artificially induced radioactivity (Curie et.al 1934) and in the same year Ernest Lawrence in his thesis published the invention of the cyclotron giving birth to resonant particle acceleration at the University of California, Berkeley. Lawrence's work established University of California, Berkeley (UCB) as one of the major pioneers of the field of nuclear science, bringing experts such as Seaborg, Segre, Hamilton, Anger, Alvarez and many more to UCB (Slater 2012). Enrico Fermi in the same year published his work in which he used a radium-beryllium neutron source to activate elements to produce various radionuclides with short half-life (Fermi 1934; Agnew 1981; Ice 1995).

Quite a number of naturally occurring radionuclides have been assessed for use in medicine. These radionuclides arise from two different sources. The primordial radionuclides which have been present since the birth of the earth or the cosmogenic radionuclides. The primordial radionuclides are further divided into two part; the primary and the secondary

primordial radionuclides. The primary primordial radionuclides include uranium-235, uranium-238 and thorium-232, while the secondary primordial radionuclides, which are the decay products of the primary primordial radionuclide. The primordial radionuclides have half-lives similar to the estimated age of the earth, about 4.5-billion years or more. Examples of each of primary and secondary primordial radionuclide used in nuclear medicine include radium and potassium-40 (used to evaluate lean muscle mass in the body) respectively (Ice 1995). Cosmogenic radionuclides are those naturally occurring materials that are formed by the interaction of high-energy cosmic radiation arising from outside our solar system with target nuclei floating in the atmosphere. Some of the products of this interaction include naturally occurring H-3 and C-14, which are both used in biomedical research and many other science and engineering fields (Ice 1995).

Naturally occurring radioactive material is ubiquitous on earth, not all naturally occurring radionuclides are necessarily suitable for use in nuclear medicine, mostly because of their long half-lives (IAEA 2009). Therefore, artificially produced radionuclides are the main source of radioactive materials used in nuclear medicine. Production of artificial radionuclides can be achieved by particle-induced activation of elements using accelerators, neutron activation using nuclear reactors and/or recovery of radioactive materials produced in nuclear reactor during nuclear fission. The production of radionuclides with an accelerator involves the acceleration of charged particles to energies high enough that the charged particle can overcome the coulomb barrier of the nucleus of a target material in order to interact with the nucleus. A good example of an accelerator-induced reaction is the reaction of $\text{Te-124}(p, 2n)\text{I-123}$, where an accelerated proton interacts with the nucleons of Te-124 ejecting 2 neutrons to produce I-123. Neutrons produced during fission are used to induce nuclear interactions in the nuclei of a target material. A common example is seen in the reaction $\text{Mo-98}(n, \gamma)\text{Mo-99}$, where a Mo-98 atom absorbs a neutron

and the atom is briefly transmuted to Mo-99. The Mo-99 atom, which is in excited state decays by gamma ray emission because of the excess energy in the nucleus that was gained from the absorption of a neutron. The third method is to collect fission products i.e. (from the fission of U- 235) that are created because of nuclear fission in the reactor. Chemical separation techniques are used to obtain radionuclides (such as I-131 and Mo-99) for use in nuclear medicine.

Accelerators were the major devices used for radionuclide production between 1935 to the end of World War II. The advent of nuclear reactors after World War II brought about a decline in the use of accelerators to produce artificial radioactivity for nuclear medicine. Because reactors were used more and more for this purpose, accelerator produced radionuclide became less common. However, this is changing. As the techniques of using radiotracers becomes more sophisticated, it has become imperative for accelerators to be used to augment radionuclide production because reactor produced radionuclides cannot completely meet the growing demand or diversity. Hence, the use of accelerators to produce radioactive materials is making a comeback. The production of radioactive materials from an accelerator usually involves the irradiation of a unique target material. The target and the product should be composed of such different chemical elements that it is possible to find chemical or physical means of separating the product from the target. This helps in obtaining high specific activity high purity preparations, owing to the target and product being different. This also frequently produces fewer radionuclide impurities especially if one selects a target material, particle and energy window for irradiation to minimize the production of impurities (IAEA 2009).

2.10 Selection of Radionuclide for Potential use in Nuclear Medicine

When choosing radionuclides used in nuclear medicine several things are considered. These include the characteristics of the radionuclide, for instance, the half-life, type of particle

emitted, specific activity, energy of particle, and the toxicity of the element or compound. Another factor is if the radionuclide is going to be used for therapy or diagnosis. Considerations of the material production capacity, the method of delivery for diagnosis or therapy, also important. If it were to be used in therapy to treat cancer, one must know how the radiation will be conducted. For instance, will it be done using interstitial implants? Interstitial implant involves the direct insertion of radioactive source into a cancerous tissue to irradiate the cancer cells (Cuaron et. al 2009). The major factor or characteristic considered for radionuclide selection for nuclear medicine is the half-life of the radionuclide (Ice 1995). Usually, when considering external beam radiotherapy, teletherapy, or certain interstitial approaches, radionuclides with relatively long half-life are preferable. In contrast, short half-life radionuclides are preferable for use in diagnosis. The long half-life radionuclides are suitable for therapy because these radionuclides are permanently placed at the site of a tumor to continuously irradiate and control the tumor. Short half-life radionuclides are especially useful for diagnosis. The reason being is that shortly after administration, the radionuclide decays away leaving the patient free of exposure from the radionuclide (Ice 1995). This ensures that the patient is not exposed to excessive dose even when the procedure needs to be carried out again.

2.11 Using Accelerators for Medical Radionuclide Production and Nuclear Research

Bombarding target nuclei with charged particles from accelerators is one of the several methods used to produce radioactive materials. The use of accelerators to produce specific radionuclides has its bases in Rutherford's gold foil experiment (Graham et. al. 1984; Ice 1995). During this experiment, Rutherford used alpha particles emitted by radium to change the structure of matter (Graham et. al. 1984; Ice 1995). Similarly, charged particles that are accelerated to high energy of at least 8 to 10 MeV could penetrate the columbic barrier of a target nucleus creating a

nuclear reaction. Typically, the beam generated and accelerated should not only have sufficient energy to stimulate a nuclear reaction, but also have enough beam current to give a practical yield of the radionuclide that needs to be produced (IAEA 2009).

The yield of production of specific radionuclides from an accelerator depends on the incident particle current, emerging particle energy spectra, and reaction cross section. It is possible that the target nucleus simply scatters the charged particle, which may or may not cause the nucleus to excite. If the charged particle has sufficient energy, it may break the potential barrier of the nucleus combining with the nucleus to form a compound nucleus. The outcome of absorption depends on whether the reaction is endothermic or exothermic. Typically, the compound nucleus is highly excited because the absorbed accelerated particles represents its own kinetic energy and mass difference energy within the nucleus (IAEA 2009). The combination of the charged particle in the target nucleus and the subsequent excitation of the nucleus may cause the compound nucleus to decompose through several possible different processes, leading to a new nucleus or different nuclei (IAEA 2009). Accompanying the decomposition of a compound nucleus is the emission of radiation if the target itself is radioactive.

2.12 Beam Dump Designs

The activation of materials while running an accelerator of energy above 8 MeV is inevitable. In the case of electron LINACs, the electron beam and/or the bremsstrahlung radiation produced may activate materials. Since the target does not usually completely stop the beam, a different means of reducing or stopping the beam beyond a target is necessary. To perform this task, a beam dump device is used. The beam dump is a device in which accelerated electron bunches that travel past the target, dissipate their remaining energy. The design of such a device requires careful selection of the types of material used, depends on the power of the beam and the

type of particle that is being accelerated (NCRP 2003). Beam dumps are used in various applications ranging from radiation producing devices like traveling wave tubes to electron beam coolers, lasers, large machines like LINACs and electron colliders (Hershcovitch 2010). Due to the high temperature experienced when charged particles deposit all of their remaining kinetic energy into a beam dump, the choice of materials used for a beam dump is limited. Materials used in a beam dump must be able to withstand a great amount of heat. In addition, water or oil circulation in the beam dump or a water tank built around the beam dump to prevent the beam dump from melting is often a necessary design feature. It is important to note that the process of cooling the beam dump can result in a source of exposure to workers due to the activation of water or other cooling substances. Consequently, the water tank surrounding the beam dump needs to be shielded (Ohnishi et al 2009), (Lee et al 2005). Another issue associated with beam dump design for electron LINACs is the inevitability of Bremsstrahlung radiation production when electrons interact with high-Z material, a process that might require its own additional shielding. Electrons with energy greater than 1.022 MeV passing through a high-Z material may produce annihilation radiation; associated with pair production. The positron produced from the pair production reaction, undergoes an annihilation process producing more gamma rays, thus resulting in the phenomenon called cascade gamma production (Heshcovitch 2010). Therefore, choosing material used in beam dump construction, one must avoid materials with high-Z, and large photoneutron production cross section. These types of materials aid in photoneutron production and as a result complicate the shielding needs.

In summary, any material considered for use in building a beam dump should possess the listed qualities below:

- i. high thermal conductivity so as to provide good heat transfer to the coolant,

- ii. high melting temperature and yield low thermal stress (Smith et. al. 2004),
- iii. low photon production from electron interaction with the material,
- iv. Resistance to photoneutron production to reduce neutron production, and ultimately induced activation.

The thermal conductivity, thermal expansion coefficient and electron range in the material used to build the beam dump, along with maximum allowed temperature and thermal stresses, determine the required traverse size of the beam striking the dump, and therefore the beam dump size (Smith et. al 2004). According to (Smith et. al. 2004) from a practical point of view, beryllium, pyrolytic carbon, aluminum and copper are the most suitable materials to consider as building materials used to construct electron beam dumps.

Takei et. al. 2000, designed a beam dump using 22 separate plates fabricated from oxygen free high-purity copper. Each plate had a thickness of 5-cm. The first 18 plates had circular holes cut in the center with slightly different diameters. These were placed at the upstream end of the beam dump. The four remaining disk plates without holes were placed on the downstream side of the beam dump. The first eighteen plates were arranged in such a way that the plate with the largest ring diameter was placed upstream and the plate with the smallest-ring-diameter was placed at the downstream side. This arrangement created a cone shaped center in the array of copper plates where the beam of electrons that passed the target, or photons and neutrons, produced in this process could be absorbed. The last four disks were intended to disperse the heat created in them into the surrounding cooling water that stop the central beam.

The second design was by (Leuschner et. al. 2004) of Deutsches Elektronen-Synchrotron (DESY) in Germany. This design was developed for the Electron Positron Linear Collider. They

suggested the beam dump should be made of a cylindrical volume of water, 10-m long and 1.5-m in diameter. A static pressure of 10 bar was applied to this volume of water to improve the interaction between the beam and beam dump. To remove the heat from the beam dump, it was suggested that a secondary cooling water system be added to the facility, to remove excess energy deposited in the beam dump (Leuschner et. al. 2004).

Chapter 3: MATERIALS AND METHODS

3.1 Instruments Used

The instruments used for data collection during the experiment included a Ludlum 9-3 ion chamber to take exposure rate, and a Ludlum Model 12-4 (REM ball) to measure neutron dose equivalent rates. The LINAC was operated at the following parameters: beam energy of 40-MeV, peak current of 67 mA, pulse length 9 microseconds, repetition rate of 300 Hz, and an average power of 7.24-kW. The white room walls are made from ordinary concrete that has a density of 2.35-gcm^{-3} . Monte Carlo N-Particle version 6 (or MCNP 6²) which is a, continuous-energy, generalized-geometry, time-dependent Monte Carlo radiation-transport code that was designed specifically for radiation transport was used to perform all simulation. The MCNP6 code tracks many different particle types including gamma rays, electrons, positrons, neutrons, alpha particles and heavy ions over a wide range of energies. MCNP6 is the product of the merger of MCNP5 and MCNPX codes into one comprising all features of both (MCNP6 2013 and Mashnik et. al. 2012). This code was run using an HP pavilion laptop having 670 GB hard drive, intel(R)³ Core(TM) i7 5500 CPU a 2.40 GHz processor, and 6.00 GB installed memory (RAM).

3.2 Monte Carlo Neutral Particle Transport Code (MCNP6)

MCNP can be used to investigate a nearly infinite matrix of transport scenarios considering different geometries, types and energies of radiation. The execution of an MCNP6 problem input file can take anywhere from a few minutes to as long as several weeks depending on the complexity of the problem, the number of source particles to be simulated and the speed of the computer used.

²Los Alamos National Laboratory New Mexico 87545

³ Intel Corporation 2200 Mission College Blvd, Santa Clara, CA 95054

Input files include the geometry of the problem to be simulated, the materials that will fill the geometry, the source of the radiation, and the desired result for the calculation. There are four major blocks or sections contained in the input file namely: title, cell, surface, and data. Each of these major sections consists of one or more cards and every card consists of several components. A card is a single line of input up to 80 characters (Shultis J. K. et. al. 2006 and MCNP6 2013).

3.2.1 The Title Block

The first block of information provided in an MCNP6 input file is called the title card. The title card gives an option to write a brief description of the problem in the input file. Thus, the title card affords a means of differentiating between different input files. If required, the date and time on which an input file is created can be provided in the title card. All information on a title card is repeated in the output file in many places for easy of identification (Shultis J. K. et. al. 2006 and MCNP6 2013).

3.2.2 The Cell Block

The cell block of information that follows immediately after the title card section. In these cards, cells are used to define shapes contained in the geometry that is to be modeled. The density of materials contained in each defined volume are also given in the cell card to identify those volumes filled with different materials. Many cell cards notate the cell number. The number is used to identify a cell. The material number is used to identify the material, the density of the material occupying the space and the surface(s) bounding the cell respectively. A space is used to separate each of the previously mentioned cards. The blank line delimiter is used to separate the end of the cell block and the beginning of the surface block. A blank line delimiter is a line

intentionally left blank line that signifies the end of a block of information in the input file (Shultis et. al. 2006 and MCNP6 2013).

3.2.3 Surface Block

The surface cards follow the cell card. A blank line delimiter is required between the surface card and cell card. Surface cards in the surface block are used to provide limit(s) for cell(s) defining volumes. Surface cards are made up of a surface number, a mnemonic that defines the shape of the surface that is bordering a volume, and the dimensions of the volume (Shultis et. al. 2006 and MCNP6 2013).

3.2.4 Data Block

The data block is made up of several different cards. Examples of cards include the source definition card (SDEF), the material cards, the mode cards, the cutoff card, tally card, and the print card; there are many others. The different card needed to achieve a particular task depend on the nature of the model to be simulated. The source to be modeled is defined in the SDEF card, which tells the code the type of source, types and energy of source radiation(s), and their direction etc. The mode card defines the particle of interest pertinent to the modeled problem and therefore tells MCNP6 to run any of the particles available in the database or a combination of these particles. The cutoff card is used to let the code know at what energy to stop tracking a particle. The use of the cutoff card helps reduce the code run time. The tally card tells MCNP the type of answer to be calculated (dose, fluence, flux, energy deposited etc.) for a given modeled problem (Shultis et. al. 2006 and MCNP6 2013).

3.3 Data Acquisition

The data acquisition system used to collect data from activated materials for analysis is shown in Figure.3.1. The data acquisition system was used to count the fluence monitors used in the fluence experiment. The system consisted of several electronic modules that convert the deposited photon energy signal within a detector into a pulse. Some of these electronics included but are not limited to: ORTEC⁴ 659 (5kV) high-voltage supply, ORTEC⁵ high-purity germanium detector (HP(Ge)), ORTEC⁶ spectroscopy amplifier, preamplifier, ORTEC⁷ amplifier, a CANBERRA⁸ analog to digital converter and MPA-3⁹ software installed on a special data acquisition computer. The MPA-3 software carried out the tasks of the multichannel analyzer.

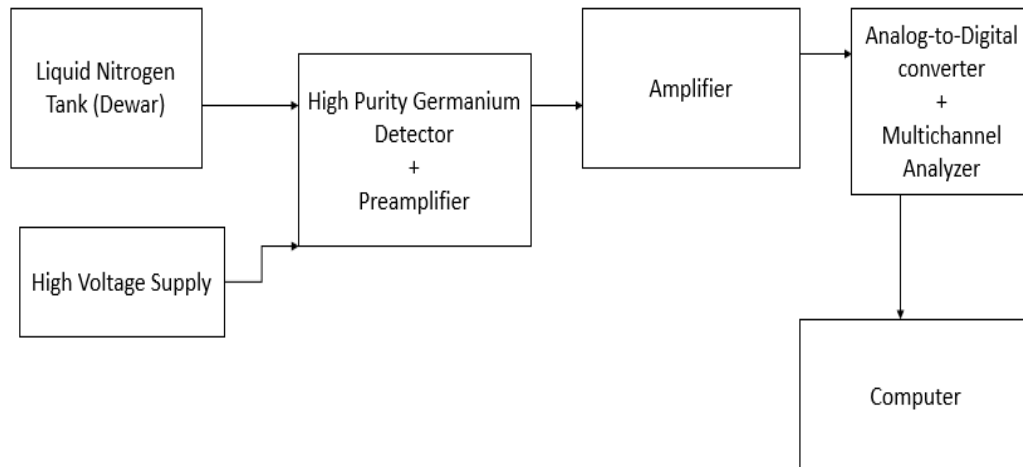


Figure 3.1. A schematic diagram of the data acquisition Station

⁴ ORTEC INC. 505 Gentry Memorial Hwy, Easley, SC 29640

⁵ ORTEC INC 505 Gentry Memorial Hwy, Easley, SC 29640

⁶ ORTEC INC 505 Gentry Memorial Hwy, Easley, SC 29640

⁷ ORTEC INC 505 Gentry Memorial Hwy, Easley, SC 29640

⁸ Canberra Inc. 800 Research Pkwy, Meridian, CT 06450

⁹ ORTEC INC 505 Gentry Memorial Hwy, Easley, SC 29640

3.4 Methodology Part I

3.4.1 Target Study

Large radiation fields may be produced when a target is placed downstream of the beam window of the 40-MeV electron LINAC. The thickness of shielding needed in this room depends on the target, the number of neutrons and/or photons (fluence rate) produced per unit time during operation, and the allowable magnitude of radiation intensity in the room. The fluence rate produced due to the irradiation of the target could result in a measurable dose equivalent rate beyond the walls of the white room and around the general vicinity of the IAC (including the top of the earthen material). Before the LINAC could be operated at full capacity (maximum power), it was important to ascertain the magnitude of dose equivalent rate that would be produced at the locations of interest at maximum power. Instead of running the accelerator at maximum power to estimate the fluence rate and have radiation worker perform radiation surveys to determine dose equivalent rate around the white room. A target study using a surrogate materials was proposed in which an experiment was performed to determine the fluence rate and dose equivalent rate that would be produced at unit power around the white room. The experiment allowed the author to eliminate the potential problem of exceeding the regulatory limit of 0.02-mSv in any one hour to the public. MCNP6 was used to develop a model of the white room. The model developed was benchmarked against measurements made during the “test run” using the parameters described previously for LINAC operation during the experiment. The fluence and dose equivalent rates predicted using the MCNP simulation model were compared to those measured during the low power study performed using the surrogate target. It was thought that if the fluence rates and the dose equivalent rate from the simulation and experiments were comparable, the code could be used in place of further experiments to determine the fluence rate and the dose equivalent rate at high

power. Therefore, based on the predictions produced using MCNP6, the required amount of shielding that would suppress the dose equivalent rate around the white room to levels below regulatory limit for the condition of high power operation could be determined.

3.4.2 The Experiment

During the experiment, the LINAC was run at a power of 0.518-kW and beam energy of 40-MeV. This power level produces an electron beam intensity of 8.5×10^{13} electrons per second. This value is linearly related to the beam intensity at other power levels. Normalized to operation at 1 kW, an 1.6×10^{14} electron per second is anticipated. The experiment to measure the fluence rate and obtain the dose equivalent rate was carried out by selecting a surrogate target material. The surrogate target was chosen to provide fluence rate and dose equivalent rate data to use in benchmarking the model that was developed in MCNP6. The steel surrogate was placed downstream from three 1.5-mm thick water-cooled tungsten converters. A set of activation foils were used to monitor fluence. Three of the activation foils were aluminum-27 (Al-27) (Schmitt et al. 1960) and three were nickel-58 (Ni-58) (Ni J. et al. 2000). These materials were chosen because they are activated by the anticipated secondary radiations produced (i.e. Al-27 is activated by neutrons and Ni-57 is activated by photons). Ni-57 is also produced through Ni-58(n, 2n) Ni-57 reaction (semkova et al. 1992). However, the cross section for this reaction is very small (about 5-micro-barn) (Horibe et al. 1992). Given the anticipated low neutron fluence for those neutrons with energy greater than 12.1-MeV produced by the 40-MeV accelerator, the possibility of this reaction is negligible. The unique property of these materials allowed the researchers to quantify neutron and photon fluence rates separately. Other criteria used for fluence monitor selection included the threshold of activation reactions of interest and the half-life of the activated material. The specific reactions of interest were Al-27(n, alpha) Na-24 with a threshold energy of 3.25 MeV

for neutrons and Ni-57 (γ, n) Ni-57 with a threshold energy of 12.1 MeV. The activation products, Na-24 and Ni-57, decay by isobaric transition with the subsequent emission of a photon with an energy of 1.369 MeV and 1.377 MeV respectively. Na-24 has a half-life of 14.98 hours and Ni-57 has a half-life of 36.6 hours. Each of the activation products has a half-life that provides sufficient time for analysis after irradiation. Before the fluence monitors were counted after a 30 minutes irradiation, they were allowed to cool for at least hours. Six flux monitors were placed on the target. The dimension of each monitor was 1-cm by 1-cm with a thickness of 0.002-cm. Three of the fluence monitors were used to monitor neutrons and the remaining three were used to monitor photons. Two fluence monitors, one for neutrons and the other for photons, a pair were placed upstream on the target (position A), downstream on the target (position B) and at the center of the length of the target (position C) as shown in Figure. 3.2.

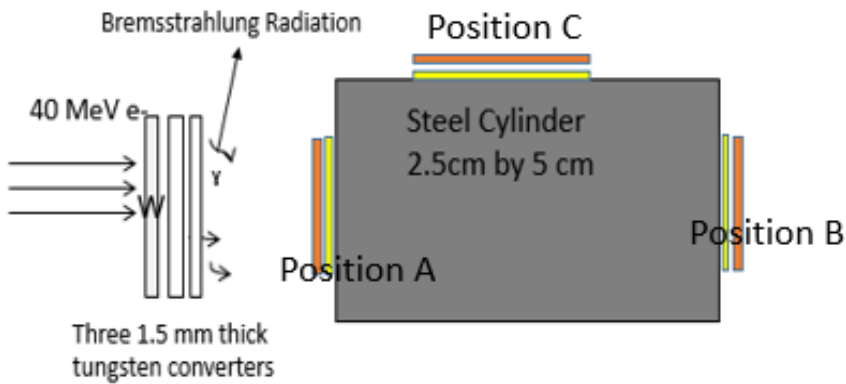


Figure 3.2 Experimental Setup

The neutron and photon fluence were calculated based on measurements obtained from activated foils. The corrected decay activity was determined using Eq. 5.

$$A(T_D) = \frac{\lambda N}{Eff \cdot BR} \quad (5)$$

$A(T_D)$ = is the activity after a giving time of decay

λ = is the decay constant of the isotope

N = is the number of counts

Eff. = is the efficiency of the detector

BR = is the branching ratio of the energy line of interest

T_C = is the time of cooling.

The activity calculated was then used in Equation 2 to calculate the activity at irradiation stop.

$A(T_i)$

$$A(T_i) = \frac{A(T_D)}{e^{\lambda T_D}} \quad (6)$$

$A(T_i)$ = is the activity when the irradiation was stopped

T_D = is the time the foil was allowed to decay before counting.

$A(T_D)$ = is the activity after a giving time of decay

λ = is the decay constant of the isotope

The activity (A) was placed into Eq. 7 and the fluence in Eq 3 was made the subject of the formula as shown in Eq. 8 to calculate the flux.

$$A(T_i) = \left(\frac{m \cdot l \cdot h}{A_r} \right) \cdot \varphi \cdot \sigma_{eff} \cdot (1 - e^{-\lambda T_i}) \quad (7)$$

$$\varphi = \frac{A(T_i) \cdot A_r}{m \cdot l \cdot h \cdot \sigma_{eff} \cdot (1 - e^{-\lambda T_i})} \quad (8)$$

φ = is the fluence in $(cm^2 \cdot s \cdot kW)^{-1}$

A_r = is the relative atomic mass of isotope

m = is the mass of element in grams

l = is Avogadro number

h = is the abundance of target isotope

σ_{eff} = is the effective cross section of the reaction of interest

T_i = is the time of irradiation (Segebade C. et. al. 1988)

Neutron dose rate and photon exposure rate meters were used to measure neutron dose equivalent rate and photon exposure rates. Exposure rate data collected using the exposure rate meter were converted to dose equivalent rates. Out of the nine locations surveyed on the top of the accelerator vault, locations 3, 6 and 9 were observed to have the highest dose equivalent rate on the top of the vault. These three locations coincided with the position directly above the LINAC in the vault below. Therefore, to reduce the number of locations to be simulated, these locations were used and dose equivalent was assumed uniform across these sections. Therefore, the dose rate at location 1, 3, 6, 9 and 11 were used as reference for dose rate calculation using MCNP6. Since it was not possible to take a large sample size, measurements of neutron and photon dose equivalent rates at each location of interest were used to calculate the uncertainty associated with each data point. The uncertainty associated with each measurement for neutron and photon dose equivalent rates were calculate based on the technical specification of the instruments used. The technical specification was quoted to be within 10% of measurement in the product manual (Ludlum 2010).

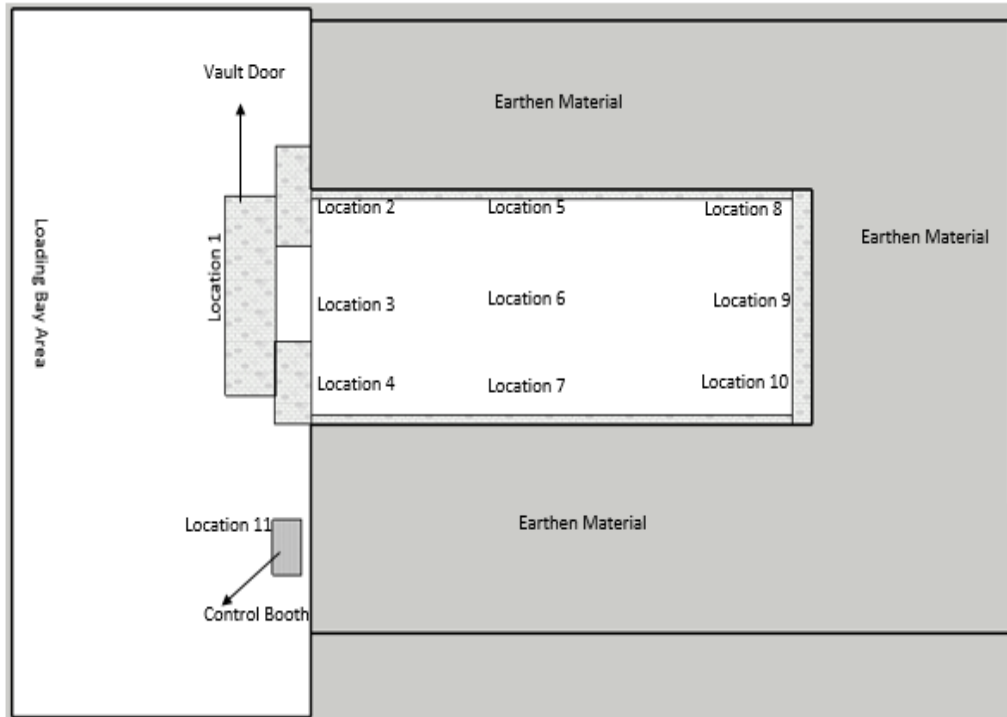


Figure 3.3 Dose equivalent Rate Map

3.4.3 Simulations

The surrogate steel target was modeled using MCNP6 to calculate the neutron and photon fluence rates as shown in Figure. 3.2. The 2.5-cm diameter by 5-cm long surrogate steel target was positioned downstream of three water-cooled tungsten converters each with a thickness of 1.5- mm. However, in the MCNP6 model the F2 tally in the code normalized the fluence emanating from the surfaces of interest to the number of particles cm^{-2} . The F2 tally is used to calculate the fluence of particles of interest averaged over a surface area (MCNP6 2013). These fluence values were later normalized using the beam current to provide the fluence rate in (number of particles $cm^{-2} \cdot s^{-1} \cdot kW^{-1}$). The setup was bombarded by the 40-MeV electron beam generated by the LINAC which was modeled as a source in the code. The neutron and photon fluence rates were calculated at position A (upstream), position B (downstream) and position C (around the

length of the cylinder). The beam of bremsstrahlung photons produced and the remaining uncollided electron beam interacted with the target to produce neutrons and photons.

The entire area around the LINAC was modeled using MCNP6 in order to predict the dose equivalent rates at various locations around the LINAC. To predict the dose rates without having to design a detector in the code, the author incorporated five (ICRU 1985; ICRU 1988) spherical phantoms into the model to represent people standing at each location of interest. A spherical phantom is composed of tissue equivalent material 30-cm in diameter with a density of 1-gcm^{-3} , and mass composition of 76.2% oxygen, 11.1% carbon, 10.1% hydrogen and 2.6% nitrogen. One of the spheres was located by representation on the north edge of the earthen material above the ceiling, the second one at mid-distance from the first, and the third on the south edge of the hall. All three spheres were placed directly above the location of the electron LINAC. These were the locations where the highest dose equivalent rates were measured during the experiment. The fourth was positioned at the center of the vault door (this location was chosen not necessary to give representative dose equivalent rate to an individual but as a means for comparison between simulation and experiment), and the last (fifth) sphere was placed at the control booth area as shown in Figure. 3.4. All dose equivalent rates were calculated at a depth of 1-cm from the surface of the phantom.

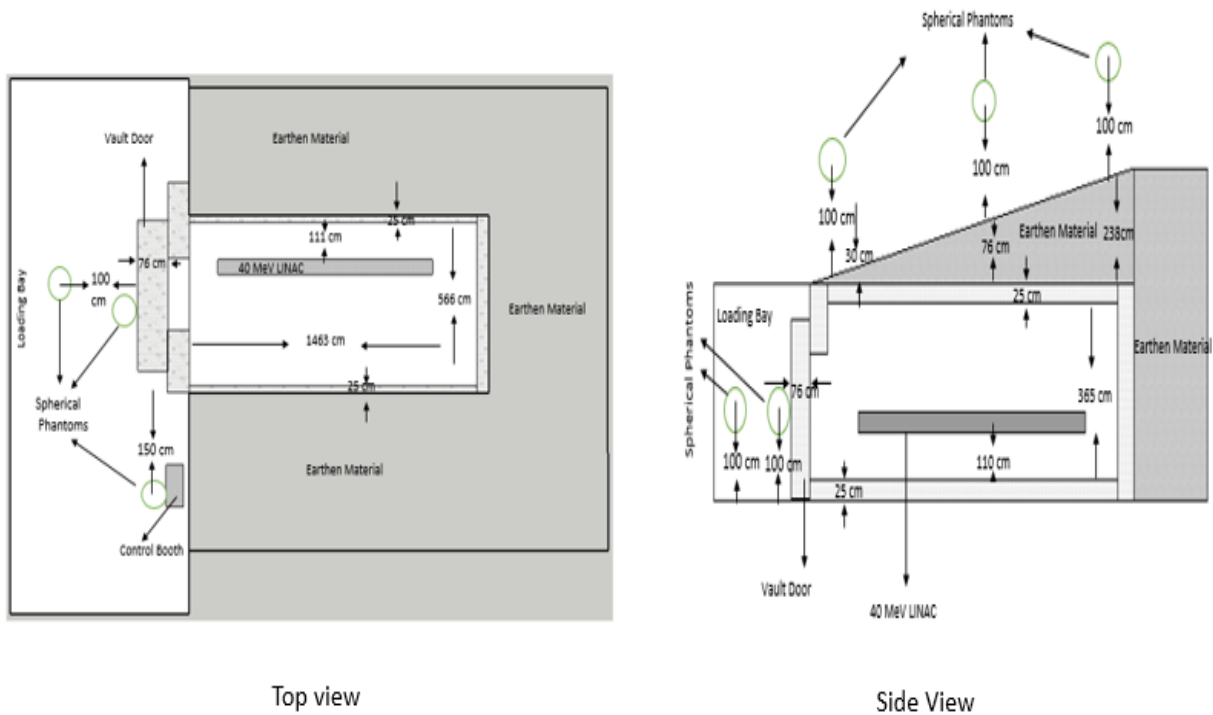


Figure 3.4. Location of the Spherical Phantoms

Although, dose equivalent rates were taken at nine locations on top of the vault (three each on the north end, south end and center) as shown on the experimental dose rate map in Figure. 3.3, only the locations with the highest dose equivalent rates were simulated. However, it was assumed that these chosen dose equivalent rates were uniform across each of the locations (north end, south end and center of the top of the vault) making the results of the simulations conservative.

The results of the fluence rate and the dose equivalent rate measurements from the simulation at low power (1 kW) were compared to the results obtained for these quantities in the experiment performed at the same power level. A base model was developed in MCNP6 (i.e. benchmark) for this shielding analysis. The model served as a platform for all simulations associated with the 40-MeV LINAC at beam powers that would cause the dose equivalent rate to exceed the allowable limit to members of the public. After benchmarking the model with measured

values, the MCNP6 code were scaled up from a 1-kW to a 10-kW beam power and the dose equivalent rates were predicted for this higher power. After every input execution, MCNP6 generates an output file. At the end of the output, MCNP6 prints one bin for each tally to give an indication of tally fluctuations (i.e. how well the tally has converged). The tally fluctuation bin is subject to some statistical checks for tally convergence, including calculation of the variance, Figure of merit, relative error, and the mean. These statistical checks are printed on a table in the output file thus providing the user with detailed information about the quality of the tally fluctuation results.

3.5 Methodology Part II

3.5.1 Benchmarking MCNP6 using Dose Equivalent Rate

The LINAC beam parameters used for Cu-67 production were, peak current of 67-mA, a pulse length of $9\mu\text{s}$, repetition rate of 300Hz and an average power output of 7.24kW. During Cu-67 production, radiation survey meters were used to measure the dose equivalent rate at all locations of interest. The measured survey data were used as reference to benchmark the MCNP6 model developed using this specific geometry for this study; an input file was developed that mimicked as many conditions of the white room and operation parameters for the 40-MeV accelerator during Cu-67 production. The input file of the MCNP model consisted of the white room as shown in Figure.3.5, the 40-MeV electron LINAC source, three 1.5-mm thick water cooled tungsten converters and a cylindrical Zn-68 target of dimensions 2.5 by 3 cm as shown in Figure. 3.2. Densities of 2.35 gcm^{-3} and 1.5 gcm^{-3} were used for the all concrete and earthen material respectively. The accelerator window and the Zn-67 target was designed inside the target vault in the white room also shown in Figure 3.5. Instead of detectors, ICRU spherical phantoms were incorporated in the input file at each of the location of interest as shown in Figure 3.3 in order

to represent a person standing at these locations. There is no provision in MCNP6 to enter parameters such as peak current, pulse length, repetition rate or power. Therefore, the average current at this power was used to calculate the number of electrons, which is given as 1.13×10^{15} electrons per second. This value was used to normalize the tallies defined in the input file, which are normalized per source particle. The predicted dose equivalent rate results were compared to the dose equivalent rate data collected during Cu-67 generation. After the MCNP model was benchmarked for the shielding analysis and beam dump design. The MCNP6 model predicted dose equivalent rates for the 7.24-kW beam power level were scaled up to obtain the dose equivalent rates for a 10-kW beam.

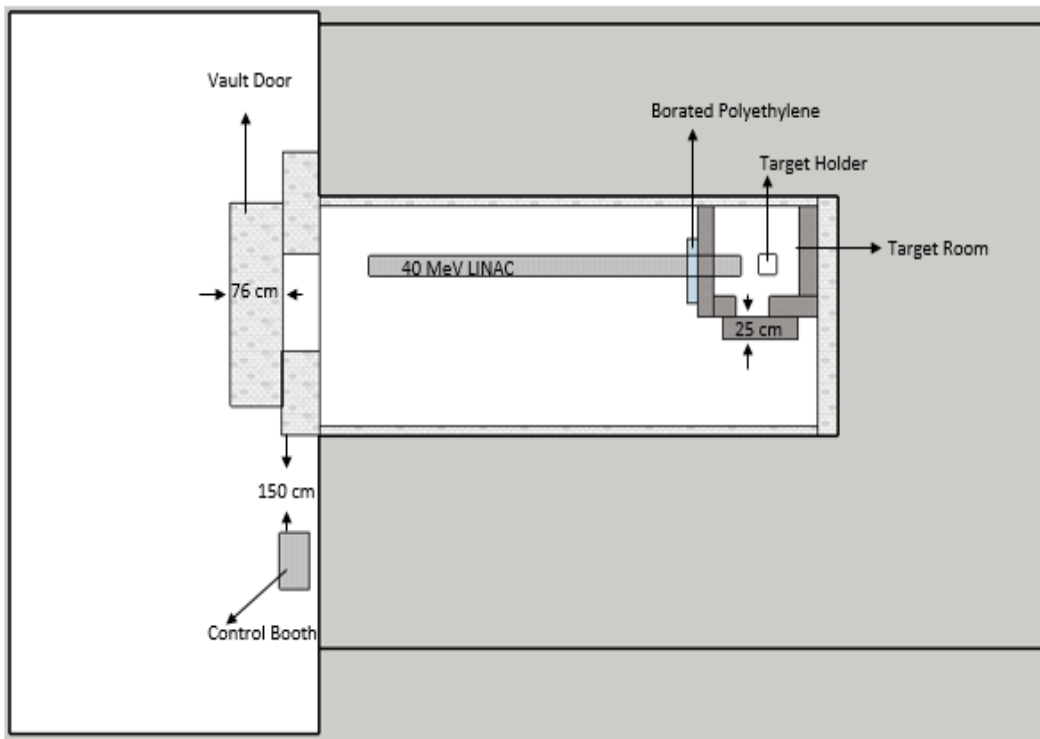


Figure 3.5. Plan View of the White Room with Shielding Upgrade

Two new input files were created based on the benchmarked model and in each file the zinc-68 target was replaced with one of the new target holder shown in Figures. 1.5 a and b. The

gases (krypton and xenon) in the target configuration were not accounted for in the model because they were unlikely to be generated in sufficient quantities to have significant effect on the dose equivalent rate calculated for the locations of interest. Therefore, only krypton gas was included in the Monte Carlo simulation of the white room model. Monte Carlo model operational-simulations were performed for each target holder using the number of electrons generated from a 7.24-kW beam as a normalization factor in the code. The predictions based on the 7.24-kW beam were scaled-up to obtain the dose equivalent rate that could be anticipated when a 10-kW beam was used. The dose equivalent rate results for the various locations of interest for the three different targets (Zn-67 and Natural Kr configurations 1 and 2) were compared to determine which of the targets would be the most important contributor to worker dose. Based on this comparison, the target that contributed most to worker exposure was selected. This target was used as the reference for beam dump design and necessary shield upgrade analyses. The approach was to determine the shield upgrade and a beam dump design that could shield the target producing the highest dose equivalent rate. It was thought the designs for shielding upgrades and the beam dump would be sufficient for the target with the greatest activity and this would predict the most conservative radiation field strength hence it would be sufficient for the other targets.

3.5.2 Shielding Upgrade and Beam Dump Design Analysis using MCNP6

Based on the literature review it was concluded that the materials selected for analyses (beryllium, pyrolytic carbon, aluminum and copper) were the most suitable material for use in building a beam dump (Takei et. al. 2000), (Smith et. al. 2005). The choice of these materials was based on a combination of unique characteristics such as high thermal conductivity, high melting temperature and relatively low z (to curb photon production). Another important factor in the selection of these materials was their potential to undergo photo-neutron production. The

production of photoneutrons need to be small so that they would not greatly contribute to the magnitude of the neutron field generated. Beryllium was not analyzed in this study because of its undesirably low photoneutron production energy. The higher the threshold energy for photoneutron production a material has, the lower the number of neutron the material would produce when bremsstrahlung photons interacts with the material. Table 3.3 shows some of the characteristic of these materials. Although, it has been established that these materials are suitable for beam dumps, the author intended to compare performance of these materials with the performance of ordinary concrete as a beam dump material for the 40-MeV electron LINAC. This comparison is appropriate because concrete is a cheaper alternative to all these elemental materials. Therefore, if concrete could perform well enough as a beam dump material, there would be no need to spend a great deal of funds to provide protection.

Table 3.1 Characteristic of Materials chosen for Beam Dump Design Analysis.

Material	Range (g.cm ⁻²)	Density (g.cm ⁻³)	Range (cm)	Specific Heat Capacity (J/Kg-K)	Melting point (°C)	Threshold Energy (MeV)
Cu	1.82	8.90	0.20	384	1084	9.91
Al	12.99	2.70	4.81	904	660	13.1
C (pyrolytic)	13.27	1.70	7.81	720	3550	18.7
Be	15.16	1.80	8.42	1825	1287	1.6
Concrete	12.66	2.34	5.41	960	1000-1300 ^a	-----

^a (Hager 2013)

It was assumed that after electrons from the beam encountered the target, the un-collided electrons that escaped the target through the downstream surface (or in the forward direction) of the target would, interact with the beam dump. MCNP6 was used to simulate the fluence of all

electrons leaving the target at the downstream (or surface B) surface for each one of the three targets (Zn-68 and the 2 krypton targets) to ascertain the maximum energy of electrons that would eventually collide with the beam dump. Hence, an input file with energy bins to calculate the energy of all electrons leaving the B surface of the target was created. Moreover, from this data the maximum energy for electron leaving the B surface was found for each of the three target configurations. To determine the thickness of material required for the beam dump, the author modeled the target assembly capable of producing the highest energy electron spectrum emerging from the B surface. The thicknesses of materials necessary for the beam stop was simply the maximum distance (range) the unabsorbed electrons with the highest energy leaving the B surface would travel in each materials. The range of electron in each material (ordinary concrete, copper, aluminum, and pyrolytic carbon) was obtained from the National Institute of Standards and Technology's (NIST) which provided the continuous slowing down approximation (CSDA) range database for electrons. The thicknesses for each material required are shown in Table 3.3.

In addition to the room-inside-a-room placed in the white room to improve shielding, the proposed design as shown on Figure. 3.5a consisted of a beam dump fabricated on the south wall in the MCNP6 model. This was used to accommodate the beam dump and to reduce beam scattering before the beam interacted with the beam dump. The south wall of the room-inside-a-room was extended towards the target by 45-cm making its thickness 150-cm. The height of the room-inside-a-room was increased from 120-cm to 130-cm and the thickness of the concrete covering it was also increased from a thickness of 17.5-cm to 23.5-cm to account for the hollow created by the inclusion of a beam dump. The thickness of borated polyethylene was also increased from 5-cm to 15-cm to further suppress neutrons scattered from the beam dump. The beam dump was made from a set of 22 disks of each of the materials aluminum, copper and carbon. Each of

the disk is 5-cm thick and the first 18 disks were designed with cut out centers such that they have the shape of a ring. The inner diameter of the first ring of all beam dump materials analyzed was 10-cm. Each subsequent disk's inner diameter was reduced by 0.5-cm such that the inner diameter of the eighteenth ring was only 1.5-cm. This gave the hollow section of the beam dump a conical shape. The outer diameter of the 22 disks was chosen in such a way that the thickness between the inner diameter and outer diameter is equal to or greater than the range of the most energetic electron leaving the target's B surface to interact with the beam dump. The outer diameter of the first five rings for each material is 13 cm for copper, 15 cm for aluminum, and 18 cm for pyrolytic carbon. The outer diameter of the second set of five ring was reduced by 2 cm. Hence, the other diameter of the second set of five rings for each beam dump material is 11 cm, 13 cm, and 16 cm for copper, aluminum and pyrolytic carbon respectively. Finally, the last 12 disks was further reduced by 2 cm. The outer diameter for beam dump materials is 9 cm, 11 cm, and 14 cm for copper, aluminum and pyrolytic carbon respectively. In addition, the last four disks have no hollow in the center. The lack of hollow in the center of the last four disks was meant to aid in heat dispersal.

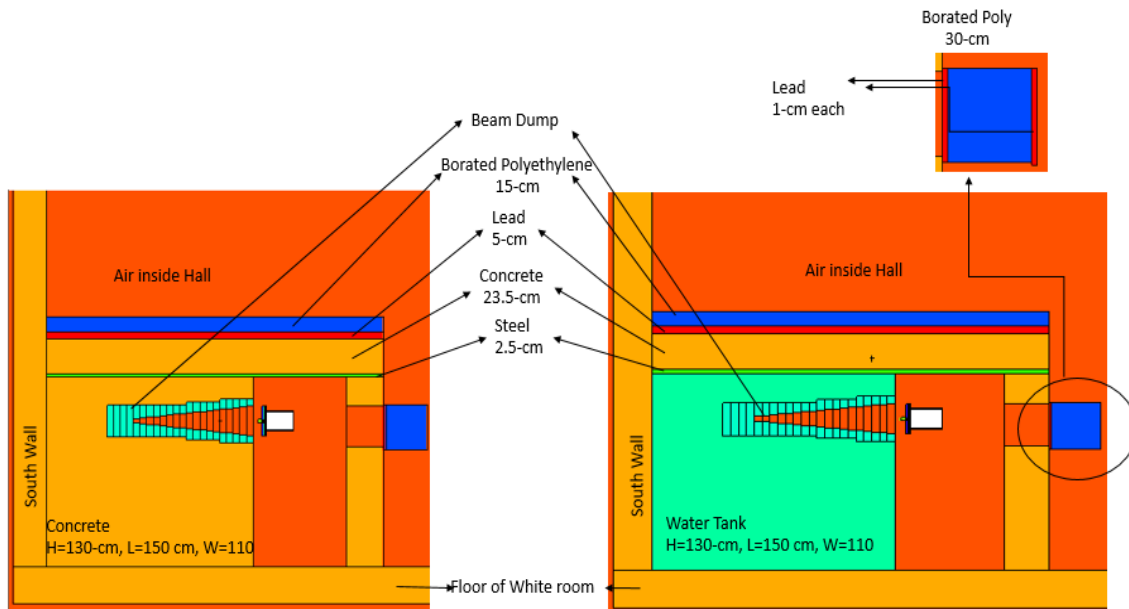
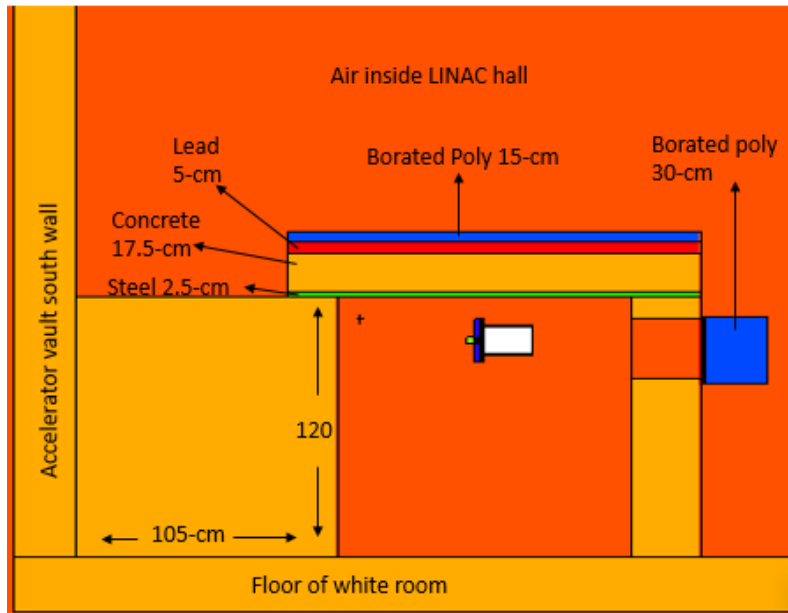


Figure 3.6. The Beam Dump Designs Modeled using MCNP: Beam Dump Encased in Concrete (Left) Beam Dump Immersed in Water Tank (Right)

Using each material and thickness required to absorb the maximum energy electron in the beam, four input files of the entire white room were created in MCNP6. Several simulations were evaluated; one for each of the four materials of interest. Each design was surrounded by the concrete of the south wall of the room-inside-a-room. This was done to be able to compare the performance of the three material (copper, aluminum and pyrolytic carbon) against ordinary concrete because the proposed beam dump would be made out of concrete. Depending on the heat generated by the interaction between the beam and beam dump, some of the materials being studied may require cooling. Therefore, another design analyzed the beam dump as it would perform if modeled in a water tank. The water tank replaced the south wall of the room-inside-a-room as shown in Figure. 3.6b. This design was simulated to provide insight on how the change from concrete to water tank would affect the performance of the materials used for th beam dump. The designs in Figure. 3.6a and 3.6b are the same in all aspects except in Figure. 3.6b the south wall

of the room-inside-a-room was replaced with a water tank. Figure. 3.7 shows how the target room looked like without the beam dump and shield upgrade.



Figures 3.7 Elevation View of the Target Room in the White Room without beam dump and shield upgrade

Chapter 4: RESULTS AND DISCUSSION

4.1. Experimental Data Collected

Table 4.1 provides the data obtained from counting the fluence monitoring foils for neutron and photons. During analysis, all neutron fluence monitors were counted for 16 hours with the goal of obtaining at least ten thousand counts thus reducing counting uncertainty to 1%. The neutron fluence monitor at position “Aluminum B” yielded only about 6,000 counts, so this goal was not always achieved. Unfortunately, obtaining lower than 10,000 counts in a fluence monitor will result in a higher uncertainty in the subsequent calculations. Moreover, the neutron fluence monitor at position “Aluminum C” did not yield reasonable counts and a result the data were discarded. All photon fluence monitors were analyzed for 30 minutes. The information provided include the position of each of the fluence monitor, the mass of the each fluence monitor, branching ratio, photon energy, half-life and the number of counts obtained.

Table 4.1. Experimental Data

Position	Mass of Foil (g)	BR (%)	Photon Energy (MeV)	T(1/2) (seconds)	Decay Time (seconds)	Counts
Al A	0.0042±0.005	100.0	1.368	5.38×10 ⁴	1.57E+04	20854
Al B	0.0093±0.005	100.0	1.368	5.38×10 ⁴	8.05E+04	6273
Al C	0.0069±0.005	100.0	1.368	5.38×10 ⁴	----- ^a	----- ^b
Ni A	0.0259±0.005	81.7	1.377	1.28×10 ⁵	3.74E+05	10752
Ni B	0.0239±0.005	81.7	1.377	1.28×10 ⁵	3.74E+05	10217
Ni C	0.0240±0.005	81.7	1.377	1.28×10 ⁵	3.77E+05	10498

a. no data, b. no data

MCNP provides a variety of standard tallies for users in the user manual. These tallies includes particle current, particle flux (across a surface, in a cell, at a detector point), energy deposition, collision heating, fission energy, energy deposition, pulse height and charge deposition. All these tallies are normalized to per source particle. The tally used to calculate the fluence, which was in turn used to calculate both fluence rates and dose equivalent rates was the F2 tally. The F2 tally in MCNP calculates the fluence averaged over a surface in number of particles per cm^{-2} . Therefore, multiplying the beam current to the value of the F2 tally yields the fluence rate. The task of multiplying the beam current to the F2 tally output was achieved using the tally multiplier card (or FM card). The multiplication card multiplies any tallied quantity. Table 4.2 shows how the MCNP F2 tally was converted to fluence rate. Column 1 give the list of neutron and photon monitor positions. Column 2 and 3 show the MCNP F2 tally output obtained for each of the monitor positions and the beam current that was used to normalize the F2 output. Colum 4 shows the predicted fluence rate from MCNP, which is the product of the MCNP F2 tally and the value of the beam current.

Table 4.2 Conversion of MCNP F2 Tally Output to Fluence Rate

Monitor Position	MCNP F2 Tally output $(\text{cm}^2\text{source particle})^{-1}$	Beam Current $(\text{s}\cdot\text{kW})^{-1}$	Predicted Fluence rate $(\text{cm}^2\cdot\text{s}\cdot\text{kW})^{-1}$
Neutron A	5.41×10^{-6}	1.60×10^{14}	8.65×10^8
Neutron B	1.36×10^{-6}	1.60×10^{14}	2.17×10^8
Neutron C	2.59×10^{-6}	1.60×10^{14}	4.15×10^8
Photon A	6.08×10^{-3}	1.60×10^{14}	9.72×10^{11}
Photon B	2.51×10^{-3}	1.60×10^{14}	4.02×10^{11}
Photon C	1.00×10^{-3}	1.60×10^{14}	1.62×10^{11}

4.2 Comparison Between Experiment Fluence and Simulated Fluence Rates

Table 4.3 compares the results of the neutron and photon fluence rates calculated for three positions A, B and C (shown in Figure 3.2) using simulation and experiment. The first column from the left gives the fluence monitor positions and the second and third columns give the simulated and experimental results respectively. There was no result for neutron fluence rate at position C. This was because the activity in the fluence monitor had decayed away before the fluence monitor could be counted. The last column shows the calculated ratios of simulated to experimental results. Except for the ratio calculated for neutron fluence rate at position B, all other ratios calculated were above unity making the simulated fluence rates higher at those positions. The variance reduction technique used was the cell importance. The cell importance is assigned in MCNP using the importance card. The importance variance reduction allow the user to assign importance to cell each cell in the input file. When a particle enters a cell with an importance of zero, MCNP would terminate the history of the particle. For instance, in these analyses, the electron fluence is not considered critical in contributing to dose equivalent rate beyond the walls of the accelerator vault. Therefore, all the cells depicting the walls of the accelerator vault were assigned an importance of zero for all electron. Whenever an electron reaches any of the walls, MCNP terminates the history of the electron. Terminating the history of the electron means computing time will not be wasted and can be diverted towards tracking the history of another particle. The particle history run for the fluence rate simulation was 10^7 particles and the F 2 tally was used to calculate the fluence rate.

Table 4.3 Predicted and Experimental Fluence Rate Results

Monitor Position	Predicted Fluence (cm ² ·s·kW) ⁻¹	Experimental Fluence (cm ² ·s·kW) ⁻¹	Ratio of Predicted to Experimental
Neutron A	8.65 × 10 ⁸ ± 4%	7.40 × 10 ⁸ ± 6%	1.2
Neutron B	2.17 × 10 ⁸ ± 6%	2.83 × 10 ⁸ ± 12%	0.8
Neutron C	4.15 × 10 ⁸ ± 4%	----- ^a	----- ^a
Photon A	9.72 × 10 ¹¹ ± 4%	8.32 × 10 ¹¹ ± 6%	1.2
Photon B	4.02 × 10 ¹¹ ± 5%	2.94 × 10 ¹¹ ± 9%	1.4
Photon C	1.60 × 10 ¹¹ ± 7%	1.11 × 10 ¹¹ ± 10%	1.4

^a Calculation was not performed due to low counts.

The predicted results from MCNP6 of the surrogate target show similarities within statistical bounds to the results obtained from the experiment. An increase in power from 1 to 10-kW would increase the neutron and photon production by a factor of ten at each position. The input file of the model design took into consideration the cutoff energies of the reactions of interest in the fluence monitor. Using the cutoff energy, the code scored only neutrons or photons with energy greater than or equals to the cutoff energy assigned for each particle. Every neutron or photon with energy above the threshold value of reactions sorted in the fluence monitor would be register when the neutron or photon crosses any of the surfaces of interest. This is not the case in the experiment. Although, a neutron or photon with energy high enough to cause a reaction does not necessarily cause a reaction 100% of the time. The energy may be high enough to cause a reaction but the reaction occurring is based on probability in the experiment. MCNP6, on the other hand, would register every neutron or photon that crosses a surface of interest. Consequently, the fluence rate calculated using MCNP6 might be more than the fluence rate calculated in the experiment. The example below gives a part of the input file that defines the source used in MCNP. The “sdef” stands for source definition. In the source definition card, “pos 0 0 0” tells MCNP that the source

is located the source position coordinate (0, 0, 0). The axis term “axs 0 0 1” tells MCNP the axis of the sampling volume is the line through (0, 0, 0), in the direction (0, 0, 1). The energy term “erg 40” defines the energy of the source particles and particles term “par e” tells MCNP the type of particle to transport, which in this case is electron. The vector term “vec 0 0 1” tells MCNP the direction in which the source particles are to be transported. The radial term “rad d1” defines the radial dimension of the source and the distribution of the particles using “si1 0 0.25” and “sp1 -21 1”. The term “si1 0 0.25” defines the radius of the source, which is from 0 (the origin) to 0.25 or 0.25 cm. While the “sp1 -21 1” tells MCNP to use the power law $p(x) = c|x|^a$ where $a=1$ to define the radial distribution of the source. Similarly, the extension term, which describes the thickness of the source using the “si2 48 49.9” and “sp2 -21 0”. The term “si1 48 49.9” tell MCNP that the source extends from a position 48 cm from the origin on the z-axis to a position 49.9 cm away. Hence, the thickness of the source is 1.9 cm thick. While the “sp1 -21 0” tells MCNP to use the power law $p(x) = c|x|^a$ where $a=0$ to define the axial distribution of the source.

```
sdef pos 0 0 0 axs 0 0 1 rad d1 ext d2 erg 40 vec 0 0 1 par e
si1 0 0.25
sp1 -21 1
si2 48 49.9
sp2 -21 0
```

Figure 4.1 shows a plot comparing the predicted and measured photon fluence rates for the surrogate target. The predicted and measured fluence rates at location photon A and photon C show no statistically significant difference when plotted within two standard deviation. This was not the case with position photon B.

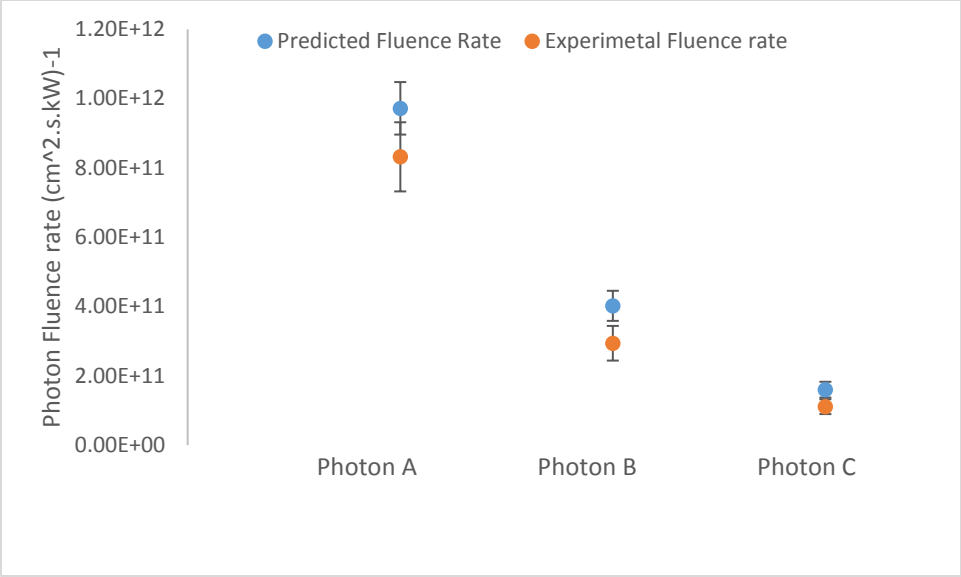


Figure 4.1 Comparing Predicted and Measured Photon Fluence Rates

Figure 4.2 show the comparison between the predicted and measured fluence rates obtained from the surrogate target. The error bars for positions neutron A and neutron B overlapped signifying that there is no statistically significant difference between the measured and predicted results, when the data was plotted within two standard deviations. Position neutron C had only predicted result.

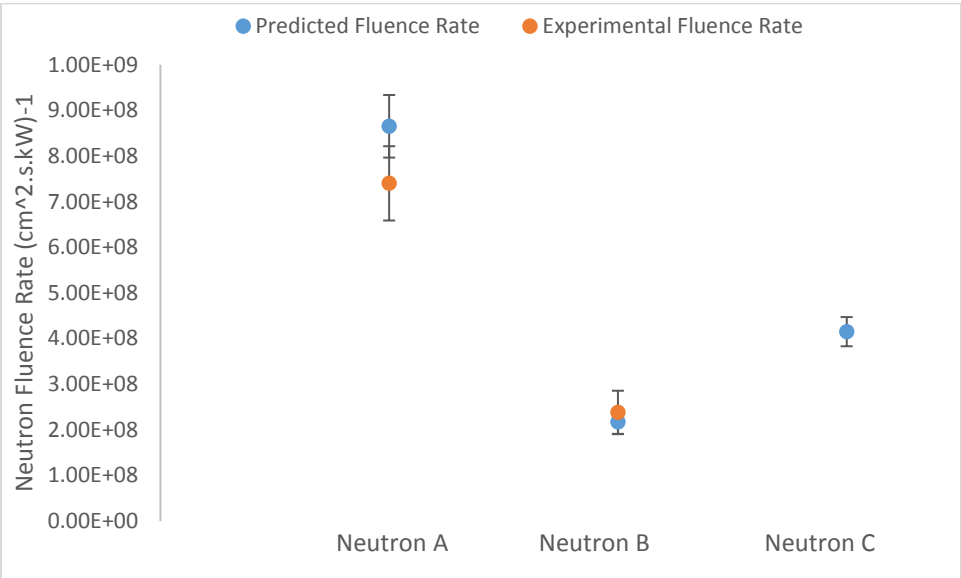


Figure 4.2 Comparing Predicted and Measured Fluence Rates

4.3 Experimental Dose Rates Map

Dose rates measured during experimental runs for the locations shown on the dose equivalent rate map are given on Table 4.4. The fonts of values for locations with the highest dose equivalent rates from the experiment for each section (north, mid and south) that were calculated in the simulation for the top of the accelerator are bolded on Table 4.2. On each of the locations, there were two values, one for neutron dose equivalent rate and the other for photon dose equivalent rate. The neutron dose rate at all location were all less than $0.0020\text{-mSv}\cdot\text{hr}^{-1}$ except the location at the center of the vault door, which had a dose equivalent rate of $0.025\text{-mSv}\cdot\text{hr}^{-1}$. All dose equivalent rates were measured at waist level on top of the earthen material on the ceiling concrete.

Table 4.4. Neutron and Photon Dose Rates for the Location Shown on the Dose Rate Map

Location	Neutron Dose rate $\text{mSv}\cdot\text{hr}^{-1}$	Photon Dose Rate $\text{mSv}\cdot\text{hr}^{-1}$
1	0.025	0.020
2	<0.0025	0.0020
3	<0.0025	0.0050
4	<0.0025	0.0030
5	<0.0025	0.0070
6	<0.0025	0.0090
7	<0.0025	0.004
8	<0.0025	0.0030
9	<0.0025	0.0050
10	<0.0025	0.0030
11	<0.0025	<0.0020

4.4 Comparison between Experimental and Predicted Dose equivalent Rates

In the case of dose equivalent rate calculation, MCNP has a function called the dose function (DF) and energy function (DE) cards, which are features that allow the user to enter a pointwise dose response function as a function of energy to modify a regular tally. Moreover, the dose conversion capability in MCNP provides several standard default fluence-to-dose conversion functions that can be invoked by omitting the DE card and using keywords on the DF card. All dose equivalent rates calculated in these analyses utilized one of the default standard dose functions. When any one of the standard default fluence-to-dose conversion factor is invoked MCNP take the values of the dose-to-fluence rate conversion factor and multiply it by the tally (F2) output to generate the dose equivalent rate. Note: there are separate standard default dose-conversion factors for neutrons and photons (MCNP 2013). The F2 tally was calculated using the ICRU phantom at a 1 cm depth from the surface of the phantom. The time cutoff card was used instead of the number of source particles card to run the simulation. The time cutoff card tells MCNP to terminate a simulation after a given time has elapsed. The cutoff time used was 2×10^4 minutes. The Table 4.5 shows the predicted and measured of dose equivalent rates obtained for the five locations of interest around the accelerator room. Three of the locations are at the top of the concrete ceiling and the other two are located in the loading bay area. The first columns after the list of location provide the predicted dose equivalent rate for photons and the uncertainty associated with these calculations. The next columns give the experiment measurement of photons for the same locations and their uncertainties. The next two columns show the same results for neutrons.

Table 4.5 Dose Equivalent Rate comparison between Predicted and experimental result at 1 kW power

Dose Location	Predicted Photon Dose Rate (mSv·hr ⁻¹)	Experimental Photon Dose Rate (mSv·hr ⁻¹)	C/E	Predicted Neutron Dose Rate (mSv·hr ⁻¹)	Experimental Neutron Dose Rate (mSv·hr ⁻¹)	C/E
Center of Vault Door	$2.3 \times 10^{-2} \pm 12\%$	$2.0 \times 10^{-2} \pm 10\%$	1.2	$2.4 \times 10^{-2} \pm 15\%$	$2.5 \times 10^{-2} \pm 10\%$	0.96
South End of Earthen Material	$1.0 \times 10^{-2} \pm 15\%$	$5.0 \times 10^{-3} \pm 10\%$	2.0	$3.9 \times 10^{-3} \pm 12\%$	$2.5 \times 10^{-3} \pm 10\%$	1.6
Top Center of Earthen Material	$1.0 \times 10^{-2} \pm 10\%$	$9.0 \times 10^{-3} \pm 10\%$	1.1	$3.0 \times 10^{-4} \pm 17\%$	$< 2.5 \times 10^{-3} \pm < 10\%$	--
North End of Earthen Material	$8.0 \times 10^{-3} \pm 8\%$	$5.0 \times 10^{-3} \pm 10\%$	1.6	0.00 ± 0.00	$< 2.5 \times 10^{-3} \pm < 10\%$	--
Control Area	$6.0 \times 10^{-4} \pm 13\%$	$< 2.0 \times 10^{-3} \pm < 10\%$	--	0.00 ± 0.00	$< 2.5 \times 10^{-3} \pm < 10\%$	--

The statistical equivalence of the predicted and experimental results are shown in Figures. 4.3 and 4.4. Figure. 4.3 is a plot comparing the predicted photon dose equivalent rate and the experimental photon dose equivalent rate with two standard deviations. The results for the all five locations show that the difference between the two sets of results at these location are not statistically different when plotted within two standard deviations. The uncertainty between the measured and predicted data could have resulted because the earthen material on the top of the concrete ceiling is not uniform in the experiment. Generally, all predicted photon dose equivalent rate results show similarity to the results obtained from the experiment. The two results were therefore assumed to be equivalent. Moreover, the simulated photon dose equivalent rate results were all greater than the experimental photon dose equivalent rate results. This make the analysis conservative.

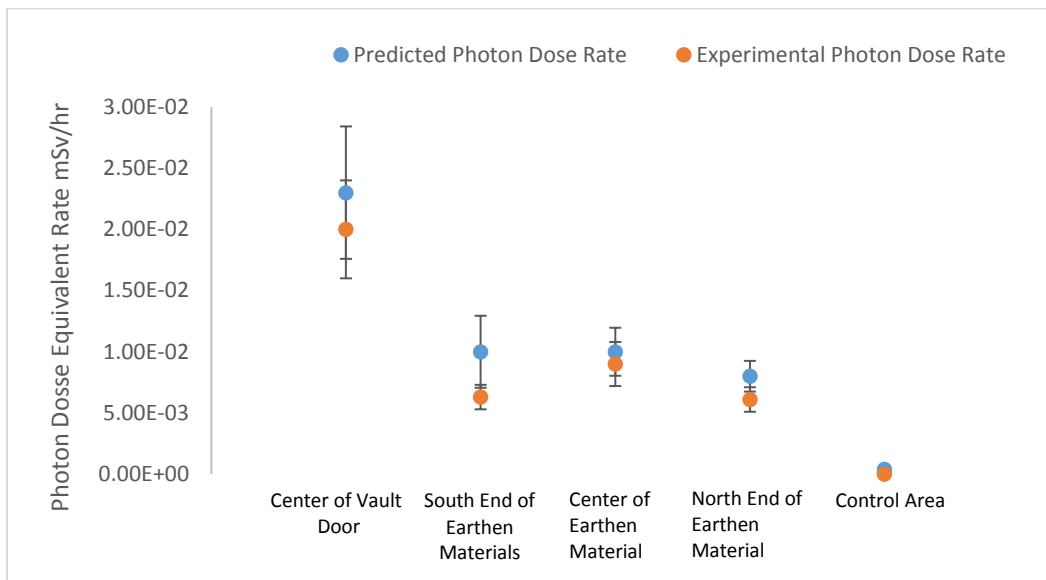


Figure 4.3 A Plot Comparing Predicted and Experimental Photon Dose Equivalent Rate

Figure 4.4 shows a plot comparing predicted neutron dose equivalent rate results to experimental neutron dose equivalent rate results for the five locations of interest. All five locations show no difference. The uncertainty in the measurements may have resulted from the unevenness of the

earthen material on the top of the concrete ceiling. The predicted neutron dose equivalent rates are greater than most of the experiment dose equivalent rate making the set of predictions conservative.

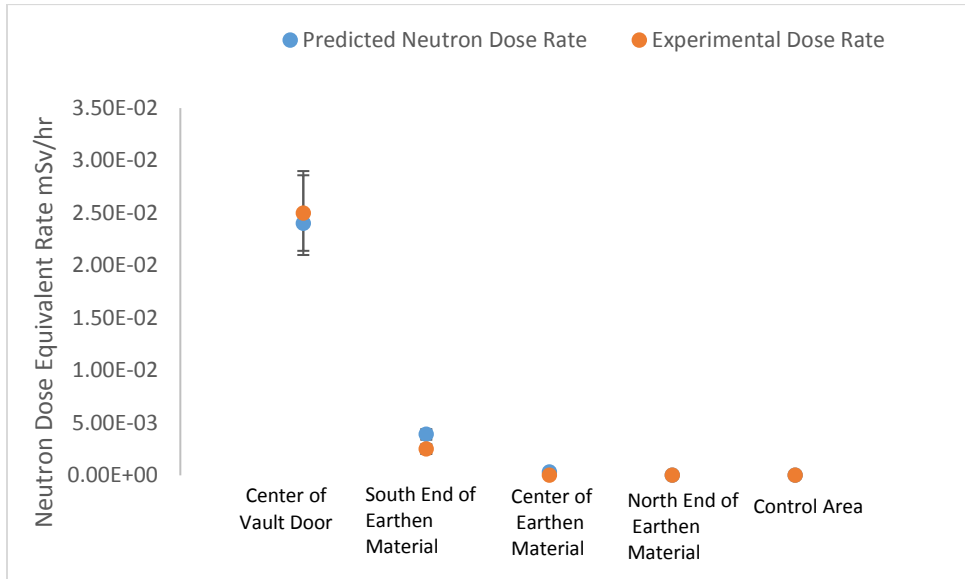


Figure 4.4: A Plot Comparing Simulated and Experimental Neutron Dose Equivalent Rate

Based on the comparisons the predicted and measured fluence rate and dose equivalent rates were concluded to be equivalent, the MCNP6 code was validated and hence this evaluation “benchmarked” MCNP used to predict the neutron and photon dose equivalent rate around the white room for this shielding study. Therefore, the code was expanded and subsequently used to predict how the increase in power from 1 to 10-kW would affect the dose equivalent rate at these locations of interest. The simulation also verified the assumption that there was a linear relationship between dose equivalent rate and power. The dose equivalent rate increased at each location of interest for both neutrons and photons by a factor of ten as shown in Table 4.6.

Table 4.6 Dose equivalent Rate Comparison between Simulation and Experiment at 10 kW Power

Dose Location	Predicted Photon Dose Rate (mSv·hr ⁻¹)	Predicted Neutron Dose Rate (mSv·hr ⁻¹)	Total Dose Equivalent Rate (mSv·hr ⁻¹)
Center of Vault Door	$0.23 \pm 2.7 \times 10^{-2}$	$0.24 \pm 3.6 \times 10^{-2}$	0.47
North end of Earthen Material	$0.10 \pm 1.5 \times 10^{-2}$	$0.039 \pm 4.6 \times 10^{-3}$	0.14
Top Center of Earthen Material	$0.10 \pm 1.0 \times 10^{-2}$	$0.003 \pm 5.1 \times 10^{-4}$	0.10
South end of Earthen Material	$0.08 \pm 6.4 \times 10^{-3}$	0.00 ± 0.00	0.08
Control Area	$0.006 \pm 7.8 \times 10^{-4}$	0.00 ± 0.00	0.006

The photon dose equivalent rate at the top of the white room at the front of the accelerator vault door were 0.10-mSv·hr⁻¹ and 0.23-mSv·hr⁻¹ respectively. The neutrons dose equivalent rate was as high as 0.039-mSv·hr⁻¹ and 0.24-mSv·hr⁻¹ for the same locations. The combined neutron and photon dose equivalent rates are also shown on the last column of Table 4.5. Out of the five locations, four would have dose equivalent rates that would be greater than the acceptable limit. The location of interest that was of most concern from a radiological protection point of view was the location of the accelerator control area. Combined dose equivalent rate for photons and neutrons at this location was calculated to be 0.006-mSv·hr⁻¹ at 10-kW of power. The summed value was below the accepted regulatory limit of 0.02-mSv in any one hour. The next location of concern outside the facility is the top of the LINAC vault. The highest combined dose equivalent rate was calculated to be 0.14-mSv·hr⁻¹ on the south end of the accelerator room. Although, the

location is open to the public, the likelihood that a member of the public would stand at this location, especially during radionuclide production, is very small. However, it is possible that a worker will be at this location to perform radiation survey during operation. Finally, the summed up neutron and photon dose equivalent rate at the center of the vault door was calculated to be $0.46\text{-mSv}\cdot\text{hr}^{-1}$ making the area beyond the accelerator vault door a high radiation area. A high radiation area is an area accessible to individuals, in which radiation levels from radiation sources external to the body could result in an individual receiving a dose equivalent in excess of 1 mSv in 1 hour at 30 cm from the radiation source or 30 cm from any surface that the radiation penetrates.

4.5 Comparison between Radiation Survey Data and Simulated Dose Equivalent Rates for Cu-67 Production

Dose equivalent rates measured for neutrons, photons and uncertainty associated with these measurements during Cu-67 production are shown on Table 4.7. Location 1 had dose equivalent rate for both neutrons and photon which when combined was greater than 0.02-mSv in any one-hour. The photon dose equivalent rate at location 2 was $0.02\text{-mSv}\cdot\text{hr}^{-1}$ and the neutron dose rate was at background level. Location 4 had a neutron dose equivalent rate of $0.016\text{-mSv}\cdot\text{hr}^{-1}$ and the photon dose equivalent rate was at background level. Locations 8 and 11 had dose equivalent rates for neutron and photons at background levels.

Table 4.7. Radiation Survey Data for Cu-67 Production

Radiation Survey		
Location	Neutron Dose equivalent Rate (mS.vhr⁻¹)	Photon Dose equivalent Rate (mSv.hr⁻¹)
1	$2.0 \times 10^{-2} \pm 2 \times 10^{-3}$	$2.0 \times 10^{-2} \pm 2.0 \times 10^{-3}$
2	$<2.5 \times 10^{-3} \pm < 2.5 \times 10^{-4}$	$1.9 \times 10^{-2} \pm 1.9 \times 10^{-3}$
4	$1.6 \times 10^{-2} \pm 1.6 \times 10^{-3}$	$<2.0 \times 10^{-3} \pm < 2.0 \times 10^{-4}$
8	$<2.5 \times 10^{-3} \pm < 2.5 \times 10^{-4}$	$<2.0 \times 10^{-3} \pm < 2.0 \times 10^{-4}$
11	$<2.5 \times 10^{-3} \pm < 2.5 \times 10^{-4}$	$<2.0 \times 10^{-3} \pm < 2.0 \times 10^{-4}$

The dose equivalent rates predicted by the model developed in MCNP6 for the same conditions but for Cu-67 production are shown in Table 4.8. Dose equivalent rate for neutrons and photons calculated for location 1 were both above the limit of 0.02-mSv in any one hour. The neutron dose equivalent rate at location 4 and the photon dose equivalent rate at location 2 were elevated as in the measured data. There was a slight increase in photon dose equivalent rate at location 8 compared to the measured data. Generally, neutron dose equivalent rates tended to be more consistent with measured data than photons.

Table 4.8: Predicted Radiation Results for Cu-67 Production

Predicted Result 7.24 kW		
Location	Neutron Dose equivalent Rate (mSv.hr ⁻¹)	Photon Dose equivalent Rate (mSv.hr ⁻¹)
1	$2.01 \times 10^{-2} \pm 3.02 \times 10^{-3}$	$2.2 \times 10^{-2} \pm 2.8 \times 10^{-3}$
2	$<2.0 \times 10^{-3} \pm < 2.5 \times 10^{-4}$	$2.2 \times 10^{-2} \pm 2.2 \times 10^{-3}$
4	$1.6 \times 10^{-2} \pm 2.08 \times 10^{-3}$	$<2.0 \times 10^{-3} \pm < 2.0 \times 10^{-4}$
8	$<2.0 \times 10^{-3} \pm < 2.5 \times 10^{-4}$	$5.0 \times 10^{-3} \pm 7.5 \times 10^{-4}$
11	$<2.0 \times 10^{-3} \pm < 2.5 \times 10^{-4}$	$<2.0 \times 10^{-3} \pm < 2.0 \times 10^{-4}$

Figure. 4.5 shows a graph comparing two sets of data; the predicted neutron dose equivalent rate from the MCNP6 model of the white room and the neutron dose equivalent rate obtained via radiation survey of the white room during Cu-67 production. The neutron dose equivalent rates at locations 2, 8 and 11 are all at background level for both data sets. Moreover, the neutron dose equivalent rates at locations 1 and 4, which had elevated dose rates, show significant overlap giving the likelihood that the two sets of data are essentially equivalent.

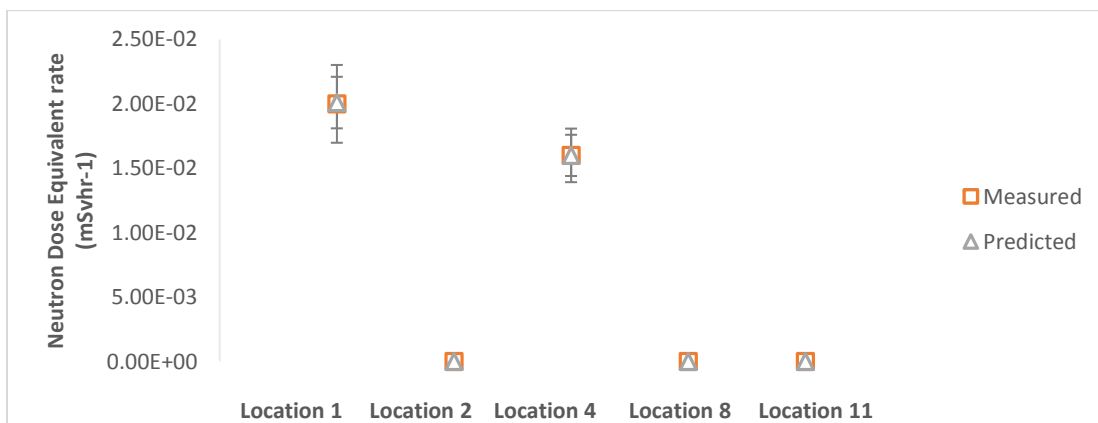


Figure 4.5: Comparing Neutron Predicted and Survey Dose Equivalent Rates around the white room During Cu-67 Production

Figure. 4.6 shows a graph comparing two sets of data; the predicted photon dose equivalent rate from the MCNP6 model of the white room and photon dose equivalent rate obtained via radiation survey of the white room during Cu-67 production. The photon dose equivalent rates at locations 4 and 11 are all at background level for both data sets. Although, the dose equivalent rate at Location 8 are at background level, the predicted value is high than the measured value. This could be because the meter used in measuring the dose equivalent rate is only sensitive to about 0.002 mSvhr^{-1} . Locations 1 and 2 have does equivalent rates that are greater than or equal to 0.02- mSv in any one hour. The error bars overlap between the predicted values and the values obtained through radiation survey. Therefore, the photon dose equivalent rates at these locations are indistinguishable. The predicted photon dose equivalent rates in Figure. 4.6 are slightly higher than the photon dose equivalent rates measured during radiation survey. However, this makes the predicted dose equivalent rate conservative. Since the predicted dose equivalent rate and the dose equivalent rate obtained from radiation survey are essentially equivalent, then MCNP6 is thought to be representative for this shielding upgrade and beam dump design study.

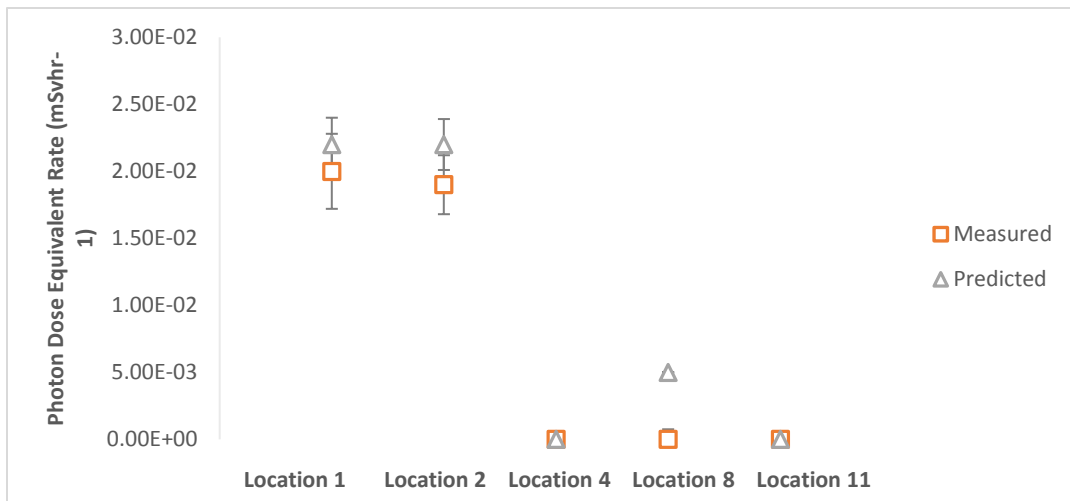


Figure 4.6: Comparing Predicted Photon Dose Equivalent Rate to Survey Dose Equivalent Rates around the white room During Cu-67 Production

4.6 Predicted Dose equivalent Rate Results for the Zn-68 Targets and that of Two Target Holders.

The model was used to predict the irradiation of the Zn-68 target with a 10-kW electron beam. The outcome of the simulation yielded the neutron and photon dose equivalent rates shown in Table 4.9. It is observed that an increase in beam power caused an increase in the dose equivalent rate at the various locations of interest. Pushing the dose equivalent to values that are beyond the 0.02-mSv allowed in any one hour.

Table 4.9. The Dose equivalent Rate results from Zn-68 for a 10-kW Beam

Predicted Result at 10 kW		
Location	Neutron Dose Equivalent Rate (mSv.hr⁻¹)	Photon Dose Equivalent Rate (mSvhr⁻¹)
1	$2.8 \times 10^{-2} \pm 4.2 \times 10^{-3}$	$3 \times 10^{-2} \pm 3.6 \times 10^{-3}$
2	$<2.0 \times 10^{-3} \pm < 2.5 \times 10^{-4}$	$3 \times 10^{-2} \pm 3.0 \times 10^{-3}$
4	$2.2 \times 10^{-2} \pm 2.9 \times 10^{-3}$	$<2.0 \times 10^{-3} \pm < 2.0 \times 10^{-4}$
8	$<2.0 \times 10^{-3} \pm < 2.58 \times 10^{-4}$	$7.0 \times 10^{-3} \pm 1.05 \times 10^{-3}$
11	$<2.0 \times 10^{-3} \pm < 2.5 \times 10^{-4}$	$<2.0 \times 10^{-3} \pm < 2.0 \times 10^{-4}$

Table 4.10 and Table 4.11 provide the predicted results of the dose equivalent rate at the locations of interest around the white room for the two new target holders. The dose equivalent values provided in these tables are for neutrons and photons produced from the targets when either configuration was irradiated with an electron beam of 10 kW. The dose equivalent rate predicted for target holder 1 were lower than dose equivalent rates predicted for target holder 2 for similar locations. These differences may be attributed to smaller mass of target holder 2 (i.e. there was in less material (aluminum) in the target holder 2).

Table 4.10. Predicted Dose Equivalent Rates for Kr/Xe Target Holder 1 at 10-kW

Location	Neutron Dose equivalent Rate (mSv.hr ⁻¹)	Photon Dose equivalent Rate (mSv.hr ⁻¹)
1	$< 2.0 \times 10^{-3} \pm < 2.5 \times 10^{-4}$	$3 \times 10^{-2} \pm 2.8 \times 10^{-3}$
2	$1.1 \times 10^{-2} \pm 9.9 \times 10^{-4}$	$< 2.0 \times 10^{-3} \pm < 2.0 \times 10^{-4}$
4	$< 2.0 \times 10^{-3} \pm < 2.5 \times 10^{-4}$	$< 2.0 \times 10^{-3} \pm < 2.0 \times 10^{-4}$
8	$3.0 \times 10^{-2} \pm 3.3 \times 10^{-3}$	$1.4 \times 10^{-2} \pm 2.1 \times 10^{-3}$
11	$< 2.0 \times 10^{-3} \pm < 2.5 \times 10^{-4}$	$< 2.0 \times 10^{-3} \pm < 2.0 \times 10^{-4}$

Table 4.11. Predicted Dose Equivalent Rates for Kr/Xe Target holder 2 at 10 kW

Location	Neutron Dose equivalent Rate (mSv.hr ⁻¹)	Photon Dose equivalent Rate (mSv.hr ⁻¹)
1	$2.9 \times 10^{-2} \pm 3.5 \times 10^{-3}$	$2.6 \times 10^{-2} \pm 3.1 \times 10^{-3}$
2	$8.0 \times 10^{-3} \pm 1.2 \times 10^{-3}$	$3.0 \times 10^{-2} \pm 4.2 \times 10^{-3}$
4	$2.2 \times 10^{-2} \pm 2.4 \times 10^{-3}$	$< 2.0 \times 10^{-3} \pm < 2.0 \times 10^{-4}$
8	$< 2.0 \times 10^{-3} \pm < 2.5 \times 10^{-4}$	$7.0 \times 10^{-3} \pm 9.1 \times 10^{-4}$
11	$< 2.0 \times 10^{-3} \pm < 2.5 \times 10^{-4}$	$< 2.0 \times 10^{-3} \pm < 2.0 \times 10^{-4}$

4.7 Predicted Dose Equivalent Rate around the White Room without Shield Upgrade or Beam Dump

Figure. 4.7. Shows a simulated dose equivalent rate map given neutron and photon-dose equivalent rates in mSv⁻¹ for a 10-kW beam during Cu-67 production. The dose-equivalent rates given on this dose equivalent rate map were predicted from a simulation without shield modifications around the target or beam dump. The dose-equivalent rate in red are dose-equivalent rates that were greater than 0.002-mSv⁻¹. In this map, neutron-dose equivalent rates at location 4, and 1 are all above the 0.02-mSv in any one-hour limit designated for the public. Likewise, the photon dose-equivalent rates in location 1 and 2 are above 0.02 mSv⁻¹.

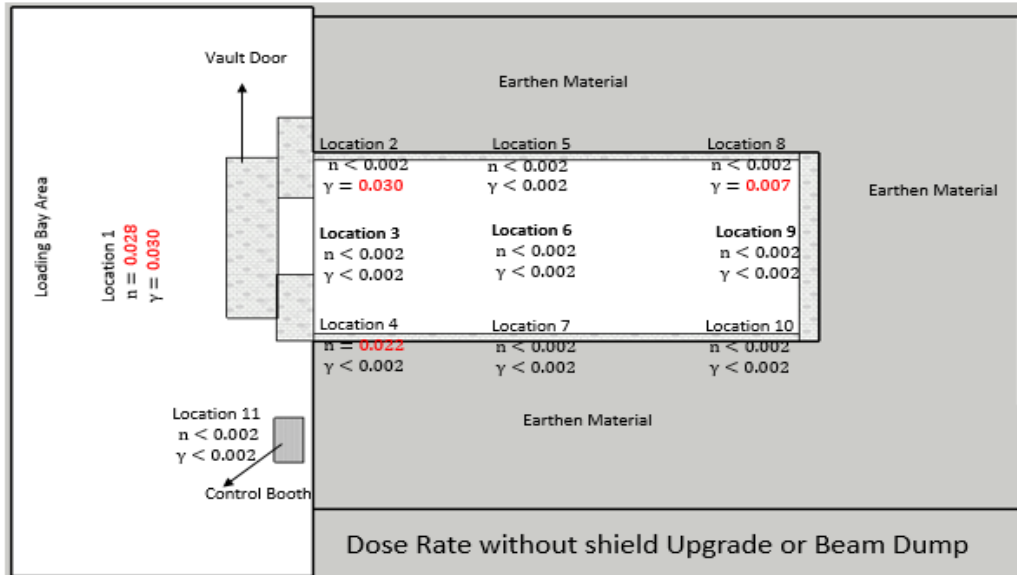


Figure 4.7. The equivalent dose rate in units of $\text{mSv}\cdot\text{hr}^{-1}$ around the white room without beam dump and shield upgrade

4.8. Predicted Dose Equivalent Rate around the White Room with Shield Upgrade and Beam Dump

Figures. 4.8, 4.9, 4.10 and 4.11. show the neutron and photon dose-equivalent rates around the white room for a 10-kW beam. The values shown on the dose rate maps are all in $\text{mSv}\cdot\text{hr}^{-1}$. Figure 4.5 shows the equivalent dose rate predicted around the white room with the shield upgrade; a beam dump made of aluminum and encased in concrete. The dose-equivalent rate in red show locations with values that are greater $0.002 \text{ mSv}\cdot\text{hr}^{-1}$. The highest dose equivalent rate predicted using an Al beam dump was at Location 4 for neutrons with a value of $0.015 \text{ mSv}\cdot\text{hr}^{-1}$. However, the equivalent dose rates at all locations were below the 0.02 mSv in any one hour.

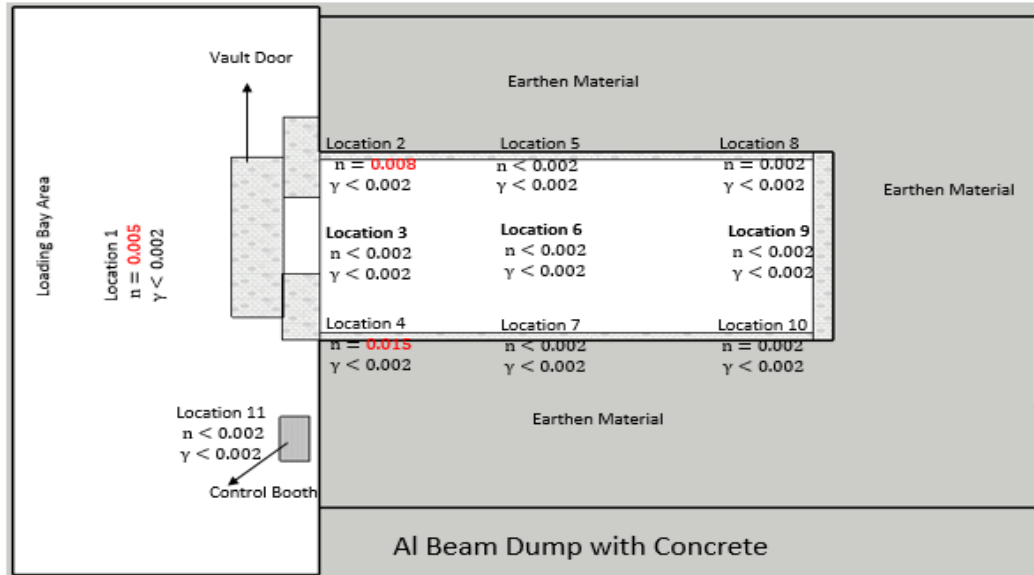


Figure 4.8. The Predicted Equivalent Dose Rate in units of $\text{mSv}\cdot\text{hr}^{-1}$ Around the White Room using Al Beam Dump Surrounded by Concrete

Figure. 4.9 shows the dose equivalent rate predicted when the beam dump material was changed from Al to pyrolytic carbon. The highest dose equivalent rate predicted by the model was at location 3 with a dose equivalent rate of $0.015 \text{ mSv}\cdot\text{hr}^{-1}$ for neutrons. Dose equivalent rates at all locations were below the 0.02 mSv in any one hour.

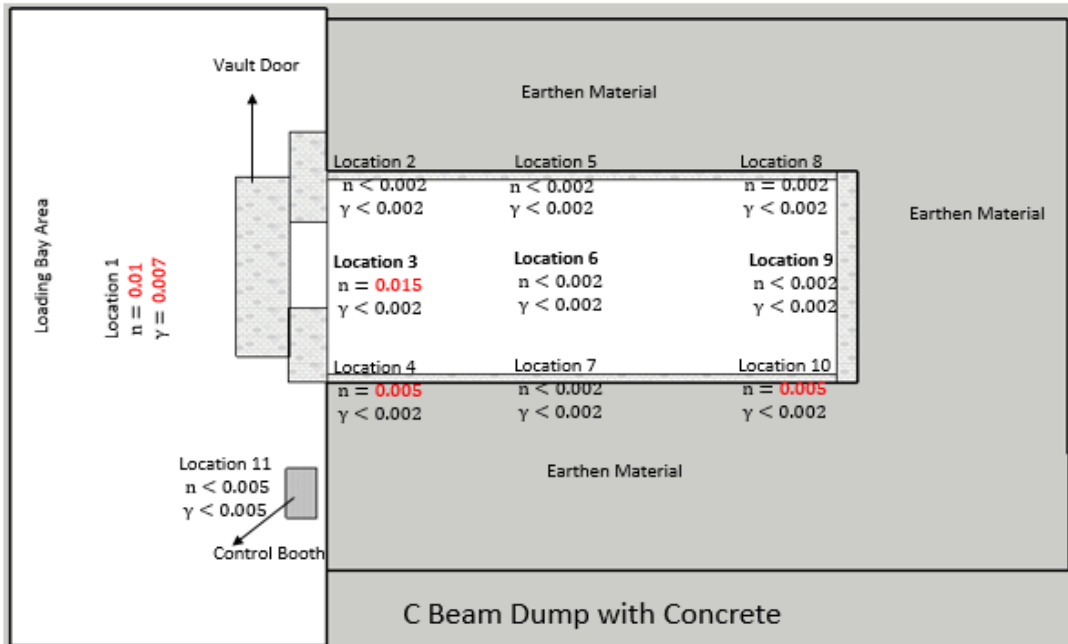


Figure 4.9. The Predicted Equivalent Dose Rate in Units of $\text{mSv}\cdot\text{hr}^{-1}$ Around the White Room using C Beam Dump Surrounded by Concrete

Figure. 4.10 shows the dose equivalent rate predicted when the beam dump material was changed to Cu. All value shown in the map have units of $\text{mSv}\cdot\text{hr}^{-1}$. The highest dose equivalent rate predicted by the model was at location 3 with a dose equivalent rate of $0.013 \text{ mSv}\cdot\text{hr}^{-1}$ for neutrons. Dose equivalent rates at all locations were below 0.02 mSv in any one hour.

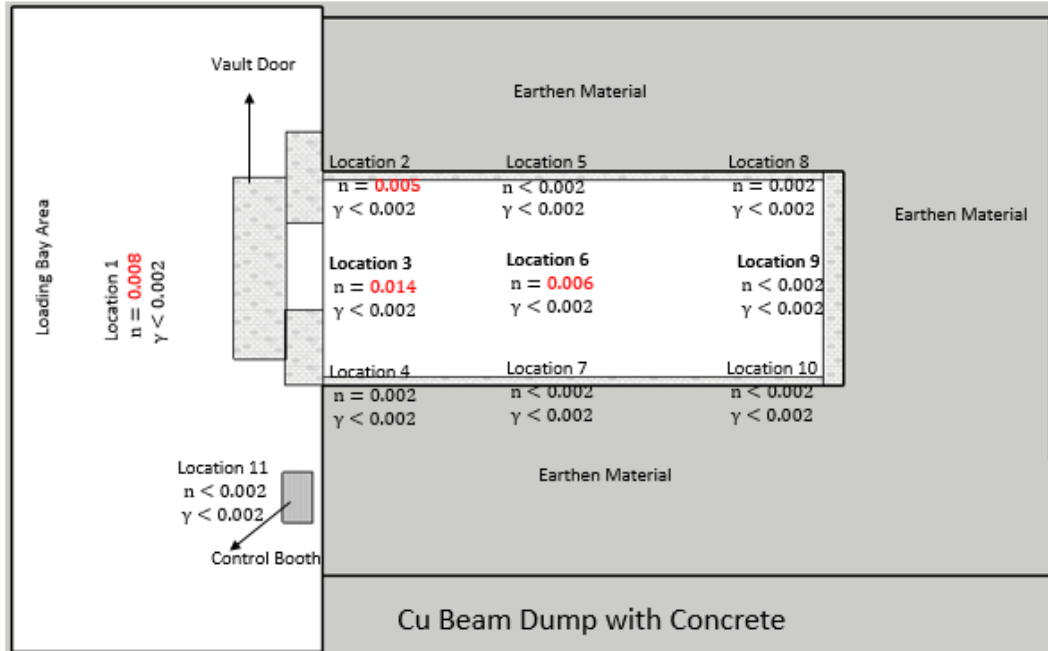


Figure 4.10 The Predicted Dose Equivalent Rate in Units of $\text{mSv}\cdot\text{hr}^{-1}$ Around the White Room using Cu Beam Dump Surrounded by Concrete

Figure. 4.11 shows the predicted dose equivalent rate around the white room for a beam dump made of ordinary concrete. The dose equivalent rate at all locations are below the limit of 0.02-mSv in any one hour. The highest dose equivalent rate was from neutrons at location 6 with a value of 0.012-mSv $\cdot\text{hr}^{-1}$. The highest dose equivalent rate predicted for photons is at location 1 for this design.

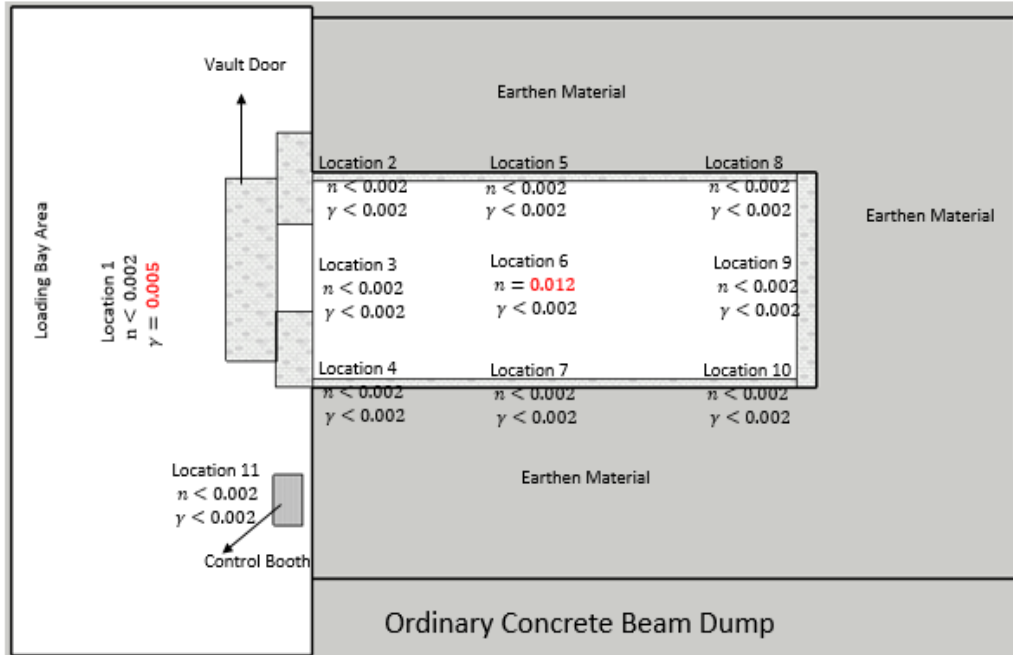


Figure 4.11 The Predicted Dose Equivalent Rate in units of $\text{mSv}\cdot\text{hr}^{-1}$ around the White Room using Ordinary Concrete as Beam Dump Material

The predicted dose equivalent rate around the white room for all materials (i.e. Cu, Al, C, and ordinary concrete) at all locations were all below the $0.02 \text{ mSv}\cdot\text{hr}^{-1}$ equivalent dose rate limit. Meaning any of the materials, provided the materials is surround by ordinary concrete and the shield modifications are in place, will be sufficient to suppress the dose equivalent rate to values below 0.02-mSv in any one hour. The down side to surrounding the beam dump materials with concrete is that there would be limited cooling. If the temperature of any of the materials rise above its melting point, especially for Al, the material will melt. Another limiting factor for using any of the other materials for construction of a beam dump is the cost of the materials.

4.9. Predicted Dose Equivalent Rate around the White Room when Beam Dump is immersed in Cooling Tank

If a design with a cooling tank was considered, the cost of construction would increase further because of investment that would be made in developing such a cooling tank. In addition to the cost of building a cooling tank, the change from concrete surrounding the beam dump to

water could likely compromise the integrity of the shielding. A modeling investigation was conducted to look at the effects of changes in dose equivalent rate around the white room. The Cu, Al and pyrolytic carbon beam dumps were immersed in a water tank in the model and simulations were carried out to predict the dose equivalent rate at the various locations of interest. Figure. 4.12 show the predicted dose equivalent rate obtained around the white room when the Al beam dump was immersed in water. All dose equivalent rates were in units of $\text{mSv}\cdot\text{hr}^{-1}$. The neutron dose equivalent rate at locations 2, 3, 4 and 10 all increased as can be seen in red fonts. The neutron dose-equivalent rate at location 2 was $0.03\text{-mSv}\cdot\text{hr}^{-1}$, which is above the recommended limit of 0.02-mSv in any one hour.

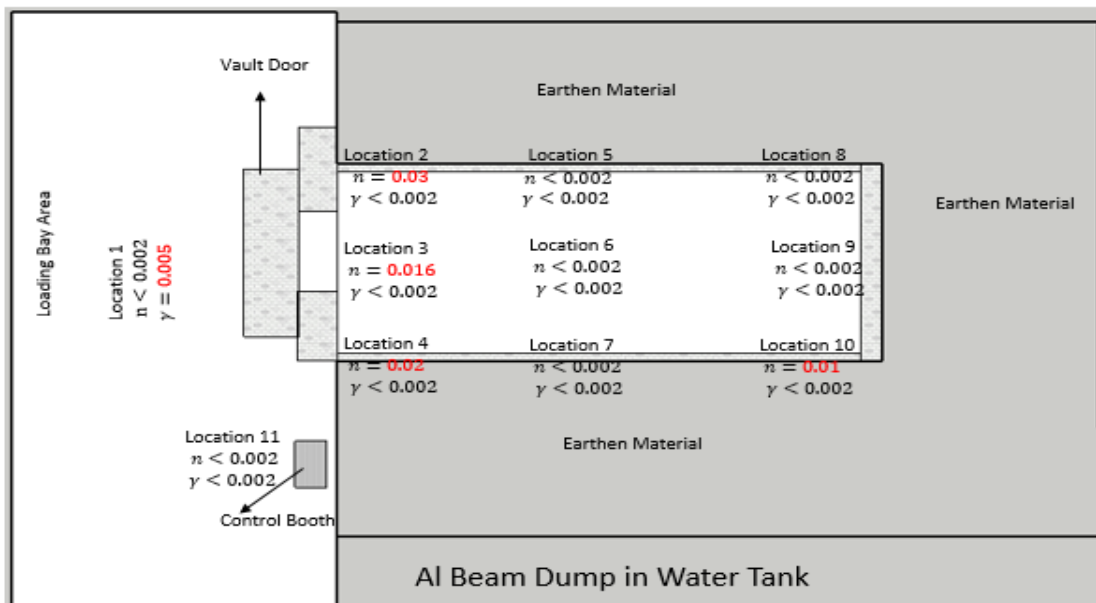


Figure 4.12. The Predicted Dose Equivalent Rate in units of $\text{mSv}\cdot\text{hr}^{-1}$ Around the White Room using Cu Beam Dump Surrounded by Water.

Figure 4.13 show the predicted dose equivalent rate around the white room for a C beam dump surrounded by tank of water. Similar to the case of an aluminum beam dump, Locations 1, 2, and 5 had elevated dose equivalent rates. Location 2 had the highest dose equivalent rate with a value of $3\text{-mSv}\cdot\text{hr}^{-1}$.

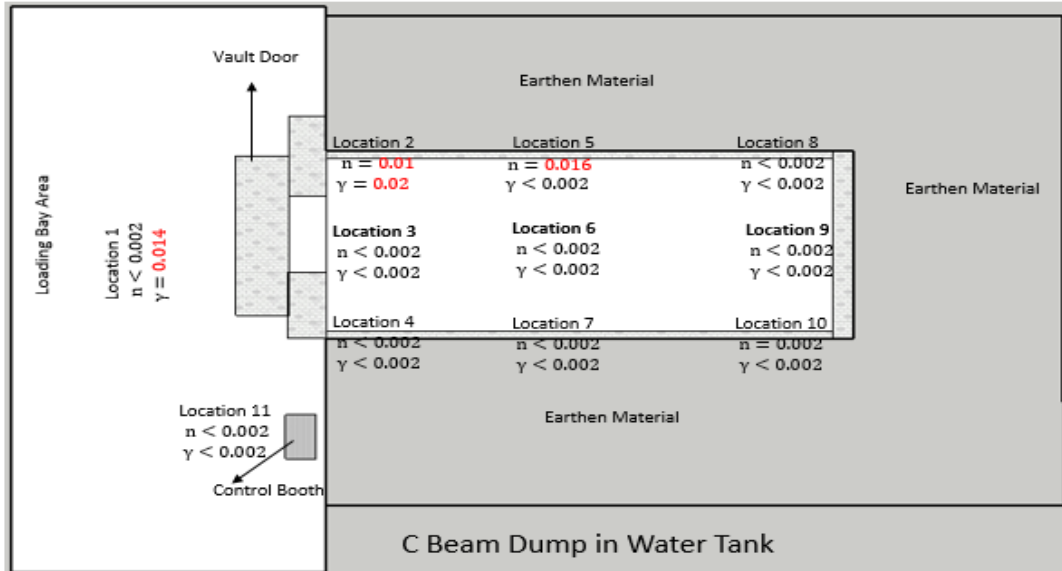


Figure 4.13. The Predicted Dose Equivalent Rate in units of $\text{mSv}\cdot\text{hr}^{-1}$ Around the White Room using C Beam Dump Surrounded by Water.

Figure. 4.14 shows the predicted dose equivalent rate around the white room for the Cu target as surrounded by water. Locations 2 and 6 show elevated dose equivalent rates. Location 2 had dose equivalent rate $0.01\text{-mSv}\cdot\text{hr}^{-1}$ and $0.02\text{-mSv}\cdot\text{hr}^{-1}$ for neutrons and photons respectively. Location 3 had a neutron dose equivalent rate of $0.03\text{-mSv}\cdot\text{hr}^{-1}$. The two location have dose equivalent rate that were greater than the recommended limit of 2-mSv in any one hour.

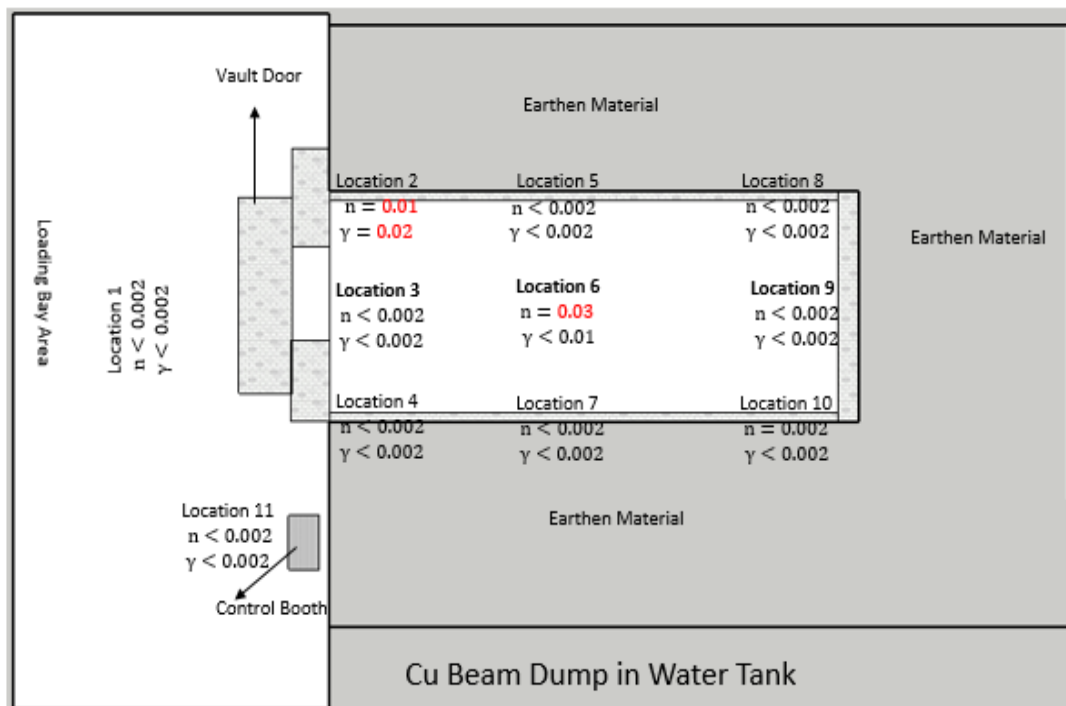


Figure 4.14. The Predicted Dose Equivalent Rate in units of $\text{mSv}\cdot\text{hr}^{-1}$ Around the White Room using C Beam Dump Surrounded by Water.

Chapter 5: CONCLUSION

A shielding analysis was performed for a new high power electron LINAC that was being built at the Idaho State University Idaho Accelerator Center. The results showed the shielding in place was adequate for all locations of interest except the front of the vault door. The combined neutron and photon dose rates calculated using MCNP6 were $0.014\text{-mSv}\cdot\text{hr}^{-1}$, $<0.0006\text{-mSv}\cdot\text{hr}^{-1}$ and $0.047\text{-mSv}\cdot\text{hr}^{-1}$ at 1-kW for the top of the LINAC vault, control area and in front of the vault door, respectively. When the predicted dose equivalent rate were scaled up for a 10 kW beam the dose equivalent rates for these locations were $0.14\text{-mSv}\cdot\text{hr}^{-1}$, $0.006\text{-mSv}\cdot\text{hr}^{-1}$ and $0.47\text{-mSv}\cdot\text{hr}^{-1}$. As a result, the need for a shielding upgrade was necessary before medical radionuclide production began.

Analyses show that at 10 kW, the room-inside-a-room in the white room was not sufficient to suppress the dose equivalent rates at some locations of interest around the white room for Cu-67 production and also for the two new target configuration at 10-kW beam power. All three targets had elevated dose equivalent rates at some locations that were above 0.02-mSv in any one hour. The combined dose equivalent rates predicted around the white room for a 10-kW beam when irradiating a Zn-68 target were, $0.058\text{-mSv}\cdot\text{hr}^{-1}$, $0.03\text{-mSv}\cdot\text{hr}^{-1}$, and $0.022\text{-mSv}\cdot\text{hr}^{-1}$ for locations 1, 2, and 4 respectively. The summed neutron and photon dose equivalent rate predicted for target holder 2 were $0.03\text{-mSv}\cdot\text{hr}^{-1}$, and $0.044\text{-mSv}\cdot\text{hr}^{-1}$ for locations 1 and 8 respectively. Finally, the combined dose equivalent rate predicted for target holder 2 were $0.055\text{-mSv}\cdot\text{hr}^{-1}$, $0.038\text{-mSv}\cdot\text{hr}^{-1}$, and $0.022\text{-mSv}\cdot\text{hr}^{-1}$ for locations 1, 2, and 4 respectively. The Zn-68 target and target holder 2 had similar and highest dose equivalent rates out of the three targets. Therefore, Zn-68 was chosen as a design basis to perform the shield upgrade and beam dump design analysis for the white room.

All materials analyzed (i.e. ordinary concrete, Cu, Al, and pyrolytic carbon) were sufficient to suppress the dose equivalent rate below 0.02-mSv in any one hour when modeled with the suggested shield upgrade and concrete surrounding the beam dump. However, it is most likely that the Al and Cu beam dumps may require cooling during operation. To see how the design would perform if the beam dumps were immersed in a water tank an additional set of Monte Carlo simulations were completed. The simulations predicted elevated dose equivalent rates that were greater than 0.02 mSv in any one hour at various locations of interest for Cu, Al, and pyrolytic carbon. The locations with dose equivalent rate greater than the limit included locations 2 and 4 for Al beam dumps, location 2 for the pyrolytic carbon beam dump, and location 2 and 6 for the Cu beam dump.

If a water tank design were to be used for shielding purposes, the thicknesses of the shield materials on top of the room-inside-a-room must be increased. Moreover, the possible need for cooling of Al and Cu beam dumps requires the addition of a water tank design thus making the system more complicated and expensive to build. Elemental materials (i.e. Cu, Al, and pyrolytic carbon) are also expensive. In view of the complications and expense, it would be prohibitive to construct a beam dump based on any of the three materials. It was suggested that the beam dump analyzed using ordinary concrete would be the most suitable to meet the shielding requirement of the white room.

FUTURE WORK

The interaction between the electron beam or Bremsstrahlung photons and the beam dump is going to produce a considerable amount of heat in the material used in constructing the beam dump. It will be important to perform heat and stress analyses on the beam dump model to determine how the high temperature produced in the beam dump because of these interactions would affect the material and the integrity of the shielding as a whole. In addition, a physical version should be constructed in the target room. After construction is done, the accelerator should be operated at unit power and a radiation survey performed to check the integrity of the upgrade. Subsequently, the power should be increased by 1-kW and each time a radiation survey should be used to check the dose equivalent rate at all locations of interest to ascertain that the 0.02-mSv limit is not exceeded. The process should be repeated until the maximum power is reached.

REFERENCES

- Ahlgren L., Olsson L. E. Induced Activity in a high-energy Linear Accelerator. *Phys. Med. Biol.*, 33, 351-354. 1988.
- Almen A., Ahlgren L., Mattsson S. Absorbed Dose to Technicians due to Induced Activity in Linear Accelerator for radiation Therapy. *Phys. Med. Biol.* 36, 815-822. 1991.
- Ayzatskiy N.I., Dikiy N.P., Dovbnaya A.N., Lyashko Y.V., Nikiforov V.I., Sramenko B.I., Tenishev A. E., Torgovkin A.V., Uvarov V.L., Comparison of Cu-67 Production at Cyclotron and Electron Accelerator. NSC "KIPT". Kharkov, 61108, Ukraine 2007.
- Bindu K. C., Harmon F., Starovoitova V., Stoner J., Wells P. D., Optimization of Commercial Scale Photonuclear Production of Radioisotopes. American Institute of Physics. 2010.
- Cossairt J.D., Vylet V., Edwards J.W., Topics in Accelerator Health Physics. Medical Physics Publishing. 2008.
- Culp P. A prediction of Accelerator- Produced Activation Products. *The Rad. Safety Journal.* 92, 2007.
- Dolley S. G., Van Der Walt T. N., Steyn G. F., Szelecsenyi F., Kovacs Z. The Production and Isolation of Cu-64 and Cu-67 from Zinc Target Materials and other Radionuclide. *Czechoslovak Journal of Phys.*, Vol. 56 2006.
- Fischer H. W., Tabot B., Poppe B. Comparison of Activation Products and Induced Dose Rates in Different High-Energy Medical Linear Accelerator. *Health Physics Society.* 94 2008.
- Hager I., Behaviour of Cement Concrete at High Temperature, *Bulletin of the Polish Academy of Sciences Technical Sciences*, Vol. 61, No. 1, 2013
- Harris E. D., Cellular Copper Transport and Metabolism. *Annu. Rev. Nutr.* 2000.
- Horibe O., Chatani H., Cross Sections of the Reactions Mn-55(n, 2n) Mn-54, Ni-58(n, 2n) Ni-57 and Ni-58(n, np) Co-50 Averaged Over the U-235 Fission Spectrum., S.M. Quim (ed.), *Nuclear Data Science and Technology*, Springer-Verlag Berlin Heidelberg, 1992.
- ICRP (1983) International Commission on Radiological Protection, Radionuclide Transformations Energy and Intensity of Emissions ICRP Publication 38 1983.
- ICRU (1985). International Commission on Radiation Unit, Determination of Dose Equivalent Resulting from External Radiation Exposure ICRU Report No. 39 1985.
- ICRU (1988) International Commission on Radiation Units, Determination of Dose Equivalents Resulting from External Radiation Exposure, ICRU Report No. 43 1988.
- Karzmark C. J., Nunan C. S., Tanabe E., *Medical Electron Accelerators* McGraw-Hill, INC. 1993
- Lee Y., Cho Y. S., Chang J., Shielding Design Calculations for Beam Dump Facility of KOMAC, *Radiation Protection Dosimetry*, Vol. 116, pp 259-263, 2005.
- Lee Y., Cho Y. S., Chang J., Preliminary Shielding Assessment for the 100MeV Proton LINAC (KOMAC), *Radiation Protection Dosimetry*, Vol. 115, pp 569-572, 2005.

Leuscher A., Schimitz M., Schwartz A. S., Tesch N., Design Study for an 18-MW Beam Dump at the Future Electron Positron Linear Collider TESLA. Deutsches Elektronen-Synchrotron, DESY. Notkestrasse 85, D-22607 Hamburg, Germany, 2004.

LUDELUM Measurements, Inc., LUDELUM Model 12-4 Ion Chamber Product Manual. Sweetwater Texas 2009

LUDELUM Measurements, Inc., LUDELUM Model 9-3 Ion Chamber Product Manual. Sweetwater Texas 2010

Monte Carlo N-Particle Code Version 6. User's Manual version 1.0 2013.

Mashnik S. G., Bull J. S., Hughes H. G., Prael R. E., Sierk A. J. Current Status of MCNP6 as a Simulation Tool useful for Space and Accelerator Applications. LANL 2012.

NCRP (2003). National Council on Radiation Protection and Measurement. Radiation Protection for Particle Accelerator Facilities, NCRP Report No. 144 (National Council on Radiation Protection and Measurement, Bethesda, Maryland) 2003.

Ni J., Block R. C., Xu X. G., Photon Activation Analysis: A Proof of Principle using a NIST Sediment Standard and an Electron Accelerator at Rensselaer Polytechnic Institute. Applied Radiation and Isotope 53. Pg. 535-540 2000.

Novak-Hofer I., Schubiger P. A., Copper-67 as a Therapy Nuclide for Radio-immunotherapy. Center for Radiopharmaceutical Science Switzerland 2002.

Ohnishi S., Maebara S., Sakaki Y., Sato S., Ochiai K., Konno C., Radiation Shielding Design for IFMIF/EVEDA Accelerator Vault. J Plasma Fusion Res. SERIES, Vol. 9 2010.

Perrin B., Walker A., Mackay R., A Model to Calculate the induced Dose Rate around an 18MeV ELEKTA Linear Accelerator. Phys. Med. Biol. 48, 75-81, 2003.

Radiation Safety Information Computational Center (RSICC) Computer Code Collection, Monte Carlo N-Particle Version 6. 2008.

Schmitt H. W., Halperin J., Al-27(n, alpha) Na-24 Cross Section as a Function of Neutron Energy. Oak Ridge National Laboratory, Oak Ridge Tennessee, Physical Review Vol. 121, #3 1960

Segebade C., Weise H., Lutz G. J., Photon Activation Analysis. W. De Gruyter, 1988.

Semkova V., Plompen A. J. M., Neutron-Induced Dosimetry Reaction Cross-Section Measurement from the Threshold up to 20 MeV. Radiation Protection Dosimetry, Vol., 126, No. 1-4, pp. 126-129 2007

Shultis J. K., Faw R. E. An MCNP Primer. Kansas State University, 2011

Smith C. H., He Y., Sinclair C. K., Design for a 1.3 MW, 13 MeV Beam Dump for an Energy Recovery LINAC. PAC pp 1877-1879 2005.

Starovoitova V., Foote D., Harris J., Makarashvili V., Segebade C. R., Sinha V., Wells P. D., Cu-67 Photonuclear Production. American Institute of Physics. 2011

Takei H., Takeda Y. Beam Dump for High Current Electron Beam at JNC. Second International Workshop on EGS. 2000.

Appendix A

Aluminum Beam Dump Dose Equivalent Rate Input File

```
MCNPX Visual Editor Version X_24E
c      Created on: Saturday, April 2, 2016 at 11:11
  1      0      -1 -3 4  $inside of beam pipe
  2      0      -2 1 -3 4  $thickness of beam pipe
  3      230 -0.001225 (2 :3 :-4 )-5 (-7 :8 :6 )(-9 :10 :6 )(-11 :12 :6
)
      (-13 :14 :6 )(-15 :16 :6 )(-17 :18 :6 )(-26 :27 :6 )
      (-28 :29 :19 )30 31 32 33 34 35 36 37 38 39 40 41 42 43 45
46 47 49
      51 53 55 57 58 60 62 64 66 68 70 72 74 79 165 166
  4      0      5  $universe
  5      160      -4.5 7 -8 -6  $ Ti 1 (Ti=Titanium)
  6      130      -1 9 -10 -6  $Water thicknes btw Ti 1 an
  7      160      -4.5 11 -12 -6  $ Ti 2
  8      230 -0.001225 13 -14 -6  $$Space btw window & target
  9      160      -4.5 15 -16 -6  $ Ti 3 in target
 10      130      -1 17 -18 -6 (-20 :21 :19 )(-22 :23 :19 ) $ space in
Target
      (-24 :25 :19 )
 11      140      -19.3 20 -21 -19  $ W 1
 12      140      -19.3 22 -23 -19  $ W 2
 13      140      -19.3 24 -25 -19  $ W 3
 14      160      -4.5 26 -27 -6  $ Ti 4
 15      190      -7.13 28 -29 -19  $ zinc Target
 16      220      -2.32 -30  $vault east wall
 17      220      -2.32 -31  $vault west wall
 18      220      -2.32 -32  $vault south wall
 19      220      -2.32 -33 44  $vault north wall
 20      220      -2.32 -34  $vault floor
 21      220      -2.32 -35 (76 :-77 :78 ) $vault Ceiling
 22      220      -2.32 -36  $beam dump west wall
 23      220      -2.32 -37 (81 :-83 :84 )(85 :-87 :88 ) $beam dump sout
      (89 :-91 :92 )(93 :-95 :96 )(97 :-99 :100 )(101 :-103 :104
)
      (105 :-107 :108 )(109 :-111 :112 )(113 :-115 :116 )(117 :-
119 :120 )
      (121 :-123 :124 )(125 :-127 :128 )(129 :-131 :132 )(133 :-
135 :136 )
      (137 :-139 :140 )(141 :-143 :144 )(145 :-147 :148 )(149 :-
151 :152 )
      (153 :-154 :155 )(156 :-157 :158 )(159 :-160 :161 )(162 :-
163 :164 )
 24      220      -2.32 -38  $beam dump east wall
 25      220      -2.32 -39 56  $beam dump north wall
 26      220      -2.32 -40  $beam dump door
 27      170      -7.87 -41  $steel layer of beam dump ceilin
 28      220      -2.32 -42  $concreat layer of beam dump cei
 29      180      -11.34 -43  $lead layer of beam dump ceiling
```

30	230	-0.001225	-44		\$vault door opening
31	220	-2.32	-45		\$vault door
32	210	-1.65	-46		\$dirt on top of vault (Changed to high density)
33	150	-1	-47	48	\$ICRU SW 2
34	150	-1	-48		
35	150	-1	-49	50	\$ICRU Center 2
36	150	-1	-50		
37	150	-1	-51	52	\$ICRU NW 2
38	150	-1	-52		
39	150	-1	-53	54	\$ICRU Door
40	150	-1	-54		
41	250	-0.9	-55		\$ borated poly layer of beam dump
42	230	-0.001225	-56		
43	180	-11.34	-57		\$ lead
44	150	-1	-58	59	\$ICRU Sphere
45	150	-1	-59		\$ICRU Spere
46	150	-1	-60	61	\$ICRU @ 1 meter
47	150	-1	-61		
48	150	-1	-62	63	\$ICRU SW 2
49	150	-1	-63		
50	150	-1	-64	65	\$ICRU SW 3
51	150	-1	-65		
52	150	-1	-66	67	\$ICRU Center 1
53	150	-1	-67		
54	150	-1	-68	69	\$ICRU Center 3
55	150	-1	-69		
56	150	-1	-70	71	\$ICRU NW 1
57	150	-1	-71		
58	150	-1	-72	73	\$ICRU NW 3
59	150	-1	-73		
60	150	-1	-74	75	
61	150	-1	-75		
62	230	-0.001225	-76	77 -78	\$ hole in ceiling
63	150	-1	-79	80	
64	150	-1	-80		
65	230	-0.001225	-82	83 -84	
66	208	-2.699	-81	83 -84 (82 :-83 :84)	
67	230	-0.001225	-86	87 -88	
68	208	-2.699	-85	87 -88 (86 :-87 :88)	
69	230	-0.001225	-90	91 -92	
70	208	-2.699	-89	91 -92 (90 :-91 :92)	
71	230	-0.001225	-94	95 -96	
72	208	-2.699	-93	95 -96 (94 :-95 :96)	
73	230	-0.001225	-98	99 -100	
74	208	-2.699	-97	99 -100 (98 :-99 :100)	
75	230	-0.001225	-102	103 -104	
76	208	-2.699	-101	103 -104 (102 :-103 :104)	
77	230	-0.001225	-106	107 -108	
78	208	-2.699	-105	107 -108 (106 :-107 :108)	
79	230	-0.001225	-110	111 -112	
80	208	-2.699	-109	111 -112 (110 :-111 :112)	

```

81 230 -0.001225 -114 115 -116
82 208 -2.699 -113 115 -116 (114 :-115 :116 )
83 230 -0.001225 -118 119 -120
84 208 -2.699 -117 119 -120 (118 :-119 :120 )
85 230 -0.001225 -122 123 -124
86 208 -2.699 -121 123 -124 (122 :-123 :124 )
87 230 -0.001225 -126 127 -128
88 208 -2.699 -125 127 -128 (126 :-127 :128 )
89 230 -0.001225 -130 131 -132
90 208 -2.699 -129 131 -132 (130 :-131 :132 )
91 230 -0.001225 -134 135 -136
92 208 -2.699 -133 135 -136 (134 :-135 :136 )
93 230 -0.001225 -138 139 -140
94 208 -2.699 -137 139 -140 (138 :-139 :140 )
95 230 -0.001225 -142 143 -144
96 208 -2.699 -141 143 -144 (142 :-143 :144 )
97 230 -0.001225 -146 147 -148
98 208 -2.699 -145 147 -148 (146 :-147 :148 )
99 230 -0.001225 -150 151 -152
100 208 -2.699 -149 151 -152 (150 :-151 :152 )
101 208 -2.699 -153 154 -155
102 208 -2.699 -156 157 -158
103 208 -2.699 -159 160 -161
104 208 -2.699 -162 163 -164
105 250 -0.9 -165
106 180 -11.34 -166

```

c Surface

```

1 c/z 0 0 6 $inner beam pipe
2 c/z 0 0 7 $outer beam pipe
3 pz 50 $top of beam window
4 pz 30 $bottom of beam window
5 so 3000 $universe
6 c/z 0 0 10 $Ti 1
7 pz 50 $bottom of Ti 1
8 pz 50.0127 $top of Ti 1
9 pz 50.0127 $bottom of water thickness
10 pz 50.872 $top of water thickness
11 pz 50.872 $bottom of Ti 2
12 pz 50.884 $top of Ti 2
13 pz 50.884 $bottom of space btw window and target
14 pz 51.646 $top of space btw window and target
15 pz 51.646 $bottom of Ti 3 in target
16 pz 51.658 $top of Ti 3 in target
17 pz 51.658 $bottom of distance btw Ti 3 and Ti 4
18 pz 53.593 $top of distance btw Ti 3 and Ti 4
19 c/z 0 0 1.25 $tungsten disk
20 pz 52.079 $Bottom of W 1
21 pz 52.228 $top of W 1
22 pz 52.482 $bottom of W 2
23 pz 52.634 $top of W 2
24 pz 52.888 $bottom of W 3

```

25 pz 53.037 \$top of W 3
26 pz 53.593 \$bottom of Ti 4
27 pz 53.605 \$top of Ti 4
28 pz 53.605 \$bottom of Target pipe
29 pz 56.605 \$stop of Target Pipe
30 rpp -136 -111 -100 523 -1248 215 \$Vault east wall
31 rpp 455 531 -100 523 -1248 215 \$vault west wall
32 rpp -136 531 -100 523 215 240 \$vault south wall
33 rpp -136 531 -100 265 -1324 -1248 \$vault north wall
34 rpp -136 480 -125 -100 -1324 240 \$vault floor
35 rpp -111 455 265 290 -1248 215 \$vault ceiling (xz reduced
by 25)
36 rpp 40 93 -100 30 39 215 \$beam dump west wall
37 rpp -72 40 -100 30 60 215 \$beam dump south wall
38 rpp -111 -72 -100 30 -10 215 \$beam dump east wall
39 rpp -111 93 -100 30 -38 -10 \$beam dum north wall
40 rpp 93 118 -100 45 -30 69 \$beam dump door
41 rpp -111 93 30 32.5 -38 215 \$steel layer of BD ceiling
42 rpp -111 93 32.5 56 -38 215 \$concrete layer of BD ceiling
43 rpp -111 93 56 61 -38 215 \$lead layer of BD Ceiling
44 rpp -10 249 -100 128 -1324 -1248 \$vault door opening
45 rpp -30 269 -100 148 -1400 -1324 \$(-z=1400 to z=-
1376)vault door
46 arb -111 290 -1248 455 290 -1248 -111 290 215 \$dirt on top
of vault
455 290
455 290
-1248 1234 3456 5612 2647 1538 0
47 s 172 628 50 15 \$ICUR South Wall (SW 2)
48 s 172 628 50 14
49 s 172 530 -542 15 \$ICRU Center 2
50 s 172 530 -542 14
51 s 172 455 -1000 15 \$ICRU North Wall (NW 2)
52 s 172 455 -1000 14
53 s 10 14 -1430 15 \$ICRU vault door (z= -1415 to -1445)
54 s 10 14 -1430 14 \$ (x= 150 to 10)
55 rpp -111 93 61 71 -38 215 \$Borated poly layer of BD
Ceiling
56 rpp -20 15 -18 10 -38 -10 \$ (x=-10, 10 to x=-20, 15)air
behind BP
57 rpp -23 20 -20 11 -39 -38 \$ Lead shield behind beam pipe
58 s 681 14 -1200 15 \$ICRU Control Area
59 s 681 14 -1200 14 \$ICRU 1 cm deep
60 s 150 14 -1500 15 \$ICRU (x=150 to x=135) @ 1 meter from
V. door
61 s 150 14 -1500 14
62 s -55 628 50 15 \$ICRU (SW 1)
63 s -55 628 50 14
64 s 400 628 50 15 \$ICRU (SW 3)
65 s 400 628 50 14
66 s -55 530 -542 15 \$ICRU Center 1
67 s -55 530 -542 14

```

68      s 400 530 -542 15  $ICRU Center 3
69      s 400 530 -542 14
70      s -55 455 -1000 15  $ICRU NW 1
71      s -55 455 -1000 14
72      s 400 455 -1000 15  $ICRU NW 3
73      s 400 455 -1000 14
74      s 135 14 -1430 15  $ICRU Center (x=150 to x=135)
75      s 135 14 -1430 14
76      c/y -91 -1224 5
77      py 265
78      py 290
79      s -91 390 -1224 15
80      s -91 390 -1224 14
81      cz 15  $beam dump disk 1
82      cz 10
83      pz 60
84      pz 65
85      cz 15
86      cz 9.5
87      pz 65
88      pz 70
89      cz 15
90      cz 9
91      pz 70
92      pz 75
93      cz 15
94      cz 8.5
95      pz 75
96      pz 80
97      cz 15
98      cz 8
99      pz 80
100     pz 85
101     cz 13
102     cz 7.5
103     pz 85
104     pz 90
105     cz 13
106     cz 7
107     pz 90
108     pz 95
109     cz 13
110     cz 6.5
111     pz 95
112     pz 100
113     cz 13
114     cz 6
115     pz 100
116     pz 105
117     cz 13
118     cz 5.5
119     pz 105

```

120	pz	110							
121	cz	11							
122	cz	5							
123	pz	110							
124	pz	115							
125	cz	11							
126	cz	4.5							
127	pz	115							
128	pz	120							
129	cz	11							
130	cz	4							
131	pz	120							
132	pz	125							
133	cz	11							
134	cz	3.5							
135	pz	125							
136	pz	130							
137	cz	11							
138	cz	3							
139	pz	130							
140	pz	135							
141	cz	11							
142	cz	2.5							
143	pz	135							
144	pz	140							
145	cz	11							
146	cz	2							
147	pz	140							
148	pz	145							
149	cz	11							
150	cz	1.5							
151	pz	145							
152	pz	150							
153	cz	11							
154	pz	150							
155	pz	155							
156	cz	11							
157	pz	155							
158	pz	160							
159	cz	11							
160	pz	160							
161	pz	165							
162	cz	11							
163	pz	165							
164	pz	170							
165	rpp	-23 20 -20 11 -70 -39	\$poly shield behind BP						
166	rpp	-23 20 -21 11 -71 -70	\$ lead						

mode	n p e				
m120	7014.70c	-0.755636	\$Air		
	8016.70c	-0.231475	18040.70c	-0.012889	
m130	1002.70c	-0.667	\$Water		

	8016.70c	-0.333				
m140	74182.70c	-0.260586	\$Tungsten			
	74183.70c	-0.142269	74184.	-0.307531	74186.70c	-
	0.289615					
m150	8016.	-0.762	\$phanthom			
	6012.	-0.111	1002.	-0.101	7014.70c	-
	0.026					
m160	22048.	-1	\$Titanium			
m170	6012.	-0.005	\$Steel, Carbon,			
	26054.70c	-0.056701	26056.70c	-0.914106	26057.70c	-
	0.021303					
	26058.70c	-0.00289				
m190	30068.70c	-1	\$Zinc 68			
m210	8016.70c	-0.5134	\$soil (dry U.S. Ave. with ENDF-VI)			
	11023.70c	-0.006	12024.70c	-0.010134	12025.70c	-
	0.001336					
	12026.70c	-0.00153	13027.70c	-0.067	14028.70c	-
	0.253938					
	14029.70c	-0.013317	14030.70c	-0.009145	20040.70c	-
	0.063341					
	20042.70c	-0.000339	20043.70c	-7.2e-005	20044.70c	-
	0.001133					
	20046.70c	-2e-006	20048.70c	-0.000112	22046.70c	-
	0.000346					
	22047.70c	-0.000322	22048.70c	-0.003326	22049.70c	-
	0.000253					
	22050.70c	-0.000253	25055.70c	-0.0007	26054.70c	-
	0.003134					
	26056.70c	-0.050528	26057.70c	-0.001178	26058.70c	-
	0.00016					
m220	1002.70c	-0.0075	\$Concrete, ordinary,			
	6012.50c	-0.055502	8016.70c	-0.492926	16032.70c	-
	0.16984					
	16033.70c	-0.001382	16034.70c	-0.007995	16036.70c	
	-4e-005					
	20040.70c	-0.221889	20042.70c	-0.009052	20043.70c	-
	0.000332					
	20044.70c	-0.005202	20046.70c	-1.1e-005	20048.70c	-
	0.000514					
	26054.70c	-0.000467	26056.70c	-0.007525	26057.70c	-
	0.000175					
	26058.70c	-2.4e-005				
m230	7014.70c	-0.755636	\$air (US S. Atm at sea level)			
	8016.70c	-0.231475	18036.70c	-3.9e-005	18038.70c	
	-8e-006					
	18040.70c	-0.012842				
m180	82206.70c	-0.253338	\$Lead,			
	82207.70c	-0.220743	82208.70c	-0.525919		
m250	1002.70c	-0.133711	\$ borated polyethylene			
	6012.70c	-0.816289	5010.70c	-0.05		
m240	29000.70c	-1	\$ copper			
m208	13027.70c	-1	\$aluminum			

```

imp:n  1          0          1          0          1 10r
$ 1, 15
      0          1          0          1          0
$ 16, 20
      1 2r          0          1 81r          $ 21, 106
imp:p  1          0          1          0          1 10r
$ 1, 15
      0          1          0          1          0
$ 16, 20
      1 2r          0          1 81r          $ 21, 106
imp:e  1          0 2r          1 10r          0 48r          1 39r
$ 1, 104
      0 1r          $ 105, 106
cut:e j 0.1
cut:p j 0.1
phys:e 5j 10 j 0
phys:p 3j 1
phys:n 50
sdef pos 0 0 0 axs 0 0 1 rad d1 ext d2 erg 40 vec 0 0 1 par e
si1 0 0.25
sp1 -21 1
si2 48 49.9
sp2 -21 0
f2:n 48
fm2 1.1298e15
df2 iu=1 ic=20
f12:n 50
fm12 1.1298e15
df12 iu=1 ic=20
f22:n 52
fm22 1.1298e15
df22 iu=1 ic=20
f32:n 54
fm32 1.1298e15
df32 iu=1 ic=20
f42:n 59
fm42 1.1298e15
df42 iu=1 ic=20
f52:n 61
fm52 1.1298e15
df52 iu=1 ic=20
f62:n 63
fm62 1.1298e15
df62 iu=1 ic=20
f72:n 65
fm72 1.1298e15
df72 iu=1 ic=20
f82:n 67
fm82 1.1298e15
df82 iu=1 ic=20
f92:n 69
fm92 1.1298e15

```

df92 iu=1 ic=20
f102:n 71
fm102 1.1298e15
df102 iu=1 ic=20
f112:n 73
fm112 1.1298e15
df112 iu=1 ic=20
f242:n 75
fm242 1.1298e15
df242 iu=1 ic=20
f262:n 80
fm262 1.1298e15
df262 iu=1 ic=20
f122:p 48
fm122 1.1298e15
df122 iu=1 ic=20
f132:p 50
fm132 1.1298e15
df132 iu=1 ic=20
f142:p 52
fm142 1.1298e15
df142 iu=1 ic=20
f152:p 54
fm152 1.1298e15
df152 iu=1 ic=20
f162:p 59
fm162 1.1298e15
df162 iu=1 ic=20
f172:p 61
fm172 1.1298e15
df172 iu=1 ic=20
f182:p 63
fm182 1.1298e15
df182 iu=1 ic=20
f192:p 65
fm192 1.1298e15
df192 iu=1 ic=20
f202:p 67
fm202 1.1298e15
df202 iu=1 ic=20
f212:p 69
fm212 1.1298e15
df212 iu=1 ic=20
f222:p 71
fm222 1.1298e15
df222 iu=1 ic=20
f232:p 73
fm232 1.1298e15
df232 iu=1 ic=20
f252:p 75
fm252 1.1298e15
df252 iu=1 ic=20

```
f272:p 80  
fm272 1.1298e15  
df272 iu=1 ic=20  
print  
ctme 20000
```

Appendix B

Graphite Beam Dump Dose Equivalent Rate Input File

```
MCNPF Visual Editor Version X_24E
c      Created on: Saturday, April 2, 2016 at 11:11
  1      0      -1 -3 4  $inside of beam pipe
  2      0      -2 1 -3 4  $thickness of beam pipe
  3      230 -0.001225 (2 :3 :-4 )-5 (-7 :8 :6 )(-9 :10 :6 )(-11 :12 :6
)
      (-13 :14 :6 )(-15 :16 :6 )(-17 :18 :6 )(-26 :27 :6 )
      (-28 :29 :19 )30 31 32 33 34 35 36 37 38 39 40 41 42 43 45
46 47 49
      51 53 55 57 58 60 62 64 66 68 70 72 74 79 165 166
  4      0      5  $universe
  5      160      -4.5 7 -8 -6  $ Ti 1 (Ti=Titanium)
  6      130      -1 9 -10 -6  $Water thicknes btw Ti 1 an
  7      160      -4.5 11 -12 -6  $ Ti 2
  8      230 -0.001225 13 -14 -6  $Space btw window & target
  9      160      -4.5 15 -16 -6  $ Ti 3 in target
  10     130      -1 17 -18 -6 (-20 :21 :19 )(-22 :23 :19 ) $ space in
Target
      (-24 :25 :19 )
  11     140      -19.3 20 -21 -19  $ W 1
  12     140      -19.3 22 -23 -19  $ W 2
  13     140      -19.3 24 -25 -19  $ W 3
  14     160      -4.5 26 -27 -6  $ Ti 4
  15     190      -7.13 28 -29 -19  $ zinc Target
  16     220      -2.32 -30  $vault east wall
  17     220      -2.32 -31  $vault west wall
  18     220      -2.32 -32  $vault south wall
  19     220      -2.32 -33 44  $vault north wall
  20     220      -2.32 -34  $vault floor
  21     220      -2.32 -35 (76 :-77 :78 ) $vault Ceiling
  22     220      -2.32 -36  $beam dump west wall
  23     220      -2.32 -37 (81 :-83 :84 )(85 :-87 :88 ) $beam dump sout
(89 :-91 :92 )(93 :-95 :96 )(97 :-99 :100 )(101 :-103 :104
)
      (105 :-107 :108 )(109 :-111 :112 )(113 :-115 :116 )(117 :-
119 :120 )
      (121 :-123 :124 )(125 :-127 :128 )(129 :-131 :132 )(133 :-
135 :136 )
      (137 :-139 :140 )(141 :-143 :144 )(145 :-147 :148 )(149 :-
151 :152 )
      (153 :-154 :155 )(156 :-157 :158 )(159 :-160 :161 )(162 :-
163 :164 )
  24     220      -2.32 -38  $beam dump east wall
  25     220      -2.32 -39 56  $beam dump north wall
  26     220      -2.32 -40  $beam dump door
  27     170      -7.87 -41  $steel layer of beam dump ceilin
  28     220      -2.32 -42  $concreat layer of beam dump cei
  29     180      -11.34 -43  $lead layer of beam dump ceiling
```

30	230	-0.001225	-44		\$vault door opening
31	220	-2.32	-45		\$vault door
32	210	-1.65	-46		\$dirt on top of vault (Changed to high density)
33	150	-1	-47	48	\$ICRU SW 2
34	150	-1	-48		
35	150	-1	-49	50	\$ICRU Center 2
36	150	-1	-50		
37	150	-1	-51	52	\$ICRU NW 2
38	150	-1	-52		
39	150	-1	-53	54	\$ICRU Door
40	150	-1	-54		
41	250	-0.9	-55		\$ borated poly layer of beam dump
42	230	-0.001225	-56		\$ lead beebees
43	180	-11.34	-57		\$polyethylene at pipe
44	150	-1	-58	59	\$ICRU Sphere
45	150	-1	-59		\$ICRU Spere
46	150	-1	-60	61	\$ICRU @ 1 meter
47	150	-1	-61		
48	150	-1	-62	63	\$ICRU SW 2
49	150	-1	-63		
50	150	-1	-64	65	\$ICRU SW 3
51	150	-1	-65		
52	150	-1	-66	67	\$ICRU Center 1
53	150	-1	-67		
54	150	-1	-68	69	\$ICRU Center 3
55	150	-1	-69		
56	150	-1	-70	71	\$ICRU NW 1
57	150	-1	-71		
58	150	-1	-72	73	\$ICRU NW 3
59	150	-1	-73		
60	150	-1	-74	75	
61	150	-1	-75		
62	230	-0.001225	-76	77 -78	
63	150	-1	-79	80	
64	150	-1	-80		
65	230	-0.001225	-82	83 -84	
66	236	-1.7	-81	83 -84 (82 :-83 :84)	
67	230	-0.001225	-86	87 -88	
68	236	-1.7	-85	87 -88 (86 :-87 :88)	
69	230	-0.001225	-90	91 -92	
70	236	-1.7	-89	91 -92 (90 :-91 :92)	
71	230	-0.001225	-94	95 -96	
72	236	-1.7	-93	95 -96 (94 :-95 :96)	
73	230	-0.001225	-98	99 -100	
74	236	-1.7	-97	99 -100 (98 :-99 :100)	
75	230	-0.001225	-102	103 -104	
76	236	-1.7	-101	103 -104 (102 :-103 :104)	
77	230	-0.001225	-106	107 -108	
78	236	-1.7	-105	107 -108 (106 :-107 :108)	
79	230	-0.001225	-110	111 -112	
80	236	-1.7	-109	111 -112 (110 :-111 :112)	

```

81 230 -0.001225 -114 115 -116
82 236 -1.7 -113 115 -116 (114 :-115 :116 )
83 230 -0.001225 -118 119 -120
84 236 -1.7 -117 119 -120 (118 :-119 :120 )
85 230 -0.001225 -122 123 -124
86 236 -1.7 -121 123 -124 (122 :-123 :124 )
87 230 -0.001225 -126 127 -128
88 236 -1.7 -125 127 -128 (126 :-127 :128 )
89 230 -0.001225 -130 131 -132
90 236 -1.7 -129 131 -132 (130 :-131 :132 )
91 230 -0.001225 -134 135 -136
92 236 -1.7 -133 135 -136 (134 :-135 :136 )
93 230 -0.001225 -138 139 -140
94 236 -1.7 -137 139 -140 (138 :-139 :140 )
95 230 -0.001225 -142 143 -144
96 236 -1.7 -141 143 -144 (142 :-143 :144 )
97 230 -0.001225 -146 147 -148
98 236 -1.7 -145 147 -148 (146 :-147 :148 )
99 230 -0.001225 -150 151 -152
100 236 -1.7 -149 151 -152 (150 :-151 :152 )
101 236 -1.7 -153 154 -155
102 236 -1.7 -156 157 -158
103 236 -1.7 -159 160 -161
104 236 -1.7 -162 163 -164
105 250 -0.9 -165
106 180 -11.34 -166

```

c Surface

```

1 c/z 0 0 6 $inner beam pipe
2 c/z 0 0 7 $outer beam pipe
3 pz 50 $top of beam window
4 pz 30 $bottom of beam window
5 so 3000 $universe
6 c/z 0 0 10 $Ti 1
7 pz 50 $bottom of Ti 1
8 pz 50.0127 $top of Ti 1
9 pz 50.0127 $bottom of water thickness
10 pz 50.872 $top of water thickness
11 pz 50.872 $bottom of Ti 2
12 pz 50.884 $top of Ti 2
13 pz 50.884 $bottom of space btw window and target
14 pz 51.646 $top of space btw window and target
15 pz 51.646 $bottom of Ti 3 in target
16 pz 51.658 $top of Ti 3 in target
17 pz 51.658 $bottom of distance btw Ti 3 and Ti 4
18 pz 53.593 $top of distance btw Ti 3 and Ti 4
19 c/z 0 0 1.25 $tungsten disk
20 pz 52.079 $Bottom of W 1
21 pz 52.228 $top of W 1
22 pz 52.482 $bottom of W 2
23 pz 52.634 $top of W 2
24 pz 52.888 $bottom of W 3

```

25 pz 53.037 \$top of W 3
26 pz 53.593 \$bottom of Ti 4
27 pz 53.605 \$top of Ti 4
28 pz 53.605 \$bottom of Target pipe
29 pz 56.605 \$stop of Target Pipe
30 rpp -136 -111 -100 523 -1248 215 \$Vault east wall
31 rpp 455 531 -100 523 -1248 215 \$vault west wall
32 rpp -136 531 -100 523 215 240 \$vault south wall
33 rpp -136 531 -100 265 -1324 -1248 \$vault north wall
34 rpp -136 480 -125 -100 -1324 240 \$vault floor
35 rpp -111 455 265 290 -1248 215 \$vault ceiling (xz reduced
by 25)
36 rpp 40 93 -100 30 39 215 \$beam dump west wall
37 rpp -72 40 -100 30 60 215 \$beam dump south wall
38 rpp -111 -72 -100 30 -10 215 \$beam dump east wall
39 rpp -111 93 -100 30 -38 -10 \$beam dum north wall
40 rpp 93 118 -100 45 -30 69 \$beam dump door
41 rpp -111 93 30 32.5 -38 215 \$steel layer of BD ceiling
42 rpp -111 93 32.5 56 -38 215 \$concrete layer of BD ceiling
43 rpp -111 93 56 61 -38 215 \$lead layer of BD Ceiling
44 rpp -10 249 -100 128 -1324 -1248 \$vault door opening
45 rpp -30 269 -100 148 -1400 -1324 \$(-z=1400 to z=-
1376)vault door
46 arb -111 290 -1248 455 290 -1248 -111 290 215 \$dirt on top
of vault
455 290
455 290
-1248 1234 3456 5612 2647 1538 0
47 s 172 628 50 15 \$ICUR South Wall (SW 2)
48 s 172 628 50 14
49 s 172 530 -542 15 \$ICRU Center 2
50 s 172 530 -542 14
51 s 172 455 -1000 15 \$ICRU North Wall (NW 2)
52 s 172 455 -1000 14
53 s 10 14 -1430 15 \$ICRU vault door (z= -1415 to -1445)
54 s 10 14 -1430 14 \$ (x= 150 to 10)
55 rpp -111 93 61 66 -38 215 \$Borated poly layer of BD
Ceiling
56 rpp -20 15 -18 10 -38 -10 \$ (x=-10, 10 to x=-20, 15)air
behind BP
57 rpp -23 20 -20 11 -39 -38 \$ Lead shield behind beam pipe
58 s 681 14 -1200 15 \$ICRU Control Area
59 s 681 14 -1200 14 \$ICRU 1 cm deep
60 s 150 14 -1500 15 \$ICRU (x=150 to x=135) @ 1 meter from
V. door
61 s 150 14 -1500 14
62 s -55 628 50 15 \$ICRU (SW 1)
63 s -55 628 50 14
64 s 400 628 50 15 \$ICRU (SW 3)
65 s 400 628 50 14
66 s -55 530 -542 15 \$ICRU Center 1
67 s -55 530 -542 14

```

68         s 400 530 -542 15  $ICRU Center 3
69         s 400 530 -542 14
70         s -55 455 -1000 15  $ICRU NW 1
71         s -55 455 -1000 14
72         s 400 455 -1000 15  $ICRU NW 3
73         s 400 455 -1000 14
74         s 135 14 -1430 15  $ICRU Center (x=150 to x=135)
75         s 135 14 -1430 14
76     c/y -91 -1224 5
77     py 265
78     py 290
79         s -91 390 -1224 15
80         s -91 390 -1224 14
81     cz 18  $beam dump disk 1
82     cz 10
83     pz 60
84     pz 65
85     cz 18
86     cz 9.5
87     pz 65
88     pz 70
89     cz 18
90     cz 9
91     pz 70
92     pz 75
93     cz 18
94     cz 8.5
95     pz 75
96     pz 80
97     cz 18
98     cz 8
99     pz 80
100     pz 85
101     cz 16
102     cz 7.5
103     pz 85
104     pz 90
105     cz 16
106     cz 7
107     pz 90
108     pz 95
109     cz 16
110     cz 6.5
111     pz 95
112     pz 100
113     cz 16
114     cz 6
115     pz 100
116     pz 105
117     cz 16
118     cz 5.5
119     pz 105

```

120	pz	110							
121	cz	14							
122	cz	5							
123	pz	110							
124	pz	115							
125	cz	14							
126	cz	4.5							
127	pz	115							
128	pz	120							
129	cz	14							
130	cz	4							
131	pz	120							
132	pz	125							
133	cz	14							
134	cz	3.5							
135	pz	125							
136	pz	130							
137	cz	14							
138	cz	3							
139	pz	130							
140	pz	135							
141	cz	14							
142	cz	2.5							
143	pz	135							
144	pz	140							
145	cz	14							
146	cz	2							
147	pz	140							
148	pz	145							
149	cz	14							
150	cz	1.5							
151	pz	145							
152	pz	150							
153	cz	14							
154	pz	150							
155	pz	155							
156	cz	14							
157	pz	155							
158	pz	160							
159	cz	14							
160	pz	160							
161	pz	165							
162	cz	14							
163	pz	165							
164	pz	170							
165	rpp	-23 20 -20 11 -70 -39					\$poly shield behind BD		
166	rpp	-23 20 -21 11 -71 -70					\$ lead		

mode	n p e								
m120	7014.70c	-0.755636	\$Air						
	8016.70c	-0.231475	18040.70c				-0.012889		
m130	1002.70c	-0.667	\$Water						

	8016.70c	-0.333				
m140	74182.70c	-0.260586	\$Tungsten			
	74183.70c	-0.142269	74184.70c	-0.307531	74186.70c	-
	0.289615					
m150	8016.70c	-0.762	\$phanthom			
	6012.70c	-0.111	1002.70c	-0.101	7014.70c	
	-0.026					
m160	22048.70c		-1 \$Titanium			
m170	6012.70c	-0.005	\$Steel, Carbon,			
	26054.70c	-0.056701	26056.70c	-0.914106	26057.70c	-
	0.021303					
	26058.70c	-0.00289				
m190	30068.70c		-1 \$Zinc 68			
m210	8016.70c	-0.5134	\$soil (dry U.S. Ave. with ENDF-VI)			
	11023.70c	-0.006	12024.70c	-0.010134	12025.70c	-
	0.001336					
	12026.70c	-0.00153	13027.70c	-0.067	14028.70c	-
	0.253938					
	14029.70c	-0.013317	14030.70c	-0.009145	20040.70c	-
	0.063341					
	20042.70c	-0.000339	20043.70c	-7.2e-005	20044.70c	-
	0.001133					
	20046.70c	-2e-006	20048.70c	-0.000112	22046.70c	-
	0.000346					
	22047.70c	-0.000322	22048.70c	-0.003326	22049.70c	-
	0.000253					
	22050.70c	-0.000253	25055.70c	-0.0007	26054.70c	-
	0.003134					
	26056.70c	-0.050528	26057.70c	-0.001178	26058.70c	-
	0.00016					
m220	1002.70c	-0.0075	\$Concrete, ordinary,			
	6012.50c	-0.055502	8016.70c	-0.492926	16032.70c	-
	0.16984					
	16033.70c	-0.001382	16034.70c	-0.007995	16036.70c	
	-4e-005					
	20040.70c	-0.221889	20042.70c	-0.009052	20043.70c	-
	0.000332					
	20044.70c	-0.005202	20046.70c	-1.1e-005	20048.70c	-
	0.000514					
	26054.70c	-0.000467	26056.70c	-0.007525	26057.70c	-
	0.000175					
	26058.70c	-2.4e-005				
m230	7014.70c	-0.755636	\$air (US S. Atm at sea level)			
	8016.70c	-0.231475	18036.70c	-3.9e-005	18038.70c	
	-8e-006					
	18040.70c	-0.012842				
m180	82206.70c	-0.253338	\$Lead,			
	82207.70c	-0.220743	82208.70c	-0.525919		
m250	1002.70c	-0.133711	\$ borated polyethylene			
	6012.70c	-0.816289	5010.70c	-0.05		
m240	29000.50c		-1 \$ copper			
m208	13027.70c		-1 \$aluminum			

```

m236 6012.50c -1 $graphite
imp:n 1 0 1 0 1 10r
$ 1, 15
0 1 0 1 0
$ 16, 20
1 2r 0 1 81r $ 21, 106
imp:p 1 0 1 0 1 10r
$ 1, 15
0 1 0 1 0
$ 16, 20
1 2r 0 1 81r $ 21, 106
imp:e 1 0 2r 1 10r 0 48r 1 39r
$ 1, 104
0 1r $ 105, 106
cut:e j 0.1
cut:p j 0.1
phys:e 5j 10 j 0
phys:p 3j 1
phys:n 50
sdef pos 0 0 0 axs 0 0 1 rad d1 ext d2 erg 40 vec 0 0 1 par e
si1 0 0.25
sp1 -21 1
si2 48 49.9
sp2 -21 0
f2:n 48
fm2 1.1298e15
df2 iu=1 ic=20
f12:n 50
fm12 1.1298e15
df12 iu=1 ic=20
f22:n 52
fm22 1.1298e15
df22 iu=1 ic=20
f32:n 54
fm32 1.1298e15
df32 iu=1 ic=20
f42:n 59
fm42 1.1298e15
df42 iu=1 ic=20
f52:n 61
fm52 1.1298e15
df52 iu=1 ic=20
f62:n 63
fm62 1.1298e15
df62 iu=1 ic=20
f72:n 65
fm72 1.1298e15
df72 iu=1 ic=20
f82:n 67
fm82 1.1298e15
df82 iu=1 ic=20
f92:n 69

```

fm92 1.1298e15
df92 iu=1 ic=20
f102:n 71
fm102 1.1298e15
df102 iu=1 ic=20
f112:n 73
fm112 1.1298e15
df112 iu=1 ic=20
f242:n 75
fm242 1.1298e15
df242 iu=1 ic=20
f262:n 80
fm262 1.1298e15
df262 iu=1 ic=20
f122:p 48
fm122 1.1298e15
df122 iu=1 ic=20
f132:p 50
fm132 1.1298e15
df132 iu=1 ic=20
f142:p 52
fm142 1.1298e15
df142 iu=1 ic=20
f152:p 54
fm152 1.1298e15
df152 iu=1 ic=20
f162:p 59
fm162 1.1298e15
df162 iu=1 ic=20
f172:p 61
fm172 1.1298e15
df172 iu=1 ic=20
f182:p 63
fm182 1.1298e15
df182 iu=1 ic=20
f192:p 65
fm192 1.1298e15
df192 iu=1 ic=20
f202:p 67
fm202 1.1298e15
df202 iu=1 ic=20
f212:p 69
fm212 1.1298e15
df212 iu=1 ic=20
f222:p 71
fm222 1.1298e15
df222 iu=1 ic=20
f232:p 73
fm232 1.1298e15
df232 iu=1 ic=20
f252:p 75
fm252 1.1298e15

```
df252 iu=1 ic=20
f272:p 80
fm272 1.1298e15
df272 iu=1 ic=20
print
prtmp j 1e6 1 3 1e6
ctme 20000
```

Appendix C

Ordinary Concrete Dose Equivalent Rate Input File

```
MCNPF Visual Editor Version X_24E
c Created on: Saturday, April 2, 2016 at 11:11
  1 0 -1 -3 4 $inside of beam pipe
  2 0 -2 1 -3 4 $thickness of beam pipe
  3 230 -0.001225 (2 :3 :-4 )-5 (-7 :8 :6 )(-9 :10 :6 )(-11 :12 :6
)
(-13 :14 :6 )(-15 :16 :6 )(-17 :18 :6 )(-26 :27 :6 )
(-28 :29 :19 )30 31 32 33 34 35 36 37 38 39 40 41 42 43 45
46 47 49
  51 53 55 57 58 60 62 64 66 68 70 72 74 79 165 166
  4 0 5 $universe
  5 160 -4.5 7 -8 -6 $ Ti 1 (Ti=Titanium)
  6 130 -1 9 -10 -6 $Water thicknes btw Ti 1 an
  7 160 -4.5 11 -12 -6 $ Ti 2
  8 230 -0.001225 13 -14 -6 $Space btw window & target
  9 160 -4.5 15 -16 -6 $ Ti 3 in target
 10 130 -1 17 -18 -6 (-20 :21 :19 )(-22 :23 :19 ) $ space in
Target
(-24 :25 :19 )
 11 140 -19.3 20 -21 -19 $ W 1
 12 140 -19.3 22 -23 -19 $ W 2
 13 140 -19.3 24 -25 -19 $ W 3
 14 160 -4.5 26 -27 -6 $ Ti 4
 15 190 -7.13 28 -29 -19 $ zinc Target
 16 220 -2.32 -30 $vault east wall
 17 220 -2.32 -31 $vault west wall
 18 220 -2.32 -32 $vault south wall
 19 220 -2.32 -33 44 $vault north wall
 20 220 -2.32 -34 $vault floor
 21 220 -2.32 -35 (76 :-77 :78 ) $vault Ceiling
 22 220 -2.32 -36 $beam dump west wall
 23 220 -2.32 -37 (81 :-83 :84 )(85 :-87 :88 ) $beam dump sout
(89 :-91 :92 )(93 :-95 :96 )(97 :-99 :100 )(101 :-103 :104
)
(105 :-107 :108 )(109 :-111 :112 )(113 :-115 :116 )(117 :-
119 :120 )
(121 :-123 :124 )(125 :-127 :128 )(129 :-131 :132 )(133 :-
135 :136 )
(137 :-139 :140 )(141 :-143 :144 )(145 :-147 :148 )(149 :-
151 :152 )
(153 :-154 :155 )(156 :-157 :158 )(159 :-160 :161 )(162 :-
163 :164 )
 24 220 -2.32 -38 $beam dump east wall
 25 220 -2.32 -39 56 $beam dump north wall
 26 220 -2.32 -40 $beam dump door
 27 170 -7.87 -41 $steel layer of beam dump ceilin
 28 220 -2.32 -42 $concreat layer of beam dump cei
```

29	180	-11.34	-43		\$lead layer of beam dump ceiling
30	230	-0.001225	-44		\$vault door opening
31	220	-2.32	-45		\$vault door
32	210	-1.65	-46		\$dirt on top of vault (Changed to high
density)					
33	150		-1 -47 48		\$ICRU SW 2
34	150		-1 -48		
35	150		-1 -49 50		\$ICRU Center 2
36	150		-1 -50		
37	150		-1 -51 52		\$ICRU NW 2
38	150		-1 -52		
39	150		-1 -53 54		\$ICRU Door
40	150		-1 -54		
41	250	-0.9	-55		\$ borated poly layer of beam dump
42	230	-0.001225	-56		\$ lead beebees
43	180	-11.34	-57		\$polyethylene at pipe
44	150		-1 -58 59		\$ICRU Sphere
45	150		-1 -59		\$ICRU Spere
46	150		-1 -60 61		\$ICRU @ 1 meter
47	150		-1 -61		
48	150		-1 -62 63		\$ICRU SW 2
49	150		-1 -63		
50	150		-1 -64 65		\$ICRU SW 3
51	150		-1 -65		
52	150		-1 -66 67		\$ICRU Center 1
53	150		-1 -67		
54	150		-1 -68 69		\$ICRU Center 3
55	150		-1 -69		
56	150		-1 -70 71		\$ICRU NW 1
57	150		-1 -71		
58	150		-1 -72 73		\$ICRU NW 3
59	150		-1 -73		
60	150		-1 -74 75		
61	150		-1 -75		
62	230	-0.001225	-76 77 -78		
63	150		-1 -79 80		
64	150		-1 -80		
65	230	-0.001225	-82 83 -84		
66	220	-2.32	-81 83 -84 (82 :-83 :84)		
67	230	-0.001225	-86 87 -88		
68	220	-2.32	-85 87 -88 (86 :-87 :88)		
69	230	-0.001225	-90 91 -92		
70	220	-2.32	-89 91 -92 (90 :-91 :92)		
71	230	-0.001225	-94 95 -96		
72	220	-2.32	-93 95 -96 (94 :-95 :96)		
73	230	-0.001225	-98 99 -100		
74	220	-2.32	-97 99 -100 (98 :-99 :100)		
75	230	-0.001225	-102 103 -104		
76	220	-2.32	-101 103 -104 (102 :-103 :104)		
77	230	-0.001225	-106 107 -108		
78	220	-2.32	-105 107 -108 (106 :-107 :108)		
79	230	-0.001225	-110 111 -112		

```

80 220 -2.32 -109 111 -112 (110 :-111 :112 )
81 230 -0.001225 -114 115 -116
82 220 -2.32 -113 115 -116 (114 :-115 :116 )
83 230 -0.001225 -118 119 -120
84 220 -2.32 -117 119 -120 (118 :-119 :120 )
85 230 -0.001225 -122 123 -124
86 220 -2.32 -121 123 -124 (122 :-123 :124 )
87 230 -0.001225 -126 127 -128
88 220 -2.32 -125 127 -128 (126 :-127 :128 )
89 230 -0.001225 -130 131 -132
90 220 -2.32 -129 131 -132 (130 :-131 :132 )
91 230 -0.001225 -134 135 -136
92 220 -2.32 -133 135 -136 (134 :-135 :136 )
93 230 -0.001225 -138 139 -140
94 220 -2.32 -137 139 -140 (138 :-139 :140 )
95 230 -0.001225 -142 143 -144
96 220 -2.32 -141 143 -144 (142 :-143 :144 )
97 230 -0.001225 -146 147 -148
98 220 -2.32 -145 147 -148 (146 :-147 :148 )
99 230 -0.001225 -150 151 -152
100 220 -2.32 -149 151 -152 (150 :-151 :152 )
101 220 -2.32 -153 154 -155
102 220 -2.32 -156 157 -158
103 220 -2.32 -159 160 -161
104 220 -2.32 -162 163 -164
105 250 -0.9 -165
106 180 -11.34 -166

```

c Surface

```

1 c/z 0 0 6 $inner beam pipe
2 c/z 0 0 7 $outer beam pipe
3 pz 50 $top of beam window
4 pz 30 $bottom of beam window
5 so 3000 $universe
6 c/z 0 0 10 $Ti 1
7 pz 50 $bottom of Ti 1
8 pz 50.0127 $top of Ti 1
9 pz 50.0127 $bottom of water thickness
10 pz 50.872 $top of water thickness
11 pz 50.872 $bottom of Ti 2
12 pz 50.884 $top of Ti 2
13 pz 50.884 $bottom of space btw window and target
14 pz 51.646 $top of space btw window and target
15 pz 51.646 $bottom of Ti 3 in target
16 pz 51.658 $top of Ti 3 in target
17 pz 51.658 $bottom of distance btw Ti 3 and Ti 4
18 pz 53.593 $top of distance btw Ti 3 and Ti 4
19 c/z 0 0 1.25 $tungsten disk
20 pz 52.079 $Bottom of W 1
21 pz 52.228 $top of W 1
22 pz 52.482 $bottom of W 2
23 pz 52.634 $top of W 2

```

24 pz 52.888 \$bottom of W 3
25 pz 53.037 \$top of W 3
26 pz 53.593 \$bottom of Ti 4
27 pz 53.605 \$top of Ti 4
28 pz 53.605 \$bottom of Target pipe
29 pz 56.605 \$top of Target Pipe
30 rpp -136 -111 -100 523 -1248 215 \$Vault east wall
31 rpp 455 531 -100 523 -1248 215 \$vault west wall
32 rpp -136 531 -100 523 215 240 \$vault south wall
33 rpp -136 531 -100 265 -1324 -1248 \$vault north wall
34 rpp -136 480 -125 -100 -1324 240 \$vault floor
35 rpp -111 455 265 290 -1248 215 \$vault ceiling (xz reduced
by 25)
36 rpp 40 93 -100 30 39 215 \$beam dump west wall
37 rpp -72 40 -100 30 60 215 \$beam dump south wall
38 rpp -111 -72 -100 30 -10 215 \$beam dump east wall
39 rpp -111 93 -100 30 -38 -10 \$beam dum north wall
40 rpp 93 118 -100 45 -30 69 \$beam dump door
41 rpp -111 93 30 32.5 -38 215 \$steel layer of BD ceiling
42 rpp -111 93 32.5 56 -38 215 \$concrete layer of BD ceiling
43 rpp -111 93 56 61 -38 215 \$lead layer of BD Ceiling
44 rpp -10 249 -100 128 -1324 -1248 \$vault door opening
45 rpp -30 269 -100 148 -1400 -1324 \$(-z=1400 to z=-
1376) vault door
46 arb -111 290 -1248 455 290 -1248 -111 290 215 \$dirt on top
of vault
455 290
-1248 1234 3456 5612 2647 1538 0
47 s 172 628 50 15 \$ICUR South Wall (SW 2)
48 s 172 628 50 14
49 s 172 530 -542 15 \$ICRU Center 2
50 s 172 530 -542 14
51 s 172 455 -1000 15 \$ICRU North Wall (NW 2)
52 s 172 455 -1000 14
53 s 10 14 -1430 15 \$ICRU vault door (z= -1415 to -1445)
54 s 10 14 -1430 14 \$ (x= 150 to 10)
55 rpp -111 93 61 76 -38 215 \$Borated poly layer of BD
Ceiling
56 rpp -20 15 -18 10 -38 -10 \$
57 rpp -23 20 -20 11 -39 -38 \$ Lead shield behind beam pipe
58 s 681 14 -1200 15 \$ICRU Control Area
59 s 681 14 -1200 14 \$ICRU 1 cm deep
60 s 150 14 -1500 15 \$ICRU (x=150 to x=135) @ 1 meter from
V. door
61 s 150 14 -1500 14
62 s -55 628 50 15 \$ICRU (SW 1)
63 s -55 628 50 14
64 s 400 628 50 15 \$ICRU (SW 3)
65 s 400 628 50 14
66 s -55 530 -542 15 \$ICRU Center 1
67 s -55 530 -542 14

```

68      s 400 530 -542 15  $ICRU Center 3
69      s 400 530 -542 14
70      s -55 455 -1000 15  $ICRU NW 1
71      s -55 455 -1000 14
72      s 400 455 -1000 15  $ICRU NW 3
73      s 400 455 -1000 14
74      s 135 14 -1430 15  $ICRU Center (x=150 to x=135)
75      s 135 14 -1430 14
76      c/y -91 -1224 5
77      py 265
78      py 290
79      s -91 390 -1224 15
80      s -91 390 -1224 14
81      cz 13  $beam dump disk 1
82      cz 10
83      pz 60
84      pz 65
85      cz 13
86      cz 9.5
87      pz 65
88      pz 70
89      cz 13
90      cz 9
91      pz 70
92      pz 75
93      cz 13
94      cz 8.5
95      pz 75
96      pz 80
97      cz 13
98      cz 8
99      pz 80
100     pz 85
101     cz 11
102     cz 7.5
103     pz 85
104     pz 90
105     cz 11
106     cz 7
107     pz 90
108     pz 95
109     cz 11
110     cz 6.5
111     pz 95
112     pz 100
113     cz 11
114     cz 6
115     pz 100
116     pz 105
117     cz 11
118     cz 5.5
119     pz 105

```

120	pz	110							
121	cz	9							
122	cz	5							
123	pz	110							
124	pz	115							
125	cz	9							
126	cz	4.5							
127	pz	115							
128	pz	120							
129	cz	9							
130	cz	4							
131	pz	120							
132	pz	125							
133	cz	9							
134	cz	3.5							
135	pz	125							
136	pz	130							
137	cz	9							
138	cz	3							
139	pz	130							
140	pz	135							
141	cz	9							
142	cz	2.5							
143	pz	135							
144	pz	140							
145	cz	9							
146	cz	2							
147	pz	140							
148	pz	145							
149	cz	9							
150	cz	1.5							
151	pz	145							
152	pz	150							
153	cz	9							
154	pz	150							
155	pz	155							
156	cz	9							
157	pz	155							
158	pz	160							
159	cz	9							
160	pz	160							
161	pz	165							
162	cz	9							
163	pz	165							
164	pz	170							
165	rpp	-23 20 -20 11 -70 -39	\$poly	behind	BD				
166	rpp	-23 20 -21 11 -71 -70	\$Lead						

mode	n p e								
m120	7014.70c	-0.755636	\$Air						
	8016.70c	-0.231475	18040.70c					-0.012889	
m130	1002.70c	-0.667	\$Water						

	8016.70c	-0.333				
m140	74182.70c	-0.260586	\$Tungsten			
	74183.70c	-0.142269	74184.	-0.307531	74186.70c	-
	0.289615					
m150	8016.70c	-0.762	\$phanthom			
	6012.70c	-0.111	1002.70c	-0.101	7014.70c	-
	0.026					
m160	22048.70c	-1	\$Titanium			
m170	6012.70c	-0.005	\$Steel, Carbon,			
	26054.70c	-0.056701	26056.70c	-0.914106	26057.70c	-
	0.021303					
	26058.70c	-0.00289				
m190	30068.70c	-1	\$Zinc 68			
m210	8016.70c	-0.5134	\$soil (dry U.S. Ave. with ENDF-VI)			
	11023.70c	-0.006	12024.70c	-0.010134	12025.70c	-
	0.001336					
	12026.70c	-0.00153	13027.70c	-0.067	14028.70c	-
	0.253938					
	14029.70c	-0.013317	14030.70c	-0.009145	20040.70c	-
	0.063341					
	20042.70c	-0.000339	20043.70c	-7.2e-005	20044.70c	-
	0.001133					
	20046.70c	-2e-006	20048.70c	-0.000112	22046.70c	-
	0.000346					
	22047.70c	-0.000322	22048.70c	-0.003326	22049.70c	-
	0.000253					
	22050.70c	-0.000253	25055.70c	-0.0007	26054.70c	-
	0.003134					
	26056.70c	-0.050528	26057.70c	-0.001178	26058.70c	-
	0.00016					
m220	1002.70c	-0.0075	\$Concrete, ordinary,			
	6012.50c	-0.055502	8016.70c	-0.492926	16032.70c	-
	0.16984					
	16033.70c	-0.001382	16034.70c	-0.007995	16036.70c	
	-4e-005					
	20040.70c	-0.221889	20042.70c	-0.009052	20043.70c	-
	0.000332					
	20044.70c	-0.005202	20046.70c	-1.1e-005	20048.70c	-
	0.000514					
	26054.70c	-0.000467	26056.70c	-0.007525	26057.70c	-
	0.000175					
	26058.70c	-2.4e-005				
m230	7014.70c	-0.755636	\$air (US S. Atm at sea level)			
	8016.70c	-0.231475	18036.70c	-3.9e-005	18038.70c	
	-8e-006					
	18040.70c	-0.012842				
m180	82206.70c	-0.253338	\$Lead,			
	82207.70c	-0.220743	82208.70c	-0.525919		
m250	1002.70c	-0.133711	\$ borated polyethylene			
	6012.70c	-0.816289	5010.70c	-0.05		
m240	29063.70c	-1				

```

imp:n 1 0 1 0 1 10r
$ 1, 15
0 1 0 1 0
$ 16, 20
1 2r 0 1 81r $ 21, 106
imp:p 1 0 1 0 1 10r
$ 1, 15
0 1 0 1 0
$ 16, 20
1 2r 0 1 81r $ 21, 106
imp:e 1 0 2r 1 10r 0 48r 1 39r
$ 1, 104
0 1r $ 105, 106
cut:e j 0.1
cut:p j 0.1
phys:e 5j 10 j 0
phys:p 3j 1
phys:n 50
sdef pos 0 0 0 axs 0 0 1 rad d1 ext d2 erg 40 vec 0 0 1 par e
si1 0 0.25
sp1 -21 1
si2 48 49.9
sp2 -21 0
f2:n 48
fm2 1.1298e15
df2 iu=1 ic=20
f12:n 50
fm12 1.1298e15
df12 iu=1 ic=20
f22:n 52
fm22 1.1298e15
df22 iu=1 ic=20
f32:n 54
fm32 1.1298e15
df32 iu=1 ic=20
f42:n 59
fm42 1.1298e15
df42 iu=1 ic=20
f52:n 61
fm52 1.1298e15
df52 iu=1 ic=20
f62:n 63
fm62 1.1298e15
df62 iu=1 ic=20
f72:n 65
fm72 1.1298e15
df72 iu=1 ic=20
f82:n 67
fm82 1.1298e15
df82 iu=1 ic=20
f92:n 69
fm92 1.1298e15

```

df92 iu=1 ic=20
f102:n 71
fm102 1.1298e15
df102 iu=1 ic=20
f112:n 73
fm112 1.1298e15
df112 iu=1 ic=20
f242:n 75
fm242 1.1298e15
df242 iu=1 ic=20
f262:n 80
fm262 1.1298e15
df262 iu=1 ic=20
f122:p 48
fm122 1.1298e15
df122 iu=1 ic=20
f132:p 50
fm132 1.1298e15
df132 iu=1 ic=20
f142:p 52
fm142 1.1298e15
df142 iu=1 ic=20
f152:p 54
fm152 1.1298e15
df152 iu=1 ic=20
f162:p 59
fm162 1.1298e15
df162 iu=1 ic=20
f172:p 61
fm172 1.1298e15
df172 iu=1 ic=20
f182:p 63
fm182 1.1298e15
df182 iu=1 ic=20
f192:p 65
fm192 1.1298e15
df192 iu=1 ic=20
f202:p 67
fm202 1.1298e15
df202 iu=1 ic=20
f212:p 69
fm212 1.1298e15
df212 iu=1 ic=20
f222:p 71
fm222 1.1298e15
df222 iu=1 ic=20
f232:p 73
fm232 1.1298e15
df232 iu=1 ic=20
f252:p 75
fm252 1.1298e15
df252 iu=1 ic=20

```
f272:p 80
fm272 1.1298e15
df272 iu=1 ic=20
print
prtmp j 1e6 1 3 1e6
ctme 20000
```

Appendix D

Copper Beam Dump Dose Equivalent Rate Input File

```
MCNPF Visual Editor Version X_24E
c Created on: Saturday, April 2, 2016 at 11:11
  1 0 -1 -3 4 $inside of beam pipe
  2 0 -2 1 -3 4 $thickness of beam pipe
  3 230 -0.001225 (2 :3 :-4 )-5 (-7 :8 :6 )(-9 :10 :6 )(-11 :12 :6
)
(-13 :14 :6 )(-15 :16 :6 )(-17 :18 :6 )(-26 :27 :6 )
(-28 :29 :19 )30 31 32 33 34 35 36 37 38 39 40 41 42 43 45
46 47 49
51 53 55 57 58 60 62 64 66 68 70 72 74 79 165 166
  4 0 5 $universe
  5 160 -4.5 7 -8 -6 $ Ti 1 (Ti=Titanium)
  6 130 -1 9 -10 -6 $Water thicknes btw Ti 1 an
  7 160 -4.5 11 -12 -6 $ Ti 2
  8 230 -0.001225 13 -14 -6 $Space btw window & target
  9 160 -4.5 15 -16 -6 $ Ti 3 in target
 10 130 -1 17 -18 -6 (-20 :21 :19 )(-22 :23 :19 ) $ space in
Target
(-24 :25 :19 )
 11 140 -19.3 20 -21 -19 $ W 1
 12 140 -19.3 22 -23 -19 $ W 2
 13 140 -19.3 24 -25 -19 $ W 3
 14 160 -4.5 26 -27 -6 $ Ti 4
 15 190 -7.13 28 -29 -19 $ zinc Target
 16 220 -2.32 -30 $vault east wall
 17 220 -2.32 -31 $vault west wall
 18 220 -2.32 -32 $vault south wall
 19 220 -2.32 -33 44 $vault north wall
 20 220 -2.32 -34 $vault floor
 21 220 -2.32 -35 (76 :-77 :78 ) $vault Ceiling
 22 220 -2.32 -36 $beam dump west wall
 23 220 -2.32 -37 (81 :-83 :84 )(85 :-87 :88 ) $beam dump sout
(89 :-91 :92 )(93 :-95 :96 )(97 :-99 :100 )(101 :-103 :104
)
(105 :-107 :108 )(109 :-111 :112 )(113 :-115 :116 )(117 :-
119 :120 )
(121 :-123 :124 )(125 :-127 :128 )(129 :-131 :132 )(133 :-
135 :136 )
(137 :-139 :140 )(141 :-143 :144 )(145 :-147 :148 )(149 :-
151 :152 )
(153 :-154 :155 )(156 :-157 :158 )(159 :-160 :161 )(162 :-
163 :164 )
 24 220 -2.32 -38 $beam dump east wall
 25 220 -2.32 -39 56 $beam dump north wall
 26 220 -2.32 -40 $beam dump door
 27 170 -7.87 -41 $steel layer of beam dump ceilin
 28 220 -2.32 -42 $concreat layer of beam dump cei
```

29	180	-11.34	-43		\$lead layer of beam dump ceiling
30	230	-0.001225	-44		\$vault door opening
31	220	-2.32	-45		\$vault door
32	210	-1.65	-46		\$dirt on top of vault (Changed to high
density)					
33	150		-1 -47 48		\$ICRU SW 2
34	150		-1 -48		
35	150		-1 -49 50		\$ICRU Center 2
36	150		-1 -50		
37	150		-1 -51 52		\$ICRU NW 2
38	150		-1 -52		
39	150		-1 -53 54		\$ICRU Door
40	150		-1 -54		
41	250	-0.9	-55		\$ borated poly layer of beam dump
42	230	-0.001225	-56		\$ lead beebees
43	180	-11.34	-57		\$polyethylene at pipe
44	150		-1 -58 59		\$ICRU Sphere
45	150		-1 -59		\$ICRU Spere
46	150		-1 -60 61		\$ICRU @ 1 meter
47	150		-1 -61		
48	150		-1 -62 63		\$ICRU SW 2
49	150		-1 -63		
50	150		-1 -64 65		\$ICRU SW 3
51	150		-1 -65		
52	150		-1 -66 67		\$ICRU Center 1
53	150		-1 -67		
54	150		-1 -68 69		\$ICRU Center 3
55	150		-1 -69		
56	150		-1 -70 71		\$ICRU NW 1
57	150		-1 -71		
58	150		-1 -72 73		\$ICRU NW 3
59	150		-1 -73		
60	150		-1 -74 75		
61	150		-1 -75		
62	230	-0.001225	-76 77 -78		
63	150		-1 -79 80		
64	150		-1 -80		
65	230	-0.001225	-82 83 -84		
66	240	-8.96	-81 83 -84 (82 :-83 :84)		
67	230	-0.001225	-86 87 -88		
68	240	-8.96	-85 87 -88 (86 :-87 :88)		
69	230	-0.001225	-90 91 -92		
70	240	-8.96	-89 91 -92 (90 :-91 :92)		
71	230	-0.001225	-94 95 -96		
72	240	-8.96	-93 95 -96 (94 :-95 :96)		
73	230	-0.001225	-98 99 -100		
74	240	-8.96	-97 99 -100 (98 :-99 :100)		
75	230	-0.001225	-102 103 -104		
76	240	-8.96	-101 103 -104 (102 :-103 :104)		
77	230	-0.001225	-106 107 -108		
78	240	-8.96	-105 107 -108 (106 :-107 :108)		
79	230	-0.001225	-110 111 -112		

```

80 240 -8.96 -109 111 -112 (110 :-111 :112 )
81 230 -0.001225 -114 115 -116
82 240 -8.96 -113 115 -116 (114 :-115 :116 )
83 230 -0.001225 -118 119 -120
84 240 -8.96 -117 119 -120 (118 :-119 :120 )
85 230 -0.001225 -122 123 -124
86 240 -8.96 -121 123 -124 (122 :-123 :124 )
87 230 -0.001225 -126 127 -128
88 240 -8.96 -125 127 -128 (126 :-127 :128 )
89 230 -0.001225 -130 131 -132
90 240 -8.96 -129 131 -132 (130 :-131 :132 )
91 230 -0.001225 -134 135 -136
92 240 -8.96 -133 135 -136 (134 :-135 :136 )
93 230 -0.001225 -138 139 -140
94 240 -8.96 -137 139 -140 (138 :-139 :140 )
95 230 -0.001225 -142 143 -144
96 240 -8.96 -141 143 -144 (142 :-143 :144 )
97 230 -0.001225 -146 147 -148
98 240 -8.96 -145 147 -148 (146 :-147 :148 )
99 230 -0.001225 -150 151 -152
100 240 -8.96 -149 151 -152 (150 :-151 :152 )
101 240 -8.96 -153 154 -155
102 240 -8.96 -156 157 -158
103 240 -8.96 -159 160 -161
104 240 -8.96 -162 163 -164
105 250 -0.9 -165
106 180 -11.34 -166

```

c Surface

```

1 c/z 0 0 6 $inner beam pipe
2 c/z 0 0 7 $outer beam pipe
3 pz 50 $top of beam window
4 pz 30 $bottom of beam window
5 so 3000 $universe
6 c/z 0 0 10 $Ti 1
7 pz 50 $bottom of Ti 1
8 pz 50.0127 $top of Ti 1
9 pz 50.0127 $bottom of water thickness
10 pz 50.872 $top of water thickness
11 pz 50.872 $bottom of Ti 2
12 pz 50.884 $top of Ti 2
13 pz 50.884 $bottom of space btw window and target
14 pz 51.646 $top of space btw window and target
15 pz 51.646 $bottom of Ti 3 in target
16 pz 51.658 $top of Ti 3 in target
17 pz 51.658 $bottom of distance btw Ti 3 and Ti 4
18 pz 53.593 $top of distance btw Ti 3 and Ti 4
19 c/z 0 0 1.25 $tungsten disk
20 pz 52.079 $Bottom of W 1
21 pz 52.228 $top of W 1
22 pz 52.482 $bottom of W 2
23 pz 52.634 $top of W 2

```

24 pz 52.888 \$bottom of W 3
25 pz 53.037 \$top of W 3
26 pz 53.593 \$bottom of Ti 4
27 pz 53.605 \$top of Ti 4
28 pz 53.605 \$bottom of Target pipe
29 pz 56.605 \$top of Target Pipe
30 rpp -136 -111 -100 523 -1248 215 \$Vault east wall
31 rpp 455 531 -100 523 -1248 215 \$vault west wall
32 rpp -136 531 -100 523 215 240 \$vault south wall
33 rpp -136 531 -100 265 -1324 -1248 \$vault north wall
34 rpp -136 480 -125 -100 -1324 240 \$vault floor
35 rpp -111 455 265 290 -1248 215 \$vault ceiling (xz reduced
by 25)
36 rpp 40 93 -100 30 39 215 \$beam dump west wall
37 rpp -72 40 -100 30 60 215 \$beam dump south wall
38 rpp -111 -72 -100 30 -10 215 \$beam dump east wall
39 rpp -111 93 -100 30 -38 -10 \$beam dum north wall
40 rpp 93 118 -100 45 -30 69 \$beam dump door
41 rpp -111 93 30 32.5 -38 215 \$steel layer of BD ceiling
42 rpp -111 93 32.5 56 -38 215 \$concrete layer of BD ceiling
43 rpp -111 93 56 61 -38 215 \$lead layer of BD Ceiling
44 rpp -10 249 -100 128 -1324 -1248 \$vault door opening
45 rpp -30 269 -100 148 -1400 -1324 \$(-z=1400 to z=-
1376) vault door
46 arb -111 290 -1248 455 290 -1248 -111 290 215 \$dirt on top
of vault
455 290
455 290
-1248 1234 3456 5612 2647 1538 0
47 s 172 628 50 15 \$ICUR South Wall (SW 2)
48 s 172 628 50 14
49 s 172 530 -542 15 \$ICRU Center 2
50 s 172 530 -542 14
51 s 172 455 -1000 15 \$ICRU North Wall (NW 2)
52 s 172 455 -1000 14
53 s 10 14 -1430 15 \$ICRU vault door (z= -1415 to -1445)
54 s 10 14 -1430 14 \$ (x= 150 to 10)
55 rpp -111 93 61 76 -38 215 \$Borated poly layer of BD
Ceiling
56 rpp -20 15 -18 10 -38 -10 \$
57 rpp -23 20 -20 11 -39 -38 \$ Lead shield behind beam pipe
58 s 681 14 -1200 15 \$ICRU Control Area
59 s 681 14 -1200 14 \$ICRU 1 cm deep
60 s 150 14 -1500 15 \$ICRU (x=150 to x=135) @ 1 meter from
V. door
61 s 150 14 -1500 14
62 s -55 628 50 15 \$ICRU (SW 1)
63 s -55 628 50 14
64 s 400 628 50 15 \$ICRU (SW 3)
65 s 400 628 50 14
66 s -55 530 -542 15 \$ICRU Center 1
67 s -55 530 -542 14

```

68      s 400 530 -542 15  $ICRU Center 3
69      s 400 530 -542 14
70      s -55 455 -1000 15  $ICRU NW 1
71      s -55 455 -1000 14
72      s 400 455 -1000 15  $ICRU NW 3
73      s 400 455 -1000 14
74      s 135 14 -1430 15  $ICRU Center (x=150 to x=135)
75      s 135 14 -1430 14
76      c/y -91 -1224 5
77      py 265
78      py 290
79      s -91 390 -1224 15
80      s -91 390 -1224 14
81      cz 13  $beam dump disk 1
82      cz 10
83      pz 60
84      pz 65
85      cz 13
86      cz 9.5
87      pz 65
88      pz 70
89      cz 13
90      cz 9
91      pz 70
92      pz 75
93      cz 13
94      cz 8.5
95      pz 75
96      pz 80
97      cz 13
98      cz 8
99      pz 80
100     pz 85
101     cz 11
102     cz 7.5
103     pz 85
104     pz 90
105     cz 11
106     cz 7
107     pz 90
108     pz 95
109     cz 11
110     cz 6.5
111     pz 95
112     pz 100
113     cz 11
114     cz 6
115     pz 100
116     pz 105
117     cz 11
118     cz 5.5
119     pz 105

```

120	pz	110							
121	cz	9							
122	cz	5							
123	pz	110							
124	pz	115							
125	cz	9							
126	cz	4.5							
127	pz	115							
128	pz	120							
129	cz	9							
130	cz	4							
131	pz	120							
132	pz	125							
133	cz	9							
134	cz	3.5							
135	pz	125							
136	pz	130							
137	cz	9							
138	cz	3							
139	pz	130							
140	pz	135							
141	cz	9							
142	cz	2.5							
143	pz	135							
144	pz	140							
145	cz	9							
146	cz	2							
147	pz	140							
148	pz	145							
149	cz	9							
150	cz	1.5							
151	pz	145							
152	pz	150							
153	cz	9							
154	pz	150							
155	pz	155							
156	cz	9							
157	pz	155							
158	pz	160							
159	cz	9							
160	pz	160							
161	pz	165							
162	cz	9							
163	pz	165							
164	pz	170							
165	rpp	-23 20 -20 11 -70 -39	\$poly	behind	BD				
166	rpp	-23 20 -21 11 -71 -70	\$Lead						

mode	n p e								
m120	7014.70c	-0.755636	\$Air						
	8016.70c	-0.231475	18040.70c				-0.012889		
m130	1002.70c	-0.667	\$Water						

	8016.70c	-0.333			
m140	74182.70c	-0.260586	\$Tungsten		
	74183.70c	-0.142269	74184.70c	-0.307531	74186.70
	-0.289615				
m150	8016.70c	-0.762	\$phanthom		
	6012.70c	-0.111	1002.	-0.101	7014.70
	-0.026				
m160	22048.70c	-1	\$Titanium		
m170	6012.70c	-0.005	\$Steel, Carbon,		
	26054.70c	-0.056701	26056.70c	-0.914106	26057.70c
	0.021303				
	26058.70c	-0.00289			
m190	30068.70c	-1	\$Zinc 68		
m210	8016.70c	-0.5134	\$soil (dry U.S. Ave. with ENDF-VI)		
	11023.70c	-0.006	12024.70c	-0.010134	12025.70c
	0.001336				
	12026.70c	-0.00153	13027.70c	-0.067	14028.70c
	0.253938				
	14029.70c	-0.013317	14030.70c	-0.009145	20040.70c
	0.063341				
	20042.70c	-0.000339	20043.70c	-7.2e-005	20044.70c
	0.001133				
	20046.70c	-2e-006	20048.70c	-0.000112	22046.70c
	0.000346				
	22047.70c	-0.000322	22048.70c	-0.003326	22049.70c
	0.000253				
	22050.70c	-0.000253	25055.70c	-0.0007	26054.70c
	0.003134				
	26056.70c	-0.050528	26057.70c	-0.001178	26058.70c
	0.00016				
m220	1002.70c	-0.0075	\$Concrete, ordinary,		
	6012.50c	-0.055502	8016.70c	-0.492926	16032.70c
	0.16984				
	16033.70c	-0.001382	16034.70c	-0.007995	16036.70c
	-4e-005				
	20040.70c	-0.221889	20042.70c	-0.009052	20043.70c
	0.000332				
	20044.70c	-0.005202	20046.70c	-1.1e-005	20048.70c
	0.000514				
	26054.70c	-0.000467	26056.70c	-0.007525	26057.70c
	0.000175				
	26058.70c	-2.4e-005			
m230	7014.70c	-0.755636	\$air (US S. Atm at sea level)		
	8016.70c	-0.231475	18036.70c	-3.9e-005	18038.70c
	-8e-006				
	18040.70c	-0.012842			
m180	82206.70c	-0.253338	\$Lead,		
	82207.70c	-0.220743	82208.70c	-0.525919	
m250	1002.70c	-0.133711	\$ borated polyethylene		
	6012.70c	-0.816289	5010.70c	-0.05	
m240	29063.70c	-1			

```

imp:n 1 0 1 0 1 10r
$ 1, 15
0 1 0 1 0
$ 16, 20
1 2r 0 1 81r $ 21, 106
imp:p 1 0 1 0 1 10r
$ 1, 15
0 1 0 1 0
$ 16, 20
1 2r 0 1 81r $ 21, 106
imp:e 1 0 2r 1 10r 0 48r 1 39r
$ 1, 104
0 1r $ 105, 106
cut:e j 0.1
cut:p j 0.1
phys:e 5j 10 j 0
phys:p 3j 1
phys:n 50
sdef pos 0 0 0 axs 0 0 1 rad d1 ext d2 erg 40 vec 0 0 1 par e
si1 0 0.25
sp1 -21 1
si2 48 49.9
sp2 -21 0
f2:n 48
fm2 1.1298e15
df2 iu=1 ic=20
f12:n 50
fm12 1.1298e15
df12 iu=1 ic=20
f22:n 52
fm22 1.1298e15
df22 iu=1 ic=20
f32:n 54
fm32 1.1298e15
df32 iu=1 ic=20
f42:n 59
fm42 1.1298e15
df42 iu=1 ic=20
f52:n 61
fm52 1.1298e15
df52 iu=1 ic=20
f62:n 63
fm62 1.1298e15
df62 iu=1 ic=20
f72:n 65
fm72 1.1298e15
df72 iu=1 ic=20
f82:n 67
fm82 1.1298e15
df82 iu=1 ic=20
f92:n 69
fm92 1.1298e15

```

df92 iu=1 ic=20
f102:n 71
fm102 1.1298e15
df102 iu=1 ic=20
f112:n 73
fm112 1.1298e15
df112 iu=1 ic=20
f242:n 75
fm242 1.1298e15
df242 iu=1 ic=20
f262:n 80
fm262 1.1298e15
df262 iu=1 ic=20
f122:p 48
fm122 1.1298e15
df122 iu=1 ic=20
f132:p 50
fm132 1.1298e15
df132 iu=1 ic=20
f142:p 52
fm142 1.1298e15
df142 iu=1 ic=20
f152:p 54
fm152 1.1298e15
df152 iu=1 ic=20
f162:p 59
fm162 1.1298e15
df162 iu=1 ic=20
f172:p 61
fm172 1.1298e15
df172 iu=1 ic=20
f182:p 63
fm182 1.1298e15
df182 iu=1 ic=20
f192:p 65
fm192 1.1298e15
df192 iu=1 ic=20
f202:p 67
fm202 1.1298e15
df202 iu=1 ic=20
f212:p 69
fm212 1.1298e15
df212 iu=1 ic=20
f222:p 71
fm222 1.1298e15
df222 iu=1 ic=20
f232:p 73
fm232 1.1298e15
df232 iu=1 ic=20
f252:p 75
fm252 1.1298e15
df252 iu=1 ic=20

```
f272:p 80
fm272 1.1298e15
df272 iu=1 ic=20
print
prtmp j 1e6 1 3 1e6
ctme 20000
```

Appendix E

Target 1 Dose Equivalent Rate Input File

MCNPX Visual Editor Version X_24E

```
c      Created on: Saturday, April 2, 2016 at 11:11
  1      0          -1 -3 4  $inside of beam pipe
  2      0          -2 1 -3 4  $thickness of beam pipe
  3      230 -0.001225 (2 :3 :-4 )-5 (-7 :8 :6 )(-9 :10 :6 )(-11 :12 :6
)
          (-13 :14 :6 )(-15 :16 :6 )(-17 :18 :6 )(-26 :27 :6 )
          (-28 :29 :19 )30 31 32 33 34 35 36 37 38 39 40 41 42 43 45
46 47 49
          51 53 55 57 58 60 62 64 66 68 70 72 74 79 81
  4      0          5  $universe
  5      160      -4.5 7 -8 -6  $ Ti 1 (Ti=Titanium)
  6      130      -1 9 -10 -6  $Water thicknes btw Ti 1 an
  7      160      -4.5 11 -12 -6  $ Ti 2
  8      230 -0.001225 13 -14 -6  $$Space btw window & target
  9      160      -4.5 15 -16 -6  $ Ti 3 in target
 10      130      -1 17 -18 -6 (-20 :21 :19 )(-22 :23 :19 ) $ space in
Target
          (-24 :25 :19 )
 11      140      -19.3 20 -21 -19  $ W 1
 12      140      -19.3 22 -23 -19  $ W 2
 13      140      -19.3 24 -25 -19  $ W 3
 14      160      -4.5 26 -27 -6  $ Ti 4
 15      202 -0.00374 28 -29 -19  $ krypton Target
 16      220      -2.32 -30  $vault east wall
 17      220      -2.32 -31  $vault west wall
 18      220      -2.32 -32  $vault south wall
 19      220      -2.32 -33 44  $vault north wall
 20      220      -2.32 -34  $vault floor
 21      220      -2.32 -35 (76 :-77 :78 ) $vault Ceiling
 22      220      -2.32 -36  $beam dump west wall
 23      220      -2.32 -37  $beam dump south wall
 24      220      -2.32 -38  $beam dump east wall
 25      220      -2.32 -39 56  $beam dump north wall
 26      220      -2.32 -40  $beam dump door
 27      170      -7.87 -41  $steel layer of beam dump ceilin
 28      220      -2.32 -42  $concreat layer of beam dump cei
 29      180      -11.34 -43  $lead layer of beam dump ceiling
 30      230 -0.001225 -44  $vault door opening
 31      220      -2.32 -45  $vault door
 32      210      -1.65 -46  $dirt on top of vault (Changed to high
density)
 33      150      -1 -47 48  $ICRU SW 2
 34      150      -1 -48
 35      150      -1 -49 50  $ICRU Center 2
 36      150      -1 -50
 37      150      -1 -51 52  $ICRU NW 2
```

```

38 150      -1 -52
39 150      -1 -53 54 $ICRU Door
40 150      -1 -54
41 250     -0.9 -55 $ borated poly layer of beam dump
42 230 -0.001225 -56 $ beam pipe hole
43 180    -11.34 -57 $polyethylene at pipe
44 150      -1 -58 59 $ICRU Sphere
45 150      -1 -59 $ICRU Spere
46 150      -1 -60 61 $ICRU @ 1 meter
47 150      -1 -61
48 150      -1 -62 63 $ICRU SW 2
49 150      -1 -63
50 150      -1 -64 65 $ICRU SW 3
51 150      -1 -65
52 150      -1 -66 67 $ICRU Center 1
53 150      -1 -67
54 150      -1 -68 69 $ICRU Center 3
55 150      -1 -69
56 150      -1 -70 71 $ICRU NW 1
57 150      -1 -71
58 150      -1 -72 73 $ICRU NW 3
59 150      -1 -73
60 150      -1 -74 75
61 150      -1 -75
62 230 -0.001225 -76 77 -78
63 150      -1 -79 80
64 150      -1 -80
65 250     -0.9 -81

```

c Surface

```

1      c/z 0 0 6 $inner beam pipe
2      c/z 0 0 7 $outer beam pipe
3      pz 50 $top of beam window
4      pz 30 $bottom of beam window
5      so 3000 $universe
6      c/z 0 0 10 $Ti 1
7      pz 50 $bottom of Ti 1
8      pz 50.0127 $top of Ti 1
9      pz 50.0127 $bottom of water thickness
10     pz 50.872 $top of water thickness
11     pz 50.872 $bottom of Ti 2
12     pz 50.884 $top of Ti 2
13     pz 50.884 $bottom of space btw window and target
14     pz 51.646 $top of space btw window and target
15     pz 51.646 $bottom of Ti 3 in target
16     pz 51.658 $top of Ti 3 in target
17     pz 51.658 $bottom of distance btw Ti 3 and Ti 4
18     pz 53.593 $top of distance btw Ti 3 and Ti 4
19     c/z 0 0 1.25 $tungsten disk
20     pz 52.079 $Bottom of W 1
21     pz 52.228 $top of W 1
22     pz 52.482 $bottom of W 2

```

23 pz 52.634 \$top of W 2
24 pz 52.888 \$bottom of W 3
25 pz 53.037 \$top of W 3
26 pz 53.593 \$bottom of Ti 4
27 pz 53.605 \$top of Ti 4
28 pz 53.605 \$bottom of Target pipe
29 pz 56.605 \$top of Target Pipe
30 rpp -136 -111 -100 523 -1248 215 \$Vault east wall
31 rpp 455 531 -100 523 -1248 215 \$vault west wall
32 rpp -136 531 -100 523 215 240 \$vault south wall
33 rpp -136 531 -100 265 -1324 -1248 \$vault north wall
34 rpp -136 480 -125 -100 -1324 240 \$vault floor
35 rpp -111 455 265 290 -1248 215 \$vault ceiling (xz reduced
by 25)
36 rpp 40 93 -100 20 39 109 \$beam dump west wall
37 rpp -111 93 -100 20 109 215 \$beam dump south wall
38 rpp -111 -72 -100 20 -10 109 \$beam dump east wall
39 rpp -111 93 -100 20 -38 -10 \$beam dum north wall
40 rpp 93 118 -100 45 -30 69 \$beam dump door
41 rpp -111 93 20 22.5 -38 129 \$steel layer of BD ceiling
42 rpp -111 93 22.5 40 -38 129 \$concrete layer of BD ceiling
43 rpp -111 93 40 45 -38 129 \$lead layer of BD Ceiling
44 rpp -10 249 -100 128 -1324 -1248 \$vault door opening
45 rpp -30 269 -100 148 -1400 -1324 \$(-z=1400 to z=-
1376)vault door
46 arb -111 290 -1248 455 290 -1248 -111 290 215 \$dirt on top
of vault
455 290
455 290
-1248 1234 3456 5612 2647 1538 0
47 s 172 628 50 15 \$ICUR South Wall (SW 2)
48 s 172 628 50 14
49 s 172 530 -542 15 \$ICRU Center 2
50 s 172 530 -542 14
51 s 172 455 -1000 15 \$ICRU North Wall (NW 2)
52 s 172 455 -1000 14
53 s 10 14 -1430 15 \$ICRU vault door (z= -1415 to -1445)
54 s 10 14 -1430 14 \$ (x= 150 to 10)
55 rpp -111 93 45 50 -38 129 \$Borated poly layer of BD
Ceiling
56 rpp -20 15 -18 10 -38 -10 \$ (x=-10, 10 to x=-20, 15)lead
beebees
57 rpp -23 20 -20 11 -39 -38 \$lead behind BP hole
58 s 681 14 -1200 15 \$ICRU Control Area
59 s 681 14 -1200 14 \$ICRU 1 cm deep
60 s 150 14 -1500 15 \$ICRU (x=150 to x=135) @ 1 meter from
V. door
61 s 150 14 -1500 14
62 s -55 628 50 15 \$ICRU (SW 1)
63 s -55 628 50 14
64 s 400 628 50 15 \$ICRU (SW 3)
65 s 400 628 50 14

```

66      s -55 530 -542 15  $ICRU Center 1
67      s -55 530 -542 14
68      s 400 530 -542 15  $ICRU Center 3
69      s 400 530 -542 14
70      s -55 455 -1000 15  $ICRU NW 1
71      s -55 455 -1000 14
72      s 400 455 -1000 15  $ICRU NW 3
73      s 400 455 -1000 14
74      s 135 14 -1430 15  $ICRU Center (x=150 to x=135)
75      s 135 14 -1430 14
76      c/y -91 -1224 5
77      py 265
78      py 290
79      s -91 390 -1224 15
80      s -91 390 -1224 14
81      rpp -23 20 -20 11 -64 -39  $ poly behind beam pipe hole

```

```

mode  n p e
m120  7014.70c      -0.755636  $Air
      8016.70c      -0.231475 18040.      -0.012889
m130  1002.70c      -0.667  $Water
      8016.70c      -0.333
m140  74182.70c     -0.260586  $Tungsten
      74183.70c     -0.142269 74184.70c      -0.307531 74186.70c      -
0.289615
m150  8016.70c      -0.762  $phanthom
      6012.70c      -0.111 1002.70c      -0.101 7014.70c
-0.026
m160  22048.70c     -1  $Titanium
m170  6012.70c      -0.005  $Steel, Carbon,
      26054.70c     -0.056701 26056.70c      -0.914106 26057.70c      -
0.021303
      26058.70c      -0.00289
m190  30068.70c     -1  $Zinc 68
m210  8016.70c      -0.5134  $soil (dry U.S. Ave. with ENDF-VI)
      11023.70c     -0.006 12024.70c      -0.010134 12025.70c      -
0.001336
      12026.70c     -0.00153 13027.70c      -0.067 14028.70c      -
0.253938
      14029.70c     -0.013317 14030.70c      -0.009145 20040.70c      -
0.063341
      20042.70c     -0.000339 20043.70c      -7.2e-005 20044.70c      -
0.001133
      20046.70c     -2e-006 20048.70c      -0.000112 22046.70c      -
0.000346
      22047.70c     -0.000322 22048.70c      -0.003326 22049.70c      -
0.000253
      22050.70c     -0.000253 25055.70c      -0.0007 26054.70c      -
0.003134
      26056.70c     -0.050528 26057.70c      -0.001178 26058.70c      -
0.00016
m220  1002.70c      -0.0075  $Concrete, ordinary,

```

```

        6012.50c      -0.055502  8016.70c      -0.492926  16032.70c      -
0.16984
        16033.70c    -0.001382  16034.70c    -0.007995  16036.70c
-4e-005
        20040.70c    -0.221889  20042.70c    -0.009052  20043.70c      -
0.000332
        20044.70c    -0.005202  20046.70c    -1.1e-005  20048.70c      -
0.000514
        26054.70c    -0.000467  26056.70c    -0.007525  26057.70c      -
0.000175
        26058.70c    -2.4e-005
m230  7014.70c      -0.755636  $air (US S. Atm at sea level)
        8016.70c      -0.231475  18036.70c     -3.9e-005  18038.70c
-8e-006
        18040.70c    -0.012842
m180  82206.70c     -0.253338  $Lead,
        82207.70c     -0.220743  82208.70c     -0.525919
m250  1002.70c      -0.133711  $ borated polyethylene
        6012.70c      -0.816289  5010.70c      -0.05
m202  36084.70c     -1
imp:n  1           0           1           0           1 10r
$ 1, 15
        0           1           0           1           0
$ 16, 20
        1 1r       0 1r       1 40r       $ 21, 65
imp:p  1           0           1           0           1 10r
$ 1, 15
        0           1           0           1           0
$ 16, 20
        1 1r       0 1r       1 40r       $ 21, 65
imp:e  1           0 2r       1 10r       0 49r       $ 1, 65
cut:e j 0.1
cut:p j 0.1
phys:e 5j 10 j 0
phys:p 3j 1
phys:n 50
sdef pos 0 0 0 axs 0 0 1 rad d1 ext d2 erg 40 vec 0 0 1 par e
sil 0 0.25
sp1 -21 1
si2 48 49.9
sp2 -21 0
f2:n 48
fm2 1.1298e15
df2 iu=1 ic=20
f12:n 50
fm12 1.1298e15
df12 iu=1 ic=20
f22:n 52
fm22 1.1298e15
df22 iu=1 ic=20
f32:n 54
fm32 1.1298e15

```

df32 iu=1 ic=20
f42:n 59
fm42 1.1298e15
df42 iu=1 ic=20
f52:n 61
fm52 1.1298e15
df52 iu=1 ic=20
f62:n 63
fm62 1.1298e15
df62 iu=1 ic=20
f72:n 65
fm72 1.1298e15
df72 iu=1 ic=20
f82:n 67
fm82 1.1298e15
df82 iu=1 ic=20
f92:n 69
fm92 1.1298e15
df92 iu=1 ic=20
f102:n 71
fm102 1.1298e15
df102 iu=1 ic=20
f112:n 73
fm112 1.1298e15
df112 iu=1 ic=20
f242:n 75
fm242 1.1298e15
df242 iu=1 ic=20
f262:n 80
fm262 1.1298e15
df262 iu=1 ic=20
f122:p 48
fm122 1.1298e15
df122 iu=1 ic=20
f132:p 50
fm132 1.1298e15
df132 iu=1 ic=20
f142:p 52
fm142 1.1298e15
df142 iu=1 ic=20
f152:p 54
fm152 1.1298e15
df152 iu=1 ic=20
f162:p 59
fm162 1.1298e15
df162 iu=1 ic=20
f172:p 61
fm172 1.1298e15
df172 iu=1 ic=20
f182:p 63
fm182 1.1298e15
df182 iu=1 ic=20

```
f192:p 65
fm192 1.1298e15
df192 iu=1 ic=20
f202:p 67
fm202 1.1298e15
df202 iu=1 ic=20
f212:p 69
fm212 1.1298e15
df212 iu=1 ic=20
f222:p 71
fm222 1.1298e15
df222 iu=1 ic=20
f232:p 73
fm232 1.1298e15
df232 iu=1 ic=20
f252:p 75
fm252 1.1298e15
df252 iu=1 ic=20
f272:p 80
fm272 1.1298e15
df272 iu=1 ic=20
print
prtmp j 1e6 1 3 1e6
ctme 20000
```

Appendix F

Target 2 Dose Equivalent Rate Input File

```
MCNPF Visual Editor Version X_24E
c Created on: Thursday, November 12, 2015 at 10:41
  1 0 -1 -3 4 $inside of beam pipe
  2 0 -2 1 -3 4 $thickness of beam pipe
  3 230 -0.001225 (2 :3 :-4 )-5 (-7 :8 :6 )(-9 :10 :6 )(-11 :12 :6
)
(-13 :14 :6 )(-15 :16 :6 )(-17 :18 :6 )(-26 :27 :6 )
(-28 :29 :19 )30 31 32 33 34 35 36 37 38 39 40 41 42 43 45
46 47 49
51 53 55 57 58 65 67 69 71 73 75 79
  4 0 5 $universe
  5 160 -4.5 7 -8 -6 $ Ti 1 (Ti=Titanium)
  6 130 -1 9 -10 -6 $Water thicknes btw Ti 1 an
  7 160 -4.5 11 -12 -6 $ Ti 2
  8 230 -0.001225 13 -14 -6 $Space btw window & target
  9 160 -4.5 15 -16 -6 $ Ti 3 in target
 10 130 -1 17 -18 -6 (-20 :21 :19 )(-22 :23 :19 ) $ space in
Target
(-24 :25 :19 )
 11 140 -19.3 20 -21 -19 $ W 1
 12 140 -19.3 22 -23 -19 $ W 2
 13 140 -19.3 24 -25 -19 $ W 3
 14 160 -4.5 26 -27 -6 $ Ti 4
 15 208 -2.69 28 -29 -19 (60 :-61 :62 )(63 :-61 :62 ) $ Target p
(64 :-61 :62 )
 16 220 -2.32 -30 $vault east wall
 17 220 -2.32 -31 $vault west wall
 18 220 -2.32 -32 $vault south wall
 19 220 -2.32 -33 44 $vault north wall
 20 220 -2.32 -34 $vault floor
 21 220 -2.32 -35 $vault Ceiling
 22 220 -2.32 -36 $beam dump west wall
 23 220 -2.32 -37 $beam dump south wall
 24 220 -2.32 -38 $beam dump east wall
 25 220 -2.32 -39 56 $beam dump north wall
 26 220 -2.32 -40 $beam dump door
 27 170 -7.85 -41 $steel layer of beam dump ceilin
 28 220 -2.32 -42 $concreat layer of beam dump cei
 29 180 -11.34 -43 $lead layer of beam dump ceiling
 30 230 -0.001225 -44 $vault door opening
 31 220 -2.32 -45 $vault door
 32 210 -1.75 -46 $dirt on top of vault
 33 150 -1 -47 48 $Phanthom NW
 34 150 -1 -48
 35 150 -1 -49 50 $Phantom Center
 36 150 -1 -50
 37 150 -1 -51 52 $Phantom SW
```

```

38 150      -1 -52
39 150      -1 -53 54 $Phanthom Door
40 150      -1 -54
41 250     -0.98 -55 $ borated poly layer of beam dump
42 230    -0.001225 -56 $ air beam pipe passage
43 180    -11.34 -57 $polyethylene at pipe
44 150      -1 -58 59 $ICRU Control Area
45 150      -1 -59
46 202    -0.003733 -60 61 -62 $Kr gas chamber
47 202    -0.003733 -63 61 -62 $Kr gas chamber
48 202    -0.003733 -64 61 -62 $Kr gas chamber
49 150      -1 -65 66 $ICRU @ 1 m from door
50 150      -1 -66
51 150      -1 -67 68 $ICRU SW 1
52 150      -1 -68
53 150      -1 -69 70 $ICRU SW 3
54 150      -1 -70
55 150      -1 -71 72 $ICRU Center 1
56 150      -1 -72
57 150      -1 -73 74 $ICRU center 3
58 150      -1 -74
59 150      -1 -75 76 $ICRU NW 1
60 150      -1 -76
61 150      -1 -77 78 $ICRU NW 3
62 150      -1 -78
63 250     -0.9 -79

```

c Surface

```

1      c/z 0 0 6 $inner beam pipe
2      c/z 0 0 7 $outer beam pipe
3      pz 50 $top of beam window
4      pz 30 $bottom of beam window
5      so 3000 $universe
6      c/z 0 0 10 $Ti 1
7      pz 50 $bottom of Ti 1
8      pz 50.0127 $stop of Ti 1
9      pz 50.0127 $bottom of water thickness
10     pz 50.872 $stop of water thickness
11     pz 50.872 $bottom of Ti 2
12     pz 50.884 $stop of Ti 2
13     pz 50.884 $bottom of space btw window and target
14     pz 51.646 $stop of space btw window and target
15     pz 51.646 $bottom of Ti 3 in target
16     pz 51.658 $stop of Ti 3 in target
17     pz 51.658 $bottom of distance btw Ti 3 and Ti 4
18     pz 53.593 $stop of distance btw Ti 3 and Ti 4
19     c/z 0 0 1.4 $tungsten disk
20     pz 52.079 $Bottom of W 1
21     pz 52.228 $stop of W 1
22     pz 52.482 $bottom of W 2
23     pz 52.634 $stop of W 2
24     pz 52.888 $bottom of W 3

```

25 pz 53.037 \$top of W 3
 26 pz 53.593 \$bottom of Ti 4
 27 pz 53.605 \$top of Ti 4
 28 pz 53.605 \$bottom of Target pipe
 29 pz 59.892 \$top of Target Pipe
 30 rpp -136 -111 -100 265 -1248 215 \$Vault east wall
 31 rpp 455 531 -100 265 -1248 215 \$vault west wall
 32 rpp -136 531 -100 265 215 240 \$vault south wall
 33 rpp -136 531 -100 265 -1324 -1248 \$vault north wall
 34 rpp -136 480 -125 -100 -1324 240 \$vault floor
 35 rpp -136 480 265 290 -1324 240 \$vault ceiling
 36 rpp 40 93 -100 20 39 109 \$beam dump west wall
 37 rpp -111 93 -100 20 109 215 \$beam dump south wall
 38 rpp -111 -72 -100 20 -10 109 \$beam dump east wall
 39 rpp -111 93 -100 20 -38 -10 \$beam dum north wall
 40 rpp 93 118 -100 45 -30 69 \$beam dump door
 41 rpp -111 93 20 22.5 -38 129 \$steel layer of BD ceiling
 42 rpp -111 93 22.5 40 -38 129 \$concrete layer of BD ceiling
 43 rpp -111 93 40 45 -38 129 \$lead layer of BD Ceiling
 44 rpp 50 249 -100 128 -1324 -1248 \$vault door opening
 45 rpp 30 269 -100 148 -1400 -1324 \$vault door
 46 arb -136 290 -1324 480 290 -1324 -136 290 240 \$dirt on top
 of vault
 480 290 240 -136 513 240 480 513 240 -136 290 -1324
 -1324 1234 3456 5612 2647 1538 0
 47 s 172 629 50 15 \$ICUR phanthom North Wall (NW)
 48 s 172 629 50 14 \$ICRU phanthom 1 cm deep NW
 49 s 172 530 -542 15 \$ICRU Phanthom Center
 50 s 172 530 -542 14 \$ICRU Phanthom 1 cm deep center
 51 s 172 455 -1000 15 \$ICRU Phanthom South Wall (SW)
 52 s 172 455 -1000 14 \$ICRU Phanthom 1 cm deep SW
 53 s 150 14 -1415 15 \$ICRU Phathom @ vault door
 54 s 150 14 -1415 14 \$ICRU phanthom 1 cm deep
 55 rpp -111 93 45 50 -38 129 \$Borated poly layer of BD
 Ceiling
 56 rpp -10 10 -18 10 -38 -10 \$lead beebees
 57 rpp -23 20 -20 11 -40 -39 \$Borated poly behind BP hole
 58 s 681 14 -1200 15 \$ICRU Control Area
 59 s 681 14 -1200 14
 60 c/z -0.6 -1 0.35 \$ krypton gas chamber
 61 pz 56.335 \$botton of Kr gas chamber
 62 pz 59.892 \$top of Kr gas chamber
 63 c/z -0.6 0.02 0.35
 64 c/z 0.6 0.02 0.35
 65 s 150 14 -1500 15 \$ICRU @ 1 meter from V. door
 66 s 150 14 -1500 14
 67 s -55 629 50 15 \$ICRU (SW 1)
 68 s -55 629 50 14
 69 s 400 629 50 15 \$ICRU (SW 3)
 70 s 400 629 50 14
 71 s -55 530 -542 15 \$ICRU Center 1

```

72      s -55 530 -542 14
73      s 400 530 -542 15  $ICRU Center 3
74      s 400 530 -542 14
75      s -55 455 -1000 15  $ICRU NW 1
76      s -55 455 -1000 14
77      s 400 455 -1000 15  $ICRU NW 3
78      s 400 455 -1000 14
79      rpp -23 20 -20 11 -65 -40  $ poly behind beam pipe hole

```

```

mode  n p e
m120  7014.70c      -0.755636  $Air
      8016.70c      -0.231475  18040.          -0.012889
m130  1002.70c      -0.667  $Water
      8016.70c      -0.333
m140  74182.70c     -0.260586  $Tungsten
      74183.70c     -0.142269  74184.70c     -0.307531  74186.70c  -
0.289615
m150  8016.70c      -0.762  $phanthom
      6012.70c      -0.111  1002.70c          -0.101  7014.70c
-0.026
m160  22048.70c     -1  $Titanium
m170  6012.70c      -0.005  $Steel, Carbon,
      26054.70c     -0.056701  26056.70c     -0.914106  26057.70c  -
0.021303
      26058.70c     -0.00289
m190  30068.70c     -1  $Zinc 68
m202  18040.70c     -1  $krypton gas
m210  8016.70c      -0.5134  $soil (dry U.S. Ave. with ENDF-VI)
      11023.70c     -0.006  12024.70c     -0.010134  12025.70c  -
0.001336
      12026.70c     -0.00153  13027.70c          -0.067  14028.70c  -
0.253938
      14029.70c     -0.013317  14030.70c          -0.009145  20040.70c  -
0.063341
      20042.70c     -0.000339  20043.70c          -7.2e-005  20044.70c  -
0.001133
      20046.70c     -2e-006  20048.70c          -0.000112  22046.70c  -
0.000346
      22047.70c     -0.000322  22048.70c          -0.003326  22049.70c  -
0.000253
      22050.70c     -0.000253  25055.70c          -0.0007  26054.70c  -
0.003134
      26056.70c     -0.050528  26057.70c          -0.001178  26058.70c  -
0.00016
m220  1002.70c      -0.0075  $Concrete, ordinary,
      6012.50c      -0.055502  8016.70c          -0.492926  16032.70c  -
0.16984
      16033.70c     -0.001382  16034.70c          -0.007995  16036.70c
-4e-005
      20040.70c     -0.221889  20042.70c          -0.009052  20043.70c  -
0.000332

```

```

20044.70c      -0.005202 20046.70c      -1.1e-005 20048.70c      -
0.000514
26054.70c      -0.000467 26056.70c      -0.007525 26057.70c      -
0.000175
26058.70c      -2.4e-005
m230 7014.70c  -0.755636 $air (US S. Atm at sea level)
      8016.70c  -0.231475 18036.70c      -3.9e-005 18038.70c
-8e-006
      18040.70c  -0.012842
m180 82206.70c  -0.253338 $Lead,
      82207.70c  -0.220743 82208.70c      -0.525919
m250 1002.70c  -0.133711 $ borated polyethylene
      6012.70c  -0.816289 5010.70c      -0.05
m208 13027.70c  -1 $aluminum
imp:n 1 0 1 0 1 10r
$ 1, 15
0 1 0 1 0
$ 16, 20
1 1r 0 1r 1 38r $ 21, 63
imp:p 1 0 1 0 1 10r
$ 1, 15
0 1 0 1 0
$ 16, 20
1 1r 0 1r 1 38r $ 21, 63
imp:e 1 0 2r 1 10r 0 29r 1 14r
$ 1, 60
0 2r $ 61, 63
cut:e j 0.1
cut:p j 0.1
phys:e 5j 10 j 0
phys:p 3j 1
phys:n 50
sdef pos 0 0 0 axs 0 0 1 rad d1 ext d2 erg 40 vec 0 0 1 par e
sil 0 0.25
sp1 -21 1
si2 48 49.9
sp2 -21 0
f2:n 48
fm2 1.1298e15
df2 iu=1 ic=20
f12:n 50
fm12 1.1298e15
df12 iu=1 ic=20
f22:n 52
fm22 1.1298e15
df22 iu=1 ic=20
f32:n 54
fm32 1.1298e15
df32 iu=1 ic=20
f42:n 59
fm42 1.1298e15
df42 iu=1 ic=20

```

f52:n 66
fm52 1.1298e15
df52 iu=1 ic=20
f62:n 68
fm62 1.1298e15
df62 iu=1 ic=20
f72:n 70
fm72 1.1298e15
df72 iu=1 ic=20
f82:n 72
fm82 1.1298e15
df82 iu=1 ic=20
f92:n 74
fm92 1.1298e15
df92 iu=1 ic=20
f102:n 76
fm102 1.1298e15
df102 iu=1 ic=20
f112:n 78
fm112 1.1298e15
df112 iu=1 ic=20
f122:p 48
fm122 1.1298e15
df122 iu=1 ic=20
f132:p 50
fm132 1.1298e15
df132 iu=1 ic=20
f142:p 52
fm142 1.1298e15
df142 iu=1 ic=20
f152:p 54
fm152 1.1298e15
df152 iu=1 ic=20
f162:p 59
fm162 1.1298e15
df162 iu=1 ic=20
f172:p 66
fm172 1.1298e15
df172 iu=1 ic=20
f182:p 68
fm182 1.1298e15
df182 iu=1 ic=20
f192:p 70
fm192 1.1298e15
df192 iu=1 ic=20
f202:p 72
fm202 1.1298e15
df202 iu=1 ic=20
f212:p 74
fm212 1.1298e15
df212 iu=1 ic=20
f222:p 76

```
fm222 1.1298e15
df222 iu=1 ic=20
f232;p 78
fm232 1.1298e15
df232 iu=1 ic=20
print
prtmp   j 1e6 1 3 1e6
ctme 20000
```